DOCTORAL THESIS

Insulation Durability and Measurement of Partial Discharge

Ivar Kiitam

TALLINNA TEHNIKAÜLIKOOL
TALLINN UNIVERSITY OF TECHNOLOGY
TALLINN 2021

TALLINN UNIVERSITY OF TECHNOLOGY
DOCTORAL THESIS
62/2021

Insulation Durability and Measurement of Partial Discharge

IVAR KIITAM

TALTECH PRESS

TALLINN UNIVERSITY OF TECHNOLOGY
School of Engineering
Department of Electrical Power Engineering and Mechatronics
This dissertation was accepted for the defence of the degree 14/11/2021

Supervisor: Paul Taklaja, PhD
School of Engineering
Tallinn University of Technology
Tallinn, Estonia

Co-supervisor: Prof Ivo Palu, PhD
School of Engineering
Tallinn University of Technology
Tallinn, Estonia

Opponents: Prof Matti Lehtonen, PhD
School of Electrical Engineering
Department of Electrical Engineering and Automation
Aalto University
Espoo, Finland

Assoc. Prof Audrius Jonaitis, PhD
Faculty of Electrical and Electronics Engineering
Department of Electric Power Systems
Kaunas University of Technology
Kaunas, Lithuania

Defence of the thesis: 20/12/2021, Tallinn

Declaration:
Hereby I declare that this doctoral thesis, my original investigation and achievement, submitted for the doctoral degree at Tallinn University of Technology has not been submitted for doctoral or equivalent academic degree.

Ivar Kiitam

----
signature

European Union
European Regional
Development Fund

Investing
in your future

Copyright: Ivar Kiitam, 2021
ISSN 2585-6898 (publication)
ISBN 978-9949-83-769-4 (publication)
ISSN 2585-6901 (PDF)
ISBN 978-9949-83-770-0 (PDF)
Printed by Auratrükk

TALLINNA TEHNIKAÜLIKOOL
DOKTORITÖÖ
62/2021

Isolatsiooni vastupidavus ja osalahenduste mõõtmine

IVAR KIITAM

TAL TECH
KIRJASTUS

Contents

List of publications 7

Author's contribution to the publications 8

Introduction 10

Abbreviations 13

Symbols 14

1 Durability of medium voltage covered conductor insulation materials 17
1.1 Background and experiences with covered conductors 17
1.2 Covered conductor insulation materials 18
1.3 Problems concerning covered conductors 19
1.4 Insulation lifetime modelling 21
1.5 Insulation durability testing of different insulating materials 22
1.6 Computer simulation of electric field at the grounding points 25
1.7 Results of material comparison experiment 26

2 The effect of electrode shape on insulation durability 29
2.1 Test setup and parameters 29
2.2 Test results 30
2.3 Failure probability functions of different electrodes 32
2.4 Statistical significance of test results 34
2.5 Electric field simulations 35
2.6 Intermediate summary 37

3 Accuracy of locating partial discharges in power cables 39
3.1 Physical background of partial discharges 39
3.2 Partial discharge types and modes 40
3.2.1 Corona discharge 41
3.2.2 Internal discharge 42
3.2.3 Surface discharge 42
3.3 Partial discharge pulse parameters 43
3.4 General diagnostic approach to partial discharge assessment 44
3.4.1 Measurement 44
3.4.2 Partial discharge signal denoising 46
3.5 Medium voltage power cable structure 47
3.5.1 Partial discharge in power cables 48
3.5.2 Determining locations of partial discharge sources 48
3.5.3 Partial discharge pattern recognition 50
3.6 Aspects of partial discharge occurrence in cables 51
3.6.1 Propagation-related pulse distortion 52
3.7 Aspects of partial discharge pulse behavior 55
3.8 Testing the accuracy of PD source location using time-delay reflectometry 55
3.8.1 Partial discharge type 1 57
3.8.2 Partial discharge type 2 59
3.8.3 Defect location accuracy and discussion 60

4 Differentiating partial discharge sources based on pulse characteristics and phase-resolved patterns 62
4.1 Data processing and partial discharge related parameters 63

4.2 Partial discharge measurement results and discussion 66
4.2.1 Pulse count 67
4.2.2 Maximum peak value of the pulse 68
4.2.3 Mean peak value of the pulse 68
4.2.4 Phase span 68
4.2.5 Pulse width parameters 68
4.2.6 Pulse interval parameters 68
4.2.7 Voltage difference parameters 69
4.2.8 Correlation of pulse shape at maximum and minimum pulse widths 69
4.3 Applicability of the parameter-based approach in distinguishing PD sources 69
4.4 Intermediate summary 70
Conclusion 72
Future work 74
List of figures 75
List of tables 77
References 78
Abstract 85
Lühikokkuvõte 86
Appendix 1 87
Appendix 2 93
Appendix 3 101
Appendix 4 115
Curriculum vitae 122
Elulookirjeldus 123

List of publications

The list of author’s publications, on the basis of which the thesis has been prepared:

I **Kiitam, I.**; Taklaja, P.; Tuttelberg, K. (2018). Voltage Withstand Properties of the Insulation of Different Types of Medium Voltage Covered Overhead Line Conductors. 19th International Scientific Conference Electric Power Engineering (EPE), Brno, Czech Republic. IEEE, 18–21.

II **Kiitam, I.**; Taklaja, P.; Tuttelberg, K. (2018). Effect of Electrode Shape on Medium Voltage Covered Conductor Insulation Durability Under Electric Stress. IEEE 59th International Scientific Conference on Power and Electrical Engineering of Riga Technical University (RTUCON). IEEE, 1–6.

III Shafiq, M.; **Kiitam, I.**; Taklaja, P.; Kütt, L.; Kauhaniemi, K.; Palu, I. (2019). Identification and Location of PD Defects in Medium voltage Underground Power Cables Using High Frequency Current Transformer. IEEE Access, 7, 103608−103618.

IV **Kiitam, I.**; Shafiq, M.; Taklaja, P.; Parker, M.; Palu, I.; Kütt, L. (2021); Characteristic Pulse Pattern Features of Different Types of Partial Discharge Sources in Power Cables. IEEE PES/IAS PowerAfrica Conference. IEEE, 1–5.

Author’s contribution to the publications

Contribution to the papers in this thesis are:

I I. Kiitam is the main author of the paper. He contributed to the preparation and execution of tests on which the paper is based, the analysis of results and preparation of the manuscript.

II I. Kiitam is the main author of the paper. He contributed to the preparation and execution of tests on which the paper is based, the analysis of results and preparation of the manuscript.

III I. Kiitam is a co-author of the paper. He contributed to the preparation and execution of tests on which the paper is based, the analysis of results and preparation of the manuscript.

IV I. Kiitam is the main author of the paper. He conducted the analysis of test results on which the paper is based and contributed to the preparation of the manuscript.

List of the author's other recent publications not included in the thesis

- Shafiq, M.; Kiitam, I.; Taklaja, P.; Parker, M.; Palu, I.; Kütt, L. (2021). Study of the Behaviour of Partial Discharges for Proactive Diagnostics in Medium Voltage Cables. IEEE PES/IAS PowerAfrica. IEEE, 1–5.
- Shafiq, M.; Kiitam, I.; Kauhaniemi, K.; Taklaja, P.; Kütt, L.; Palu, I. (2020). Performance Comparison of PD Data Acquisition Techniques for Condition Monitoring of Medium Voltage Cables. Energies, 13 (16), #4272.
- Shafiq, M.; Kiitam, I.; Taklaja, P.; Hussain, A.; Kütt, L.; Kauhaniemi, K. (2020). Characterization of Corona and Internal Partial Discharge Under Increasing Electrical Stress using Time Domain Analysis. IEEE Electrical Insulation Conference (EIC). IEEE, 217–220.
- Kiitam, I.; Saarna, M.; Taklaja, P.; Tealane, M.; Palu, I. (2020). Electrical and Mechanical Properties of Service-aged Medium Voltage Porcelain Support Insulators. 6th IEEE International Energy Conference (ENERGYCon), Gammarth, Tunisia, IEEE, 702–706.
- Kiitam, I.; Taklaja, P.; Pohlak, M.; Põdra, P.; Palu, I. (2019). Strength Analysis of Medium Voltage Overhead Line Crossarms for Updating Conductor. 2019 Electric Power Quality and Supply Reliability Conference (PQ2019) and Symposium of Electrical Engineering and Mechatronics (SEEM2019), Kärdla, Estonia, IEEE, 1–6.

Introduction

Reliability is a core tenet of modern power systems. Interruptions in electricity supply can impose significant costs on consumers, grid utilities, energy producers and society in general. It is desirable to decrease the duration and frequency of power outages and the performance of electrical utilities is predominantly assessed based on parameters which are related to the continuity and quality of power delivery. Regardless of the primary energy sources used for generation of electrical power, a necessity to convey that energy to the consumers and ensure sufficient security of supply is a reality of contemporary technology-dependent civilization. This central aspect of power grid operation is not expected to change in the foreseeable future.

The proliferation of smart technologies is increasingly influencing the expectations regarding the operation of power grids, their associated systems, and the functionalities these should incorporate. Consequently, the implementation of condition monitoring technologies has increased and there is interest to expand the scope of equipment surveillance efforts. Continuous information regarding grid component status enables condition-based maintenance, which is more efficient and possibly more effective in most circumstances compared to the historically more prevalent practice of performing regular interval-based maintenance inspections. Monitoring also enables the identification of incipient insulation faults and timely application of countermeasures to avoid functional component failure. Monitoring systems can also aid in managing damage control efforts following extreme weather events in vulnerable infrastructure, e.g., rural medium voltage (MV) overhead lines (OHL).

An important issue for utilities is estimating the amount of time available for responding to a developing fault situation. Techniques like partial discharge (PD) monitoring can aid in detecting potential problems in MV and high voltage (HV) systems, although the pattern of PD activity from inception to component failure does not often follow a predetermined and predictable trajectory. An abundance of relevant and up-to-date information regarding the condition of its physical assets is necessary for any enterprise operating an extensive technological system, primarily to facilitate effective asset management.

A practical example of an acute problem electrical utilities encounter is the clearance of fallen trees and other debris from OHLs after a storm or other severe weather event. In case a tree falls on a covered conductor (CC) power line, it creates a point of electrical stress in the insulation, which will eventually fail. The utility must manage its resources to locate and eliminate such problematic occurrences. A clearer understanding of the mechanisms and circumstances determining the rate of insulation deterioration, e.g., the choice of materials, the shape of the offending object in contact with the conductor, moisture, fluctuations in voltage, etc. will enable more accurate estimation of the time until an insulation fault occurs. This can aid utility personnel in making informed decisions regarding, e.g., the construction of new OHLs, deployment of grid monitoring equipment, and triage principles implemented during intensive and time-sensitive grid maintenance operations, particularly under circumstances encountered immediately after a severe storm and high winds.

The measurement of PD on-line is another aspect of this subject matter, which has developed considerably in recent years. Although numerous advancements have been made regarding the measurement of PD apparent charge based on the traditional methodology specified in IEC 60270, this is not applicable to on-line scenarios in most cases. The interest in non-traditional methods to detect and quantify PD, e.g., the deployment of high-frequency current transformers (HFCT), ultrasound transducers, and antennas has increased.

Some important aspects of PD measurement are the location of the source and diagnosing the nature of the PD activity, i.e., determining whether or not the detected PD is likely to be a cause for concern or it is merely an innocuous abnormality unlikely to have a notable impact on the functionality of equipment and, by extension, the operation of the grid. In cases where PD activity is an indicator of an incipient fault, the timely application of countermeasures to mitigate insulation failure and prevent loss of power delivery is warranted, requiring swift action on behalf of the grid operator. In conjunction with distribution grids, this problem is further aggravated by the tendency to shift towards favoring inconspicuous underground cable lines over OHLs, which are not as expensive to build, but are seen as a source of visual pollution by the general public and pose a non-negligible degree of elevated electrical hazard. Furthermore, in most MV and HV applications, the dominant trend over the past few decades has been the use of polymer-insulated power cables, predominantly utilizing XLPE (cross-linked polyethylene) as the main insulation material. While possessing numerous advantageous features over the historically more prevalent oil-impregnated paper-insulated cables, durability under the influence of PD is not amongst those. Distinguishing actual PD pulses from sources of noise during measurement, e.g., pulses generated by power converter operation, is also an issue, as this may cause misinterpretation of PD activity.

The problem of distinguishing between different PD sources is multifaceted. The types of defects most likely to cause insulation failure are referred to as internal discharge, i.e., the discharges are generated inside gaseous voids, cavities, or cracks in solid insulation. These can cause the inception and growth of carbonized channels in the insulation, which can eventually expand across the entire thickness of the insulation and precipitate the occurrence of an electrical fault. As the resilience of XLPE to PD is low, identifying these defects early and taking remedial action is desirable. PD can also occur along the interfaces between solid insulation and air, i.e., in cable terminations. These surface discharges are normally not as acutely detrimental as internal discharges, although they might indicate the presence of surface pollution or some type of defect. Surface discharge may also eventually precipitate a fault, although the timeframe might be considerably longer, depending on the circumstances of its occurrence. Corona discharge is the third primary type of PD and is usually considered innocuous, as the discharge is not in direct contact with the insulation. The capability to differentiate between these types of PD enables a more rational approach when reacting to PD in case it is identified in power grid components.

Despite the fact that while measuring PD, the primary objective is usually to determine the presence of internal discharge, any or all of the previously mentioned discharge types may be present and appear in the gathered data, alongside noise. This complicates the assessment of PD measurement results and usually interpretation by an experienced specialist is required to elucidate the nature and possible source or sources of PD. As these kinds of knowledge and skills are rare, it would be beneficial for cable grid operators, who are interested in measuring PD, but cannot independently perform reliable interpretation, to have access to software-based tools which can accomplish this task based on parameters extracted from the measured PD data.

This thesis is an investigation regarding these problems related to PD. It was motivated by the prevailing trends in the field of high voltage engineering, the practical issues faced by domestic grid utilities, and the general interest of the author, oriented towards gaining a deeper insight into the issues concerning electrical insulation. The primary methodologies used in the thesis include performing laboratory experiments and analyzing the results of those tests, using computational software (e.g., MATLAB) to process data and perform supportive simulations, including field calculations using the finite element method.

The theoretical and practical novelties of the thesis are:

- Finding evidence to suggest that regular polyethylene is more resistant to the effects of PD compared to XLPE in CC insulation.
- Finding evidence to suggest that in CCs, the susceptibility to breakdown under long-term elevated electrical stress is dominated by the degree of oxidative damage to the insulation and the size of the stressed area, rather than the maximum strength of the electric field affecting it.
- Finding evidence to suggest that employing the time-delay reflectometry technique for PD detection and source location in short cables using high-frequency current transformers has the potential to provide very accurate positioning, even without the use of pulse calibrators pre-measurement under some circumstances.
- Identifying some novel parameters to describe PD activity and aid in differentiating between various types of PD sources.

The results of the studies, on which the thesis is based, have been disseminated in three conference publications and one journal publication.

Abbreviations

AC	Alternating current
ACSR	Aluminium conductor steel reinforced
CC	Covered conductor
CI	Confidence interval
CVD	Capacitive voltage divider
DSO	Digital storage oscilloscope
DWT	Discrete wavelet transform
FEM	Finite element method
FFT	Fast Fourier transform
GIS	Gas insulated switchgear
HDPE	High-density polyethylene
HFCT	High-frequency current transformer
HV	High voltage
IEC	International Electrotechnical Commission
LDPE	Low-density polyethylene
MI	Measurement impedance
MV	Medium voltage
OHL	Overhead line
PD	Partial discharge
PDEV	Partial discharge extinction voltage
PDIV	Partial discharge inception voltage
PE	Polyethylene
PILC	Paper insulated lead-coated cable
PRPD	Phase-resolved partial discharge
PVC	Polyvinyl chloride
SD	Standard deviation
TDR	Time-domain reflectometry
TO	Test object
UHF	Ultra-high frequency
UV	Ultraviolet
UWB	Ultra-wide band
XLPE	Cross-linked polyethylene

Symbols

C_c	Coupling capacitance
E_1	Electric field strength inside solid insulation
E_2	Electric field strength inside a void in solid insulation
f	Frequency
I_i	Pulse interval-to-peak value ratio of *i*-th pulse
k	No. of samples per pulse waveform
L	Length of cable
N	Total number of failure events
n	Pulse count
P_1	Waveform of 1st partial discharge pulse
$\overline{P_1}$	Sample mean of 1st pulse waveform
P_{1_i}	*i*-th discrete sample of 1st pulse waveform
P_2	Waveform of 2nd partial discharge pulse
$\overline{P_2}$	Sample mean of 2nd pulse waveform
P_{2_i}	*i*-th discrete sample of 2nd pulse waveform
p_i	Peak value of *i*-th pulse
p_{max}	Maximum peak pulse value
p_{min}	Minimum peak pulse value
r	Pearson's correlation coefficient
s_1	Mechanically measured distance of defect 1 from cable end
s_2	Mechanically measured distance of defect 2 from cable end
T	Temperature
t	Time
t_I	Time instant at which a partial discharge pulse is detected at end 1
t_{II}	Time instant at which a partial discharge pulse is detected at end 2
Δt	Time delay between a pulse and its reflection
Δt_{cal}	Time delay between original and reflected calibration pulse
t_f	Minimum discharge epoch
t_i^F	Time instant of *i*-th failure event
Δt_{ij}	Time difference between pulses *i* and *j*
t_i	Time instant at which the pulse with sequence number *i* occurs
t_l	Maximum discharge epoch
t_{PD}	Partial discharge phase span
U_e	Partial discharge extinction voltage
U_i	Partial discharge inception voltage
u_i	Instantaneous voltage value during *i*-th partial discharge
Δu_{max}	Maximum voltage difference between partial discharge pulses
Δu_{min}	Minimum voltage difference between partial discharge pulses
U_{thr}	Partial discharge pulse detection threshold voltage

V_i	Ratio of partial discharge pulse voltage difference-to-peak value
v_p	Pulse propagation velocity
w_{max}	Maximum pulse width
w_{min}	Minimum pulse width
w_{span}	Pulse width span
x	Partial discharge source distance from cable end
x_1	Partial discharge source 1 distance from cable end measured using time-domain reflectometry
x_2	Partial discharge source 2 distance from cable end measured using time-domain reflectometry
Y	Equivalent shunt admittance
y_1	Shunt admittance of inner semiconducting layer
y_2	Shunt admittance of XLPE insulation
y_3	Shunt admittance of outer semiconducting layer
Z_1	Characteristic impedance of medium 1
Z_2	Characteristic impedance of medium 2
Z_m	Measurement impedance
Z_s	Series impedance
α	Weibull scale parameter
$\tilde{\alpha}$	Estimated Weibull scale parameter
α_p	Attenuation constant
β	Weibull shape parameter
$\tilde{\beta}$	Estimated Weibull shape parameter
β_p	Phase constant
Γ_{12}	Relative reflection magnitude
γ	Propagation constant
Δ	Difference between mechanically and electrically measured PD source distances
Δ_1	Difference between mechanically and electrically measured distance of PD source 1
Δ_2	Difference between mechanically and electrically measured distance of PD source 2
ε_1	Relative dielectric permittivity of solid insulation
ε_2	Relative dielectric permittivity of gaseous void
ε_r	Relative dielectric permittivity
μ_I	Mean pulse interval-to-peak value ratio
μ_p	Mean peak pulse value
$\mu_{\Delta u}$	Mean voltage difference between pulses
μ_V	Mean partial discharge pulse voltage difference-to-peak value ratio
μ_w	Mean pulse width
μ_τ	Mean pulse interval
σ_I	Standard deviation of pulse interval-to-peak value ratios

σ_{In}	Normalized standard deviation of pulse interval-to-peak value ratios
σ_{P_1}	Standard deviation of 1st pulse waveform
σ_{P_2}	Standard deviation of 2nd pulse waveform
σ_{p}	Standard deviation of pulse peak value
σ_{pn}	Normalized standard deviation of pulse peak value
$\sigma_{\Delta u}$	Standard deviation of voltage difference between pulses
$\sigma_{\Delta un}$	Normalized standard deviation of voltage difference between pulses
σ_{V}	Standard deviation of pulse voltage difference-to-peak value ratios
σ_{Vn}	Normalized standard deviation of pulse voltage difference-to-peak value ratios
σ_{W}	Standard deviation of pulse width
σ_{τ}	Standard deviation of pulse interval
$\sigma_{\tau n}$	Normalized standard deviation of pulse interval
τ_{max}	Maximum pulse interval
τ_{min}	Minimum pulse interval

1 Durability of medium voltage covered conductor insulation materials

1.1 Background and experience with covered conductors

The issue of reliability has always been a central concept and point of concern regarding the operation of electrical grids worldwide. The merit of distribution grid utilities is often assessed based on metrics which reflect the frequency and duration of consumer supply discontinuities, such as the System Average Interruption Duration Index (SAIDI). OHLs are the major source of faults affecting the grid and substantial efforts have been made to decrease the vulnerability of these assets to adverse weather events, negative consequences of human and animal activity, and other factors with the potential to endanger normal operation. A relatively cost-effective measure to increase OHL reliability, particularly in the medium voltage (MV) range, is the adoption of CCs.

CCs are, in principle, traditional overhead line conductors, e.g., ACSR (Aluminium Conductor Steel Reinforced) with an insulating layer consisting of a polymeric compound extruded onto its exterior surface (Figure 1). Exchanging traditional bare overhead line conductors for CCs has emerged as a common practice in many parts of the world over the last few decades [1]. Experience with using CCs has indicated that it is possible to achieve a significant decrease in the frequency of supply interruptions to consumers at a reasonable overall cost level. Constructing power lines with CCs is approximately 20% more expensive initially than using bare conductors [2].

In particular, CCs are a preferable solution for grid construction in sparsely populated rural areas, where the deployment of underground cable lines would entail unreasonably large costs considering the relatively marginal gain in reliability when compared to CCs, whereas leaving the grid more vulnerable by opting for regular bare conductors would fail to meet necessary reliability metrics. Based on prior Finnish experience, the fault rates of CC lines from most causes are approximately 10% or lower compared to bare conductor lines, except for faults mediated by wildlife activity, the rate of which is reduced by approximately 60% [3].

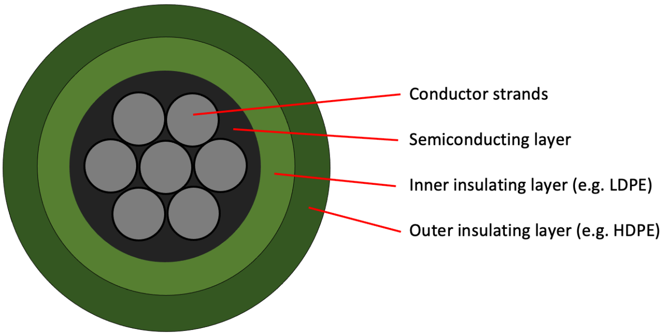
Conductor strands
Semiconducting layer
Inner insulating layer (e.g. LDPE)
Outer insulating layer (e.g. HDPE)

Figure 1. Radial cross-section of a typical medium voltage covered conductor with two layers of insulating material

Another advantage of CCs is that these enable the use of smaller clearances between conductors and hence a smaller general OHL footprint. Incidental contact between adjacent phases due to, e.g. wind, will not result in a short-circuit, and imminent earth faults following structural malfunction of the line are also avoided in most cases. A small decrease in the magnetic field strength in the proximity of the line at a level of approximately 2 m above the ground is also achieved [4].

In addition, there is a notable aspect of safety in using CCs. The insulating layer, provided that it remains intact, will prevent electrocution in the event that a person accidentally comes into contact with or deliberately handles a downed energized conductor. Testing has indicated that the combined leakage and capacitive current which will pass through a person under these circumstances might be perceptible [5] alongside the effects arising from a strong electric field. However, the amperage will remain significantly below the range of tens of milliamperes, which is generally accepted to pose a significant risk of electrically induced tetany, injury, or death due to cardio-respiratory arrest or arrhythmia in a generally healthy person. Decreases in human fatality rates related to MV OHLs have been observed in numerous countries across the world which have adopted the use of CCs [1].

1.2 Covered conductor insulation materials

The predominant materials used to produce the insulating layer of CCs are different varieties of polyethylene (PE): low-density PE (LDPE), high-density PE (HDPE) and cross-linked PE (XLPE). All of these are polymers with the general chemical formula $(CH_2 - CH_2)_n$, albeit with a slightly different molecular composition and general properties. As the eventual structure of polymers is highly dependent on the production process parameters, the material properties are also somewhat variable and the precise cut-off values determining whether a specific sample of PE is considered low-, medium-, or high-density are also slightly different depending on the source of information. However, some general qualitative metrics to distinguish between these subtypes do apply.

LDPE is a thermoplastic polymer with a density of 917 … 930 kg/m^3. A larger degree of branching occurs in its molecular structure compared to HDPE, which causes the molecules to occupy space less efficiently, resulting in a slightly lower density compared to HDPE. The side branches in the molecular structure also determine the magnitude of intermolecular forces in the material, affecting its physical properties. The density of HDPE is 944 … 965 kg/m^3 and it is also a thermoplastic polymer, however, its relative lack of side chains compared to LDPE results in stronger intermolecular forces, which contribute to its higher stiffness. It is also characterized by a higher tensile strength, a higher degree of crystallinity and lower transparency in its pure form.

Both LDPE and HDPE possess good resistance to common polar solvents, most notably water. The insulating properties of both LDPE and HDPE are also excellent, a typical value of the dissipation factor ($\tan \delta$) is 10^{-4} … 10^{-3} and the dielectric strength is approximately 20 kV/mm. The relative dielectric permittivity of both is considered to be 2.3, however this is somewhat dependent on temperature.

The notable disadvantages of both materials are relatively poor resilience to UV radiation and nonpolar solvents, also susceptibility to cracking under stress. It has been identified that the surface exposed to direct sunlight exhibits more pronounced features of degradation compared to the opposite side of the same conductor and the properties of conductors operating in a dryer, higher temperature environment deteriorate faster compared to those operating in a milder, more humid environment [6]. PE is most sensitive to UV-B radiation at wavelengths of around 300 nm [1]. This has necessitated the inclusion of pigments and fillers in the materials to augment resistance to solar radiation. The use of CCs is also contraindicated in environments subjected to a substantial pollution load as CCs are susceptible to surface tracking [6].

In contrast to LDPE and HDPE, XLPE is a thermoset polymer, i.e., it contains covalent bonds linking individual monomer chains, which form an extensive 3-D structure, and it cannot be melted and reshaped. In terms of material properties, it shares more similarities with HDPE, however, the presence of cross-links confers some notable advantages to the material. The maximum permissible temperature for continued operation is ≈65 °C for both LDPE and HDPE, whereas temperatures up to ≈90 °C are acceptable for XLPE. However, XLPE is more difficult to recycle compared to HDPE/LDPE, rendering it less lucrative from an environmental perspective. The differences in the molecular structure of these PE varieties are illustrated in Figure 2.

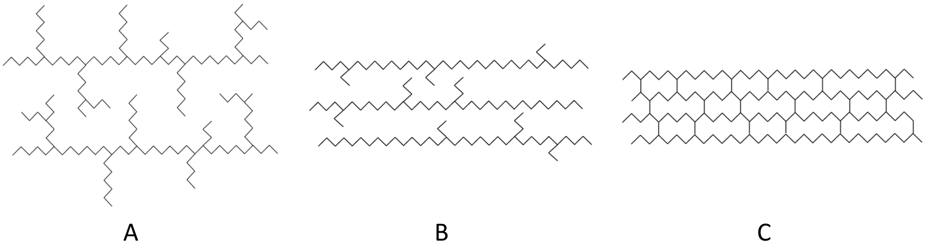

Figure 2. Macromolecular structure of different types of polyethylene: A) LDPE, B) HDPE, C) XLPE

In some CC types, the insulating cover consists of two extruded layers of different materials (e.g., HDPE and LDPE) or an even higher number in case of CC types designed for voltages beyond the MV range. These have been developed to attain improvement over the properties of conductors with a single layer of insulation. Usually, a semiconductive layer is also included as a buffer between the insulating material and conductor strands, with the primary purpose of reducing the degree of non-uniformity of the electric field inside the insulation.

One study found that the withstand level of CCs to a standard 1.2/50 µs lightning impulse voltage is approximately 50% higher in double-layer HDPE/LDPE insulation compared to single-layer XLPE and that HDPE exhibited superior abrasion resistance [7]. However, the strength of these findings is diluted somewhat by the fact that the HDPE/LDPE insulation thickness was approximately 20% greater than the thickness of the XLPE insulation. The same study also found that the mechanical, thermal, and electrical properties of XLPE can vary quite substantially between manufacturers.

Oxidation is a notable cause of CC insulation deterioration. Inadequate manufacturing conditions can promote chemical degradation, as well as normal weathering of the CC insulation. There have been instances where carbonyl moieties (C=O), which indicate oxidation, have already been detected in the unaged insulation of newly manufactured CCs [8].

1.3 Problems concerning covered conductors

Despite their numerous benefits, there are some problems which have emerged in the process of utilizing CCs in OHLs. For example, CCs are more susceptible to the breakage of conductors caused by short-circuits ("burndown") and require sophisticated overvoltage protection accessories [9]. The larger diameter and mass per unit length of CCs compared to bare conductors can also prove to be problematic due to aeolian vibration and cause problems with span geometry when retrofitted to existing power lines [10].

Field experience has also indicated that the choice of insulators is crucially important for CC insulation longevity. CCs are more compatible with polymeric insulators rather than traditionally installed porcelain insulators. In the latter case, a large difference in relative dielectric permittivity (≈6 for porcelain) results in a larger proportion of electric stress on the CC insulation, resulting in premature degradation of the insulating layer [1].

The interaction of trees and CCs is a particular point of interest, as this is the most likely source of non-transient faults affecting OHLs in forested areas of the world. The primary function of CCs is the mitigation of earth faults and short-circuits, particularly when coming into contact with vegetation. The insulating cover on the conductors would allow utilities a substantially longer period of time to survey the grid after, e.g. a storm, to locate and remove any fallen trees from their OHL infrastructure. The benefit to grid management is more efficient allocation of personnel and resources during restoration of normal grid condition as well as the possibility to introduce longer OHL inspection intervals. Failing to remove the trees fast enough causes further issues for the utility. A fallen tree can lean against the conductor with substantial force and significantly disrupt the OHL's normal catenarian span geometry and bring the conductor unacceptably close to ground level, or even cause catastrophic failure of line components. During windy weather conditions, trees can cause wear on the insulating layer due to mechanical friction. These problems are exemplified by the fact that in some forested areas, deployment of CCs has paradoxically resulted in a decline in grid reliability [11].

Another issue with fallen trees is the increased electric stress in and around the insulation near the contact area between the tree and conductor. Over time, the insulation in that location will degrade at an accelerated rate, puncture, and potentially cause an earth fault. For more efficient asset management, it is necessary to determine the approximate duration conductors can withstand concentrated electric stress due to fallen trees or other objects. To study this problem, it is necessary to examine in detail how the shape of the object in contact with the conductor affects the insulation durability. Naturally, the other aspect of this problem is the actual detection of contact between CCs and vegetation or other grounded objects. Efforts have been made to develop tools to achieve this goal, based on the measurement of PDs, which occur as a result of trees leaning on OHL CCs [12, 13].

In case of trees having fallen on the conductor, the concentration of electric field is dependent on the shape of the limb or trunk which is in contact with the conductor. Although wood is generally a poor conductor of electricity in comparison to most metals, its resistivity is still several magnitudes smaller than the resistivity of the insulating layer materials [14, 15]. As a result, the electric field concentration is significant in the insulation and surrounding air. It can be reasoned that in case of a smaller branch, the electric field is stronger due to its smaller radius, resulting in a higher electric field intensity on the surface of the branch and in the air directly near the point of contact. This should cause the puncturing of insulation after a shorter period of time in comparison to contact with a branch of a larger diameter. Alternatively, a larger tree or branch will have a more substantial mechanical impact on the conductor. It has also been determined that the presence of branches slightly dampen the maximum force the conductor is subjected to during the process of a tree falling onto the OHL, compared to a situation where only the trunk of the tree makes contact with the conductor [16].

Generally, it is expected that the insulation should endure at least two weeks of contact with a tree branch [17] and prior testing has indicated that puncture may not occur even until months of electric stress [16]. The deterioration of insulation should increase over the duration of contact and be visually observable through changes in the appearance of the conductor insulation. Previous tests employing PD measurements have indicated an increase in PD activity after prolonged contact with a grounded conductive object [18]. It has also been reasoned that if a tree makes contact with a CC, there can be many parts of the same tree leaning on the conductor at various locations and the different parts of a tree are not necessarily equipotential due to the considerable resistance of wood, which is also dependent on the temperature, and therefore, the time of year [19]. This also results in variable resistance to ground, particularly in areas which are far from the Earth’s equator, e.g., several countries in temperate climate zones, where CCs have been adopted.

Several factors affect the timespan before insulation breakdown of the CC occurs. These include the quality and thickness of the insulating material, operating voltage of the power line, species and age of the tree in contact with the conductor, contact force and abrasivity of the tree bark, as well as the resistance to ground, which affects the magnitude of leakage current. Previous research performed on covered PAS type conductors in Finland has also indicated that small holes may appear in the insulation when the line is energized, creating potential weak spots in the insulation [17]. The cause of this pitting was not specified. A tree making contact with this type of weak spot could cause insulation failure over a very short duration of time.

For utilities employing CCs it is beneficial to determine which insulating materials perform best and are most durable in use. An experiment was performed in the high voltage laboratory to investigate the resiliency of CCs exposed to elevated levels of electric stress. This involved testing 10 different types of CCs from various manufacturers. The aim of the experiment was to determine the duration CCs could withstand continuous AC voltage stress and to ascertain whether the types of polyethylene (PE, LDPE/HDPE and XLPE) used for the insulation have any significant differences in performance, i.e., if any material could be conclusively considered superior to the others for field operation purposes. A supplementary research objective was to verify if the results are concordant with the findings of preceding studies, which have concluded that a combined insulating layer consisting of HDPE and LDPE tends to perform better than a single-layer XLPE coating [7]. In this prior study, the XLPE conductors were at a disadvantage due to their inferior insulating layer thickness.

1.4 Insulation lifetime modelling

The lifetime of insulation under electrical stress can be approximated using a two-parameter Weibull distribution, which has been implemented extensively in failure analysis [20]. The two-parameter Weibull distribution density function in terms of time is presented in (1) and the cumulative distribution function is presented in (2).

$$f(t,\alpha,\beta) = \frac{\beta}{\alpha}\left(\frac{t}{\alpha}\right)^{\beta-1} e^{-\left(\frac{t}{\alpha}\right)^{\beta}} \tag{1}$$

$$F(t,\alpha,\beta) = \begin{cases} 1 - e^{-\left(\frac{t}{\alpha}\right)^{\beta}}, & t \geq 0 \\ 0, & t < 0 \end{cases} \tag{2}$$

Where: t – time;
α – scale parameter ($\alpha > 0$);
β – shape parameter ($\beta > 0$).

The scale parameter value is equal to the time at which the cumulative distribution function attains a value of 63.2% (i.e., $1 - e^{-1}$). The shape parameter values can be varied and are useful for interpreting the nature of the failure mechanism. The Weibull distribution can also attain the characteristics of some other well-known distributions, e.g., if β = 1, it becomes an exponential distribution, if β = 2, a Rayleigh distribution, if β ≈ 3…4, it exhibits a large degree of similarity to the normal distribution.

The Weibull distribution parameters can be estimated from experimental data using a variety of methods, an effective one is maximum likelihood estimation. In case of the two-parameter Weibull distribution, the shape parameter and the scale parameter can be estimated using the following equations:

$$\frac{1}{\tilde{\beta}} = -\frac{1}{N}\sum_{i=1}^{N} \ln t_i^F + \sum_{i=1}^{N} \frac{(t_i^F)^{\tilde{\beta}} \ln t_i^F}{\sum_{i=1}^{N}(t_i^F)^{\tilde{\beta}}} \tag{3}$$

$$\tilde{\alpha} = \left[\frac{1}{N}\left(\sum_{i=1}^{N}(t_i^F)^{\tilde{\beta}}\right)\right]^{\frac{1}{\tilde{\beta}}} \tag{4}$$

Where: N – total number of failure events;
t_i^F – individual observed failure times;
$\tilde{\beta}$ – estimated Weibull shape parameter;
$\tilde{\alpha}$ – estimated Weibull scale parameter.

As $\tilde{\beta}$ cannot be explicitly expressed from (3), it has to be determined iteratively. After obtaining a satisfactory value, $\tilde{\alpha}$ can be calculated directly from (4).

The life expectancy of insulation is naturally affected by other factors besides the degree of electrical stress, most notably temperature, humidity, radiation, contaminants etc. Various models are used to estimate service life under these variable circumstances. In the tests reported in this thesis, the other environmental conditions were maintained as constant as practicable over the duration of the tests to specifically isolate the effect of voltage stress on breakdown probability over time.

1.5 Insulation durability testing of different insulating materials

For the purposes of comparing the performance of different CC insulating materials, 10 different conductor types from various manufacturers were studied [I]. The tested conductors featured variable insulation materials and similar conductor cross-sections from 50 to 99 mm^2. The rated voltage of all examined conductors was 20 kV. Although the insulation thickness for all conductors was 2.3 mm as specified in [21], some deviations were observed when samples of the studied conductors were examined under microscope. The minimum insulating layer thicknesses ranged from 2.06 mm to 2.58 mm and a degree of eccentricity was present. The main parameters of the tested CC insulation are presented in Table 1.

Table 1. Insulation composition and presence of semiconducting layer on the studied conductors

Conductor No.	Insulating material (inner layer/outer layer in case of two layers)	Semiconducting layer
1	PE	Yes
2	XLPE	Yes
3	PE	Yes
4	LDPE/HDPE	Yes
5	XLPE	Yes
6	XLPE	Yes
7	XLPE/PE	Yes
8	LDPE/HDPE	Yes
9	LDPE/HDPE	Yes
10	XLPE	No

In order to simulate the voltage stress that affects the CC insulation when in contact with a grounded conducting object, a test setup was constructed in accordance with the requirements of standard [21] (Annex B: Measurement of the leakage current). In principle, this is a 10 cm long winding applied to the surface of the conductor, consisting of a bare copper wire with a diameter of 2 mm (Figure 3). The standard prescribes this setup for leakage current measurement. However, in this case, it was chosen as a suitable configuration for voltage withstand testing purposes and has a precedent for being used as such [2]. While conforming to most provisions of the standard, the requirement of immersing the tested conductors in water over a 24-hour period prior to testing was disregarded and the conductors were effectively dry throughout the duration of the experiment.

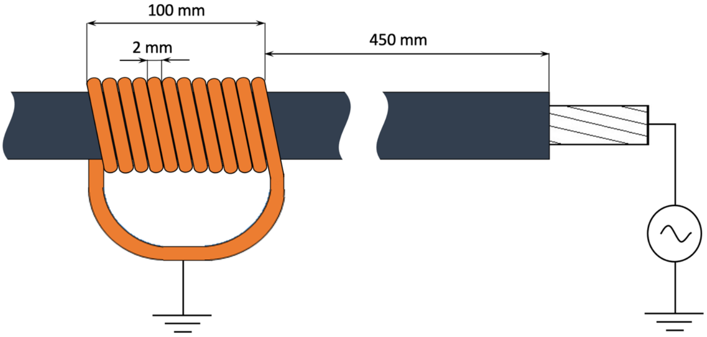

Figure 3. Principle schematic illustrating grounded copper wire winding placement on covered conductor surface during voltage stress tests

For comparison, a total of 3 windings were applied to each tested conductor. The distance between adjacent windings and the edges of the CC insulating cover was chosen to be approximately 45 cm, which would reduce the mutual effect of windings on the electric field shape to a practically acceptable minimum. This amounted to a total of 30 grounding points applied to the 10 tested conductors. The CCs were fitted with cable lugs at the ends of the exposed conductors and suspended horizontally with the application and suitable tensioning of insulating ropes. These were installed at either end of the CC segments and fastened to brackets installed onto opposing walls of the laboratory.

The general setup for one CC is illustrated in Figure 4. In practice, it was not possible to ensure a perfectly uniform construction of the windings. The outermost turns of the windings tended to diverge slightly, as can be observed in Figure 5.

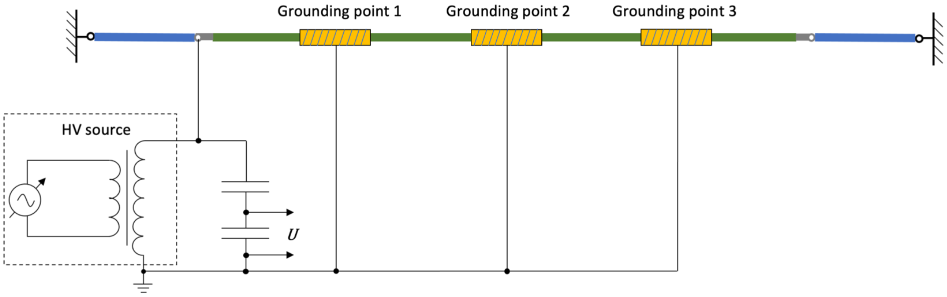

Figure 4. Principle schematic depicting the general arrangement and connections of the test setup for covered conductor insulation durability testing

The conductors were energized to the voltage level specified in [21], equal to 0.7 times the conductor rated phase-to-phase voltage. This resulted in a test voltage of 14 kV, which approximately corresponds to the maximum permissible phase-to-ground voltage level (24/√3 kV) in a 20 kV grid under normal circumstances. The test voltage was applied using a HV test transformer supplied by a programmable AC power source, which outputs a practically pure sine wave. The test voltage was free of visually noticeable distortions and higher harmonic frequencies, which are usually present, to a variable degree, in the voltage waveform of mains power supply. The test voltage was continuously applied to the conductors until a breakdown occurred in one of the grounding points, precipitating a short-circuit and tripping the power supply's overcurrent protection. The voltage applied to the conductors was measured using a capacitive voltage divider (CVD).

The objective of the test was to determine the accumulative time under voltage before the insulation punctured. Previous tests have indicated that testing at a higher voltage level, which corresponds to the highest permissible continuous phase-phase voltage (24 kV), can result in puncture of the conductor insulation within 5 minutes of voltage application, with a higher probability of breakdown in case the conductor has already aged in service. Previously unused conductors, which have not been subjected to stresses related to grid operation, have exhibited higher durability [2]. Considering these results from previous research, it was estimated that the insulation of the tested conductors would puncture over a time frame of some hours or days of consistent application of voltage.

The resulting electric field, which concentrates around the grounded winding, affects the insulating layer by initiating rapid degradation. The strong electric field causes breakdown and decomposition of air surrounding the insulation, resulting in PD activity. This is accompanied by the creation of highly corrosive substances generated from the constituents of air interacting with free charge carriers liberated and accelerated as a consequence of the PDs and electric field. Chemical byproducts of PD activity include, most notably, ozone and other reactive oxygen species (O_3, O_2^-, O, OH^-, H_2O_2), nitrogen oxides (NO_x), and nitric acid (HNO_3). After a period of a few days, the effect of the oxidative attack becomes apparent on the insulating layer, causing noticeable discoloration near the edges of and under the grounded copper winding. Air decomposition products also oxidize the copper wire, and after a few weeks, the copper starts to develop a grayish coating, which can be observed primarily near the outermost turns of the winding (Figure 5).

The PDs occurring during the test are clearly audible and can also be observed visually when the test laboratory is darkened. Even under these circumstances, the PDs are faintly discernible after a period of approximately one minute of visual acclimatization to the low-light conditions. Figure 5 also depicts a photographic image of the PD at the location of the winding, acquired in the dark using a 30 second shutter delay. It appears that the surface discharges exhibit the highest intensity at the edges of the winding, although test results eventually indicated that the overwhelming majority of locations where puncture occurred were situated somewhere under the midsection of the winding, not at the edges of it.

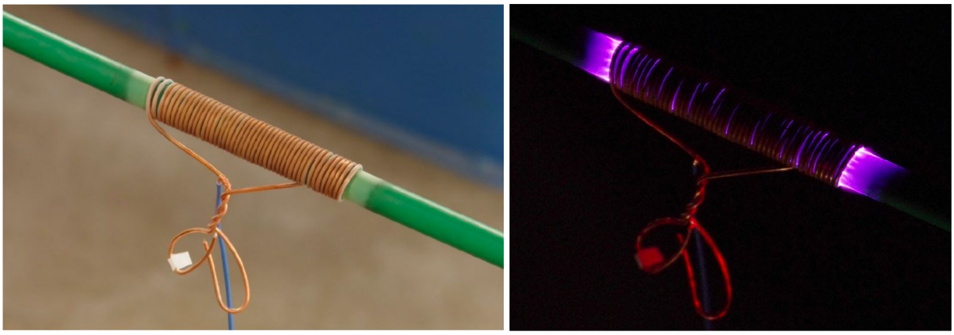

Figure 5. Photograph of grounded copper wire winding around covered conductor (left). The discoloration of insulation caused by prolonged surface discharges at the edges of the winding is evident. Photograph of winding acquired in a darkened room using a 30 second shutter delay (right) reveals notable surface discharge activity.

1.6 Computer simulation of electric field at the grounding points

Initially it was assumed that the electric field is strongest at the outermost turns of the winding due to the edge effect. Computer simulation using the finite element method (FEM), presented in Figure 6, indicates that the electric field in the surface layers of the insulation is indeed strongest under the outermost turn of the winding and starts to successively decrease and increase in the direction towards the center of the winding. In the inner layer of the insulation close to the conductor, the electric field strength increases to its highest value 2…3 turns from the ends of the winding and essentially remains constant (Figure 7). In the field simulation, the relative permittivity of the insulation and air were chosen as 2.3 and 1, respectively. The results of modelling the electric field around the grounded winding indicate that the electric field strength is sufficiently high in the air surrounding the winding to initialize breakdown and PDs (exceeding 3 kV/mm). The experimentally observed discharge activity is therefore consistent with the results of the field simulation.

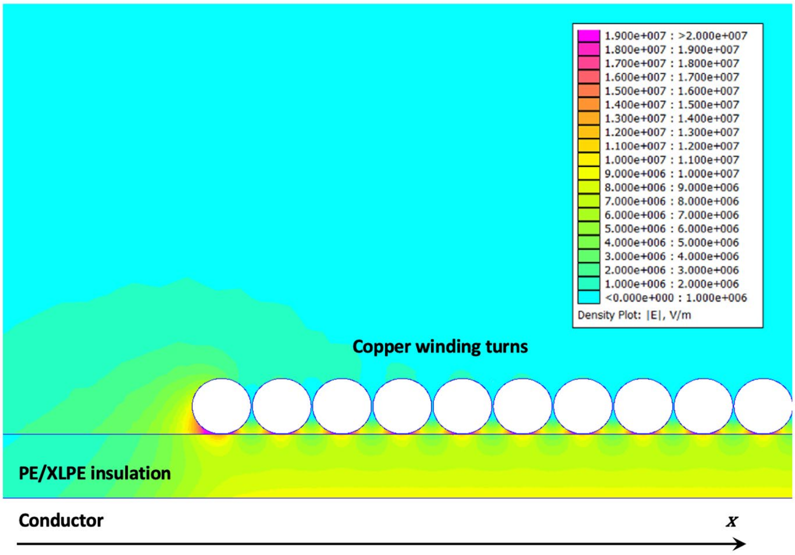
1.900e+007 : >2.000e+007
1.800e+007 : 1.900e+007
1.700e+007 : 1.800e+007
1.600e+007 : 1.700e+007
1.500e+007 : 1.600e+007
1.400e+007 : 1.500e+007
1.300e+007 : 1.400e+007
1.200e+007 : 1.300e+007
1.100e+007 : 1.200e+007
1.000e+007 : 1.100e+007
9.000e+006 : 1.000e+007
8.000e+006 : 9.000e+006
7.000e+006 : 8.000e+006
6.000e+006 : 7.000e+006
5.000e+006 : 6.000e+006
4.000e+006 : 5.000e+006
3.000e+006 : 4.000e+006
2.000e+006 : 3.000e+006
1.000e+006 : 2.000e+006
<0.000e+000 : 1.000e+006
Density Plot: |E|, V/m
Copper winding turns
PE/XLPE insulation
Conductor
x

Figure 6. FEM simulation of electric field strength in covered conductor insulation and surrounding air at test voltage instantaneous peak value 19.8 kV (cross-section along the longitudinal axis of the conductor). The x-axis is provided in reference to the values presented in Figure 7.

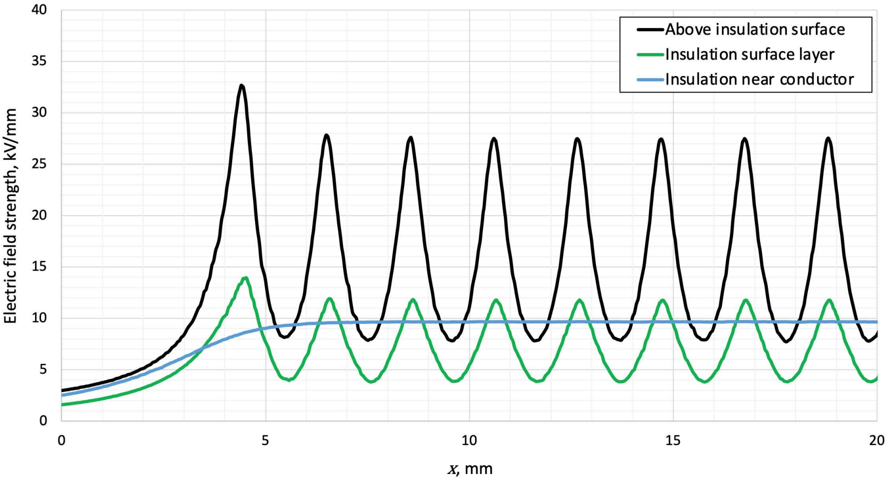

Figure 7. Modelled electric field strength at different depths in the insulation and air across the grounded copper wire winding at test voltage instantaneous peak value (19.8 kV).

1.7 Results of insulation material comparison experiment

The general results of the voltage durability test are provided in Figure 8. It is notable how variable the puncture times are for the same type of conductor for some of the test samples. For example, the minimum puncture time from test initiation for conductor No. 9 is 2.1 days and the maximum time is 48.6 days. The remaining third location punctured at 48 days, so the mean durability is 32 days. However, the ratio of maximum to minimum puncture times is approximately 24, making this a highly durable conductor in comparison to the other CCs when considering the average or maximum puncture times, but a very nondurable conductor when considering the minimum puncture time. Similar, yet smaller discrepancies between minimum and maximum puncture times were recorded for conductors 6, 7, 8 and 10. For conductors 1, 2, 3, 4 and 5, the relative difference in withstand durations for grounding points is significantly smaller.

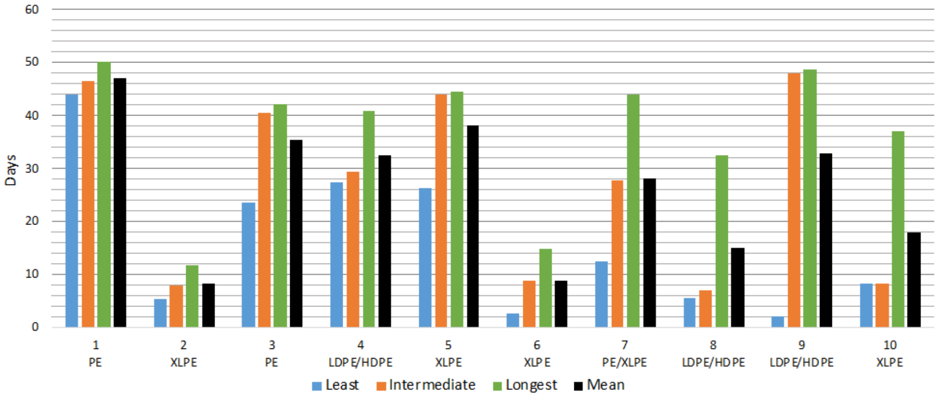

Figure 8. Electric durability test results for different covered conductors. The columns represent the three puncture times of grounding points ranked from shortest to longest and the mean.

While some variation in withstand times is anticipated, a high degree of scattering in the test results was unexpected and may indicate inconsistencies in insulation quality along the conductor length. The existence of weak spots is possibly a side effect of inadequate manufacturing quality. The large variability in breakdown times cannot be attributed to the type of material used, because in case of both XLPE and PE insulated conductors there were occurrences of large and small variance in breakdown times. The variability of workmanship during application of individual copper wire windings might also have some influence on the test results.

Another peculiar outcome is that although the electric field across the insulating layer should be the strongest at the outermost turn of the winding, only one tested grounding point out of 30 punctured at the edge of the winding. A possible reason is, that due to PDs occurring under the copper winding, air becomes ionized and partially conductive, reducing the degree of non-uniformity of the electric field in the exterior part of the insulation. The FEM simulation does not account for the effect PD exerts on electric field shape. As soon as space charges appear in the electrically stressed area near the winding, the shape of the electric field is deformed compared to that produced by means of computational tools, as the modulus and direction of the electric field vector in any location is the result of electric fields generated by different charge carriers being superimposed on each other. The actual electric field in the insulation may therefore be considerably less variable than presented in Figure 7, if the effect of partial breakdown of air is also accounted for.

If the mean durability is stratified by different insulation materials, the time until puncture amounted to:

- 32.5 days for PE insulated conductors
- 18.3 days for XLPE insulated conductors
- 28.0 days for the PE/XLPE insulated conductor

As these conductors, while consisting of the same types of materials, originate from different suppliers, drawing firm conclusions from this comparison is not possible. The high variability in withstand times indicates that there are other relevant factors besides the insulation material itself, which influence the performance of CCs under continuous AC voltage stress. Also, the number of test points used in this study is rather small, a larger number of grounding points per conductor would have enabled more reliable conclusions and estimation of the variability of puncture times. It is also notable that conductor No. 10, which lacked a semiconductive layer under the XLPE insulation, actually performed relatively well compared to other XLPE insulated conductors.

If the performance of single- and multi-layer conductors is contrasted, the mean puncture times are:

- 41.2 days for single-layer PE conductors
- 26.8 days for multi-layer PE conductors
- 27.1 days for multi-layer conductors, including the PE/XLPE insulated conductor

Drawing a highly reliable conclusion from this comparison is also not possible, although it does appear that the single-layer PE insulated conductors performed better. This points toward the possibility that the extrusion of multiple layers of insulation, through some mechanism, renders it less durable or that the combination of different PE varieties does not perform as well as a single layer under electrical stress. Both conjectures appear plausible, however, further testing will need to be conducted to assess their validity. A possible explanation as to why XLPE seems to perform worse than regular PE relates to the cross-linking process it is subjected to during manufacture. Chemical cross-linking with peroxides produces water as a by-product and this escapes from the insulation, creating small pores, which are detectable in aged insulation [8]. It is also plausible that the presence of residues from additives required for cross-linking adversely affect the insulation durability.

The results of these experiments tend to support the conclusion that PE is a superior material for employing in MV CCs, in case durability under a concentrated electric field is the primary concern. The voltage withstand time for XLPE insulated conductors was 56% of the withstand time for PE insulated conductors on average, and the conductor with a combined XLPE/PE insulation reached 86% of the average withstand time of PE insulation. To further support the results of this study, analogous tests could be conducted with a larger number of test samples. Varying the shape of the grounding electrode could also provide interesting results, as the dimensions can be altered to resemble parts of actual trees more accurately and using various electrode geometries could aid in elucidating subtle nuances which impact the gradual processes eventually culminating in the breakdown of CC insulation. These questions are addressed in the experiment described in the following section.

2 The effect of electrode shape on insulation durability

2.1 Test setup and parameters

A test was devised to investigate the effect of electrode shape on the durability of CC insulation under electrical stress [II]. The test setup included grounded conductors in contact with the XLPE insulation of a typical MV CC used in distribution grid construction. In the experiment, five sections of a covered MV conductor, each laden with a specific electrode type, were energized to a voltage of 14 kV. The conductor parameters were:

- Cover: XLPE insulated with semiconducting layer
- Conductor cross-section: 70 mm^2
- Conductor diameter: 9.7 mm
- Overall diameter: 14.9 mm
- Insulation thickness: 2.3 mm
- Semiconductive layer minimum thickness: 0.3 mm
- Rated voltage (phase-to-phase): 20 kV

Each section of the conductor included 10 locations where a grounded electrode of a specific shape was placed into direct contact with the insulating layer. The shape of the grounded conductor was different in each of the five sections, amounting to a total of 50 grounding points. The distance between grounding points, or the minimal distance between parts of adjacent grounding electrodes was 45 cm. This limit was implemented to minimize the mutual effect of ground electrodes on the electric field at each grounding point. The general setup of the test was analogous to that of the durability test comparing different insulation materials described in the previous section.

Three of the five conductors were round (metal pipes or wire) and intended to simulate tree branches of different sizes through their varying radii of curvature. The diameter of the round conductors was chosen such that it differs by a factor of five across the different electrodes: 125 mm, 25 mm, and 5 mm. The round shape would result in an electric field similar to what a tree branch in contact with a CC would produce.

The surface of the round electrodes was polished prior to applying these to the CC insulation, with the intent to minimize the effects of field concentrations surrounding miniature protrusions on the electrode. The round conductors were secured to the CC by applying zip ties. Minimal fastening strength was used upon application of zip ties as the purpose of using these was to mitigate possible displacement of the electrode relative to the CC over the duration of the test. This was necessary to prevent accidentally shifting the area of insulation affected by the electric field concentration. Excessive tightening of the zip ties would also have resulted in increased mechanical stress and slight deformation of the insulation at the point of contact. Without a possibility to accurately determine the contact pressure, minimal application of force was opted for.

The fourth type of grounding conductor was an aluminium adhesive tape wound tightly around the conductor. The width of the tape was 100 mm. It is assumed this type of grounding point would produce a strong electric field around the edges of the tape, contributing to a rapid degradation of insulation in that area. It shares some similarities with the winding-type electrode, although it is expected to produce a more uniform and relatively strong electric field in the insulation directly under the tape. Discharges would mostly occur only near the edges of the electrode.

The fifth type of conductor was a copper wire, 2 mm in diameter, wound densely around the CC, with a total coil length of 10 cm. This electrode shape is the same used in the durability test discussed in the previous section (Figure 3). Depictions of the grounding points with different electrode types are presented in Figure 9.

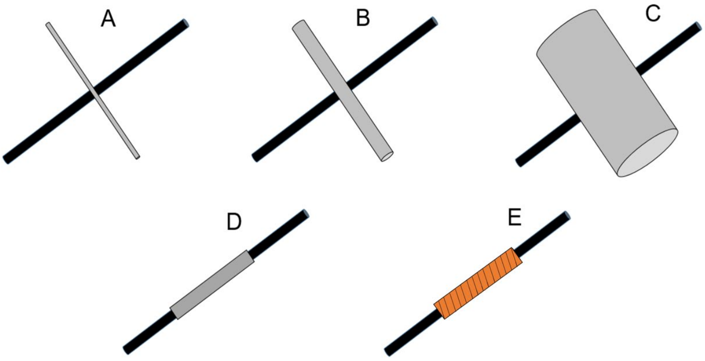

Figure 9. Principle schematic of grounding electrode types used in the study of covered conductor durability. A – 5 mm round wire, B – 25 mm round pipe; C – 125 mm round pipe; D – aluminium tape; E – copper wire winding.

After insulation failure, the punctured grounding point was manually disconnected from ground (in case of the winding and Al tape electrode types) or completely removed from the test assembly (in case of the round electrodes). The conductors were re-energized, and the test resumed until the next puncture occurred. The performance of the grounding points was quantified based on the cumulative amount of time the CC remained energized prior to the insulation breakdown at any specific grounding point.

2.2 Test results

The amount of time the various types of grounding points withstood the applied voltage stress differed significantly. The test was eventually discontinued due to practical considerations, because some grounding points withstood in excess of 7 months of accumulated electric stress, which was more than originally anticipated. Over the test period, breakdown occurred in all of the 10 grounding points in case of three of the five different types of grounding electrodes used. Some grounding points with the aluminium tape and 5 mm round conductor did not suffer breakdown over the duration of the experiment and the estimates for breakdown time regarding these two electrode types are therefore not directly comparable to the other three electrode types, which produced puncture at all the grounding points.

The test results are presented in Figure 10. Based on the results, the sequence of insulation durability for different grounding electrodes can be inferred and the ranking based on breakdown time characteristics is presented in Table 2. It should be noted that the first breakdown of a winding-type electrode grounding point occurred after only a very brief period of electric stress application, approximately 12 hours. Other grounding points of the same type punctured following 13 to 31 days of electric stress, which suggests the insulation at the first punctured location was abnormally fragile. However, this outlying result does not impart a significant impact on the main conclusions regarding the experiment.

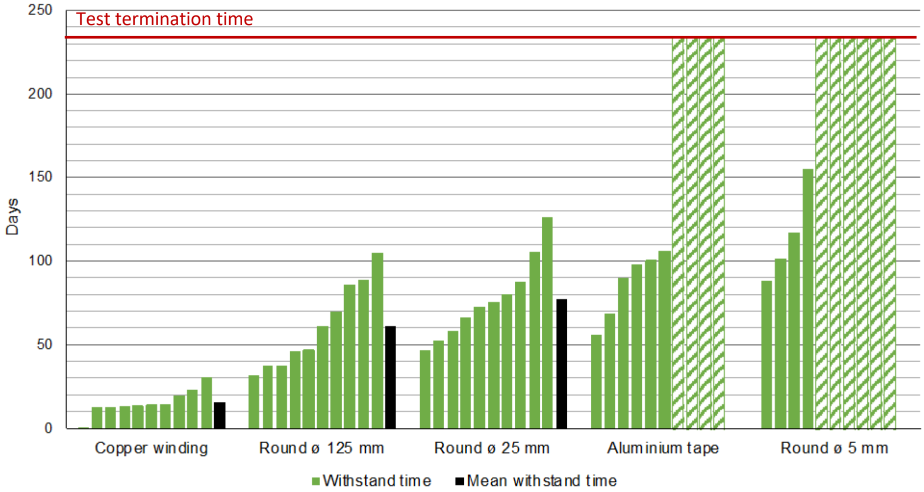

Figure 10. Withstand times of individual grounding points and overall mean withstand times of electrode types in sequence of increasing durability. Mean withstand time is not provided for electrode types regarding which some grounding locations did not puncture over the duration of the test.

Based on some rudimentary parameters, the ranking of the insulation durability for different ground electrodes is equivalent regardless of the breakdown time characteristic it is based on. The minimum, maximum and mean breakdown times all increase in the following sequence: copper winding, 125 mm round and 25 mm round electrode. Although some of the grounding points of the Al tape and 5 mm round conductors did not puncture over the duration of the test, it can be deduced with some degree of certainty that the latter ranks higher due to the following considerations:

- The minimum puncture time for the 5 mm round electrode is higher than that of the Al tape electrode;
- The mean withstand time based only on the grounding points that punctured over the duration of the test is higher for the 5 mm round electrode;
- The number of grounding points that punctured is lower in case of the 5 mm round electrode compared to the Al tape electrode.

Table 2. Tentative ranking of different grounding electrodes based on expected covered conductor insulation puncture time characteristics (in order of decreasing expected puncture time)

Insulation durability rank	**Grounding electrode type**	**Puncture time characteristic (days)**		
		Min	**Max**	**Mean**
I	Round ø 5 mm	88	*N/A*	*N/A*
II	Aluminium tape	56	*N/A*	*N/A*
III	Round ø 25 mm	47	106	77
IV	Round ø 125 mm	32	89	61
V	Copper winding	0.5	23	16

The test results in general indicated a notable variation in the amount of time until breakdown in some of the different grounding points of the same type. This might imply that there is significant variation of the insulation layer quality over the length of the conductor with several weak spots present. There was one major outlier among all the tested grounding points, the one winding-type point, which punctured first.

The results also indicated that the mean time until breakdown was shorter for the round grounding conductors with a larger diameter. This observation contradicts the conjecture that a smaller diameter of the grounding conductor would cause a breakdown faster due to higher electric field strength. This can be explained by the fact that a larger diameter would result in a wider area of elevated electric stress in the insulation and therefore a higher probability for the inclusion of weak spots in the stressed area of the insulation. Also, in a few cases the breakdown occurred some millimeters away from the point of contact between the CC insulation and round electrode, which further supports the notion that a weak spot, if it is located at an area which is subjected to elevated electric stress, will manifest as the site of the eventual puncture.

The mean time until breakdown was smallest in case of the copper winding grounding points. The stress on insulation in this instance was elevated due to high discharge activity in the air between the copper windings and insulation surface. As discussed previously, this generated highly reactive oxidizing gases in significant amounts, which contributed to the rapid degradation of the insulating layer. The highly stressed area was also significantly larger compared to the round electrodes due to the field concentration at each turn, the width of the winding, and the fact that the entire circumference of the CC was equally affected, whereas in case of the round electrode, the stressed region was confined to a substantially smaller area centred at the point of contact. Furthermore, only two of the punctures occurred at the outermost turns of the copper winding, the remaining eight occurred under the inner turns, where the electric field was not as strong according to FEM simulations (Figure 13, Figure 14, Figure 15).

The performance of the Al tape grounding points exhibited unexpected characteristics as well. The time until breakdown was rather long on average, despite the highest electric stress based on electric field simulations (Figure 14), and all the punctures occurred at the edge of the electrode. In addition, the area of increased electric stress was continuous along the surface of the conductor, so weak spots should have caused breakdown in the insulation under the aluminium tape considerably faster. This, contrary to observations made in conjunction with other grounding points, implies the absence of weak spots in the insulating layer. Apparently, because the insulation located under the tape was not exposed to air, this inhibited the progression towards a complete breakdown of insulation to a degree that it was not observed over the duration of the experiment. These observations suggest that the dominant feature of contact with a grounded object, which rapidly degrades CC insulation, is not the electric field strength *per se*, but rather the chemical degradation due to oxidative damage. The failure rate of grounding points appears to correlate positively with the surface area of the insulation affected by PD.

2.3 Failure probability functions of different electrodes

The failure times for all of the tested electrode types are presented in Figure 11 in the form of a Kaplan-Meier plot for more convenient comparison. This graph illustrates the difference in failure events over time, as there is almost no overlap between the curves corresponding to different electrodes in the intermediate section of the graph. The only exception to this general trend is the intersection of traces representing 125 mm and 25 mm electrodes around the 80…90-day mark. The other noteworthy features are the steep failure rate of copper winding electrodes around the 15-day mark and the high failure rate of CCs treated with Al tape at the 90…110-day mark, followed by a complete cessation of puncturing until the test was terminated after 234 days of accumulated electric stress. Similarly to the Al tape electrode, the 5 mm round electrodes failed to precipitate any additional punctures beyond day 155 of the experiment.

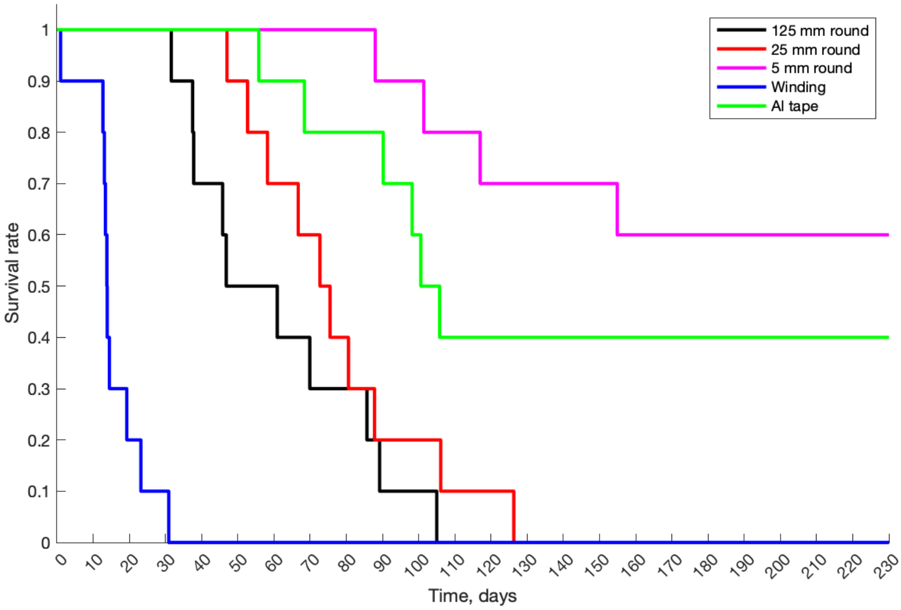

Figure 11. Kaplan-Meier plot for the survival rate of all tested electrode configurations during withstand testing of the XLPE-insulated conductor

The Weibull distribution curves for the electrode types which produced a puncture at all the tested grounding points are presented in Figure 12 alongside dot markers which correspond to individual puncture events. The distribution parameter estimator values, based on which these curves are plotted, are presented in Table 3. It is evident that there is no substantial difference between the failure dynamic of the 125 mm and 25 mm round electrodes, whereas the failure rate of the copper winding electrode was significantly higher than that of any of the other electrodes. As several of the Al tape and 5 mm round electrodes did not produce insulation puncture, the Weibull distribution curves are not plotted for those types. A heavily right-censored dataset is a source of substantial uncertainty.

Table 3. Estimated Weibull distribution parameters of the three electrode types which produced failures at all grounding locations, with 95% confidence intervals

Parameter estimate	Round ø 125 mm	Round ø 25 mm	Copper winding
$\tilde{\alpha}$ (95% CI)	68.9 (54.5 … 87.4)	86.0 (71.3 … 103.5)	17.0 (12.0 … 24.1)
$\tilde{\beta}$ (95% CI)	2.77 (1.71 … 4.49)	3.53 (2.23 … 5.60)	1.84 (1.09 … 3.10)

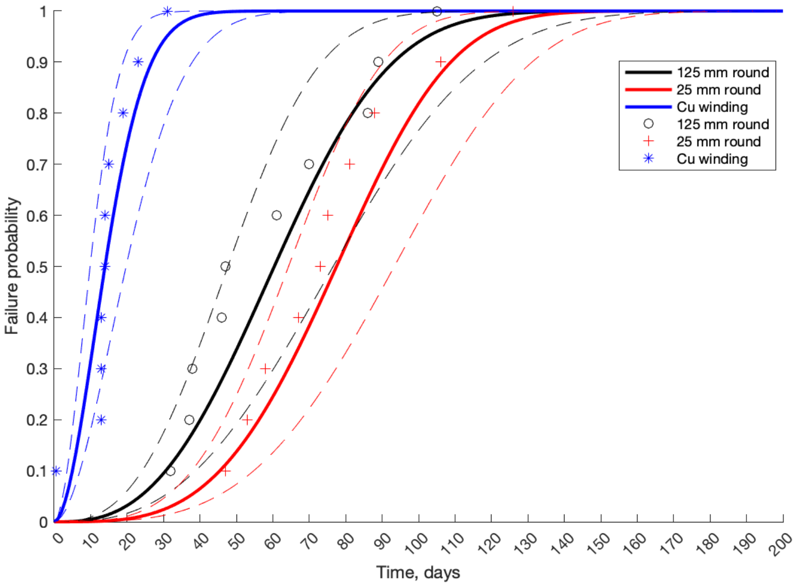

Figure 12. Estimated two-parameter Weibull cumulative distribution functions describing the failure rates of the 125 mm round conductor, 25 mm round conductor and copper wire winding electrodes. Dashed lines represent cumulative distribution function curves corresponding to 95% confidence interval boundaries for scale parameter $\tilde{\alpha}$.

2.4 Statistical significance of test results

The difference in survival across electrodes was evaluated using a series of log-rank tests. The statistical tests were performed primarily to assess the potential difference in performance between electrodes with a similar survival curve (Figure 11) and the results are presented in Table 4. Although the range of electrode types included in the experiment permit C_5^2 = 10 different pairs of comparisons, studying all of these combinations is not necessary. If a statistically significant difference between closely matched electrodes was detected, further statistical tests to evaluate the durability discrepancy between electrodes with a more substantial difference in performance were omitted. For example, because the difference in survival between the copper wire electrode and the 125 mm round electrode was found to be highly statistically significant ($p < 0.001$) and their traces on Figure 11 are adjacent, comparing the performance between the copper wire and 5 mm round electrode or, in fact, any of the other electrode types, becomes redundant due to the obvious statistical significance.

The notable outcomes of the statistical analysis are:

- The difference in survival between the 125 mm and 25 mm round electrodes was not statistically significant ($p = 0.22$)
- The difference in survival between the 25 mm and 5 mm round electrodes was highly statistically significant ($p < 0.001$), which, by extension, implies that the difference between 125 mm and 5 mm electrodes also reaches statistical significance

- The difference in survival between the 5 mm round and aluminium tape electrodes was not statistically significant ($p = 0.28$)
- The durability of the copper wire electrode was significantly lower than in case of any other electrode ($p < 0.001$)

Table 4. Results of log-rank tests to evaluate the difference in durability between different electrode types

Electrodes under comparison		χ^2	p**-value**
Copper winding	Round ø 125 mm	15.1	<0.001
Round ø 125 mm	Round ø 25 mm	1.48	0.22
Round ø 25 mm	Round ø 5 mm	13.2	<0.001
Aluminium tape	Round ø 25 mm	5.35	<0.05
Aluminium tape	Round ø 5 mm	1.16	0.28

It follows that any other comparison between electrode types not previously discussed also reached statistical significance. It can be assumed that if the tests were replicated with a suitably high number of samples and continued for a longer duration, a statistically significant difference would also be detected for both the 125 mm *vs* 25 mm and aluminium tape *vs* 5 mm round electrode cases. The conducted experiment was underpowered to confirm a difference between the larger round electrodes and it also did not reach an adequate duration to ascertain the difference in survival between the aluminium tape and 5 mm round electrode types. This resulted in a high degree of right-censoring in the datasets concerning these two electrodes with the additional consequence of a high p-value obtained in the corresponding statistical test.

2.5 Electric field simulations

In order to investigate the electric field at the grounding locations, a number of FEM simulations were performed. The field strength at test voltage amplitude value (19.8 kV) is presented for the Al tape electrode, copper winding electrode and 5 mm round electrode in Figure 13. The field for only the outermost turns of the winding-type electrode is presented, because it is known from preceding simulations that the field strength is highest at the edges of the winding and exhibits a regular undulating pattern in the midsection of the winding.

For ease of comparison of the electric fields generated using different electrodes, the field strength directly above the insulation across the grounding electrodes is presented in Figure 14 and Figure 15. The location of the highest electric stress is chosen as the origin of the axis representing distance across the surface of the insulation, parallel to the axis of the CC. In Figure 14, a zoomed-in view of the field strength in the area of highest simulated field strength is provided, whereas a wider perspective of the electric field strength is presented in Figure 15.

From these plots, it is apparent that the electric stress is the highest in case of the Al tape electrode, although in a very narrow area. Electric field strength is the second highest at the winding-type electrode, which has a smaller maximum value, but a substantially wider area of elevated electric stress. Under each turn of the winding is a point of contact and the peak values of field strength are only slightly smaller than under the outermost turn.

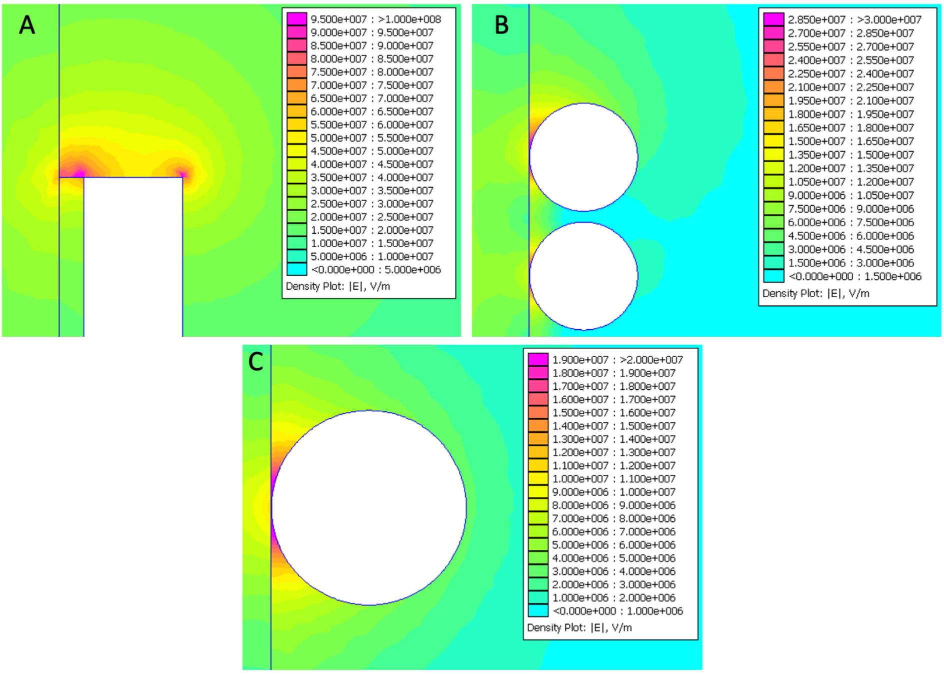

Figure 13. Electric field strength (FEM model) at the highest stressed sites of the different electrode types used: A) aluminium tape; B) copper wire winding; C) 5 mm round conductor

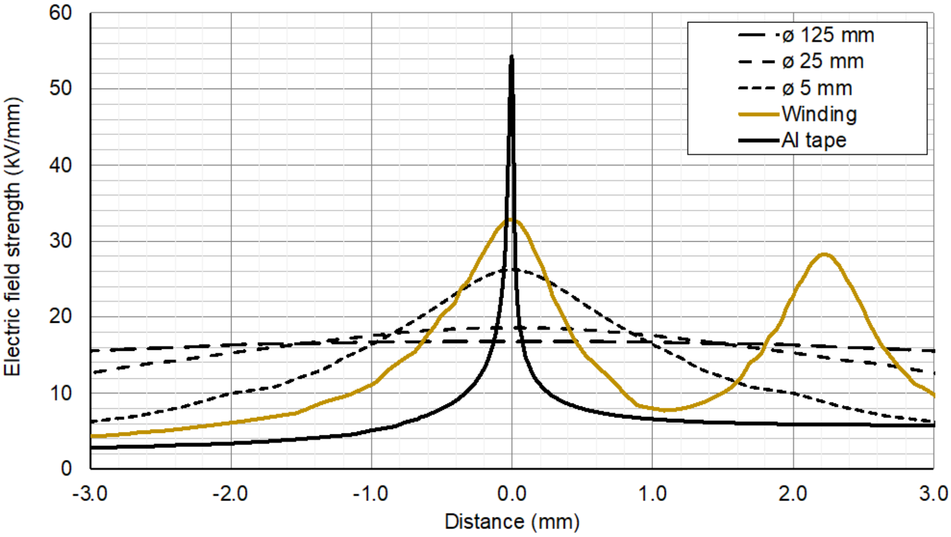

Figure 14. Modelled electric field strength at test voltage instantaneous peak value (19.8 kV) directly above the surface of the insulation for different electrode types. The locations corresponding to the highest electric stress are aligned with the origin of the x-axis (zoomed-in view).

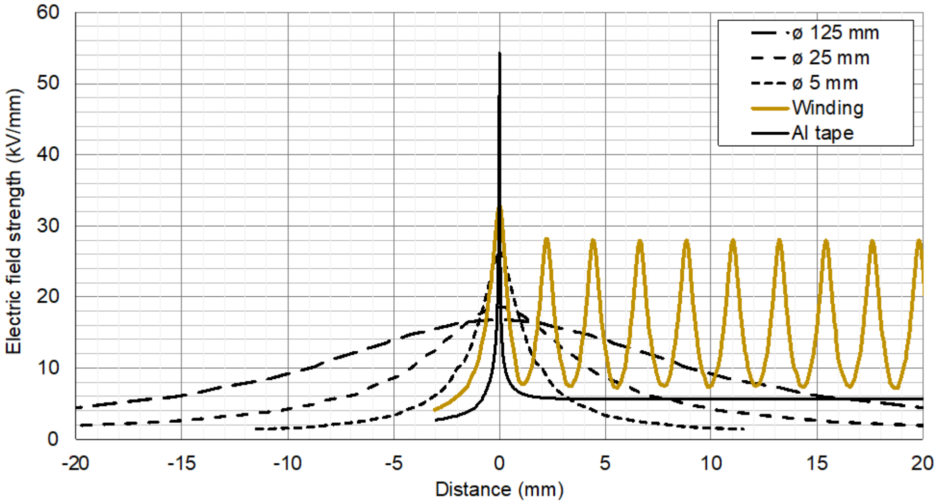

Figure 15. Modelled electric field strength at test voltage instantaneous peak value (19.8 kV) directly above the surface of the insulation for different electrode types. The locations corresponding to the highest electric stress are aligned with the origin of the x-axis (wide view).

The large overall area of high electric stress is apparently the main reason why the winding-type electrode caused puncture of the insulation over the shortest period of time. The three round electrodes exhibit a smaller value of maximum field intensity in the sequence of increasing diameter, but also a wider area of elevated electric stress as the diameter increases. This is clearly visible in Figure 14, although the difference in maximum field strength between the 125 mm and 25 mm electrodes is noticeably smaller than the difference between 25 mm and 5 mm electrodes.

The caveats discussed previously concerning the interpretation of FEM field simulations performed *in silico* apply in this instance as well. Field strength values remain somewhat indicative, because beyond the field strength high enough to initiate discharges in the air surrounding the electrode, these have an impact on the shape of the electric field due to ionization, the increase in conductivity of air and appearance of space charges. However, before any discharges occur during any given AC half-cycle and in the absence of space charges, the field strength is proportional to the computed values and therefore the areas in which the simulated electric stress is higher will accumulate a longer time under elevated stress and increased oxidative damage from PD chemical byproducts.

2.6 Intermediate summary

The performed tests indicated that the electric stress caused by contact with an object which has a substantially higher electrical conductivity compared to the insulating material of the CC causes puncture of the insulation over a timespan which ranges from hours to months, possibly even years, under normal operating voltage, depending on the shape of the object. If the object is round, a larger diameter causes breakdown faster, possibly because a wider area of insulation is stressed and there is a higher probability of insulation weak spots in the affected area. An electrode with a smaller diameter will elicit a stronger electric field, but over a narrower region of insulation, and will probably cause puncture after a longer period of time in most cases. The size of the total area under stress is apparently more significant than the strength of the electric field under the test conditions, provided the field strength is insufficient to precipitate puncture *via* another more rapid mechanism (e.g., thermo-electric breakdown). In the case of the winding-type electrode, the insulation suffered a combination of high electric stress and a large area of insulation influenced, which resulted in punctures over a significantly shorter period of time compared to other tested electrodes.

The tests also indicate that the degree of chemical degradation is a paramount factor in determining the time until failure. This is supported by the observation that the winding-type electrodes survived the least amount of time, while generating the highest degree of perceived PD activity. If this fact is considered in conjunction with the results of the Al tape electrodes, which survived for a substantially longer period of time, despite a similarly high electric stress in the insulation located underneath the electrode, the importance of oxidative damage becomes apparent. The punctures at Al tape electrodes only occurred at the edges of the tape, where the PD activity was most intense.

Four of the tested electrode types did not cause puncture in the insulation sooner than after four weeks of voltage application for any single test point. Four of the winding electrode grounding points punctured within two weeks, one of which punctured within 12 hours. This electrode shape, however, is not entirely representative of the objects that could make contact with actual energized CCs in the grid. It can be used to imitate worst-case electric stresses, because the electrode did cause the shortest insulation withstand times.

In terms of practical considerations, it appears that distribution grid operators should be most concerned about larger diameter trees and branches falling onto OHLs equipped with CCs. In addition to the faster progression to breakdown due to purely electrical effects demonstrated in the experiments, larger branches also have a more significant mechanical impact on the CC, which can also contribute to the attrition rate of insulation. Because of the high variability of breakdown time depending on the insulation strength at the point of contact, it would be prudent to eliminate any unwanted objects coming into contact with CC power lines with minimal delay. The size of the area exposed to a stronger electric field will also gradually increase in reality, as it has been observed that an indentation will start to form at the point of contact due to the effects of PD on the surface of the tree trunk, which virtually causes the conductor to “dig” into the tree [16]. Considering the importance of PD activity, monitoring of CC power lines can also be economically feasible, depending on the priorities and available resources of the grid utility.

3 Accuracy of locating partial discharges in power cables

3.1 Physical background of partial discharges

Measurement of partial discharges (PD) is one of the most important techniques utilized in HV insulation diagnostics. PDs are localized electrical discharges, which occur in the insulating space between two electrodes at different electrical potentials, and which do not penetrate across the entire distance between the electrodes. These discharges may occur in the immediate proximity of an electrode, e.g., in case of corona discharge, or not, e.g., in case of discharges occurring inside cavities embedded within the insulating material. PDs are generated in areas of increased electric stress and decreased dielectric strength, e.g., inside voids located in solid or liquid insulating materials and near energized conductive parts with protrusions surrounded by a gaseous insulating medium.

The generation of partial discharges can be explained through the distribution of electric field inside insulation with embedded voids. Consider an oblate cavity inside a mass of solid insulation (Figure 16). The electric field strength along the polar axis of the cavity is determined by the relative dielectric permittivity of both the insulating material ε_1 and the cavity ε_2. Because the cavity is filled with gas, it is usually considered that $\varepsilon_2 \approx 1$, while $\varepsilon_1 \approx 2.3$ in case of XLPE. Under such conditions, the ratio of electric field strength inside the insulation E_1 and cavity E_2 is determined by:

$$\frac{E_1}{E_2} = \frac{\varepsilon_2}{\varepsilon_1} \tag{5}$$

The electric field strength inside the cavity is therefore:

$$E_2 = \frac{\varepsilon_1}{\varepsilon_2} E_1 \tag{6}$$

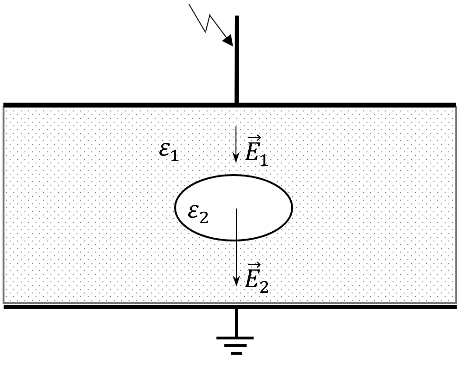

Figure 16. Electric field strength inside solid insulating material and gas-filled void in insulation

This implies the amplification of the electric field inside the cavity due to the properties of the surrounding solid dielectric. If E_2 is sufficiently high, a discharge will occur inside the cavity. The strength of this critical electric field required to initiate PD is influenced by the shape, dimensions, and position of the cavity. The precipitation of a PD event requires, in addition to a sufficiently strong electric field, an initial free electron to trigger the electron avalanche which leads to breakdown of the dielectric gas in the cavity. This electron is usually not available during the first instant the electric field strength exceeds the PD inception threshold and the discharge itself is therefore delayed until an initiatory electron appears, e.g., as a result of background radiation ionizing a gas molecule within the cavity. This statistical time lag is an inherent feature of discharge phenomena.

The primary cause of concern over PD activity is related to the deleterious effects PDs may have on the insulation over prolonged periods of time. PDs can be regarded as both a cause and a result of insulation aging, as ongoing PD activity usually establishes conditions suitable for further PD occurrence. Continuous PDs can self-perpetuate the degradation of solid and liquid insulation systems. It has been observed that organic insulating materials, particularly XLPE used in power cables, are more sensitive to PD, whereas inorganic substances like mica in rotating machine insulation can permanently tolerate the presence of mild to moderate levels of PD [22, 23]. The degradation mechanism of insulation afflicted with PD is related to the effects of free electron bombardment at the dielectric surface exposed to the discharges. Electrons with sufficiently high energy can cause scission of the C-C and C-H covalent bonds and subsequent erosion of the material resulting from chemical and physical alterations.

Some authors have drawn attention to the fact that the term “partial discharge”, although ubiquitous in the literature discussing the subject and widely encountered in general practice, is technically inaccurate [24]. A more suitable substitute to this would be “partial breakdown”, as it more adequately encapsulates the quintessential nature of the phenomenon by contrasting it to the full catastrophic breakdown of the insulation (occasionally referred to as a “disruptive discharge”). Any discharge process discussed in this specific context is complete in and of itself, regardless of the extent to which it impacts the insulation. The author of the thesis acknowledges this subtle nuance of nomenclature. However, the term “partial discharge” has been used throughout due to its historical persistence and continued widespread use in the field of high voltage engineering.

3.2 Partial discharge types and modes

Usually, three primary types of PD are distinguished: corona discharge, internal discharge, and surface discharge (Figure 17). Electrical treeing, a result of long-term internal PD is also sometimes considered to be a separate type. Also, there are subtypes to each of these and the characteristics of the PD activity in any set of circumstances is dependent on the nature of the defect which caused it.

Partial discharge may occur as a series of distinct pulses or exhibit pulseless behavior, i.e., in case of glow or pseudo-glow discharge. In practical applications, usually only pulsed PD is measured as pulseless PD is generally accompanied by pulses and the measurement of pulses is more feasible to implement [25]. In solid insulation, PD presents as a dielectric barrier discharge, which mechanistically contributes to the pulsed behavior [26]. The PD pulse characteristics at the site of measurement are highly dependent on not only the shape and nature of the PD-emitting defect, but also the parameters of the external circuit [27]. The actual rise-time of PD pulses measured at the defect can be as low as 1 ns [25].

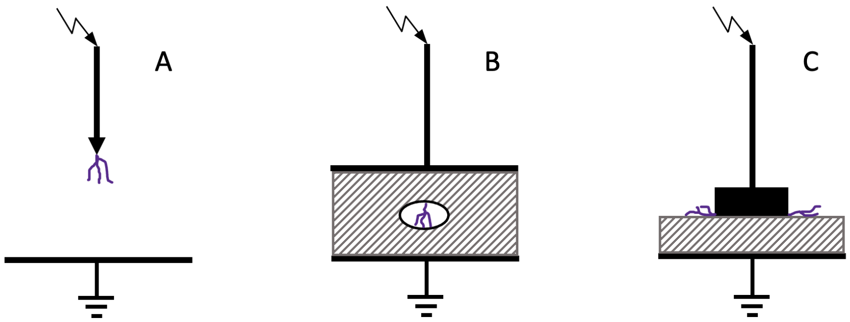

Figure 17. Types of partial discharge in an insulation system: A) corona discharge, B) internal discharge, C) surface discharge

3.2.1 Corona discharge

Corona discharge occurs at the boundary of a conductor and an extended volume of a gaseous insulating medium. Corona occurs in areas of substantial electric field non-uniformity, e.g., at protrusions and sharp edges. Corona is usually not considered to be harmful to solid insulation, because the insulating materials are not directly influenced by the energized particles accompanying the discharges. Corona can impact the insulation indirectly *via* the corrosive effect of generated gases (e.g., O_3 and NO_x) and UV radiation, although in practice, the magnitude of these effects is probably negligible, except under some very specific circumstances. PD in gaseous media can exhibit a variety of behaviors depending on the type of gas, pressure, electrical polarity, electric field parameters etc. In practical applications, i.e., reference or near-reference barometric pressure and a typical range of ambient air temperature as well as humidity, corona discharge presents as one of a few typical modalities briefly discussed as follows [28].

When the corona-producing protrusion is positively charged, the corona starts at voltage levels near or slightly beyond the inception voltage, as a phenomenon termed as onset streamers. Upon further elevation of the voltage, the corona progresses to a glow discharge. Approaching the air gap sparkover voltage, breakdown streamers may also be observed. When the protrusion is negatively charged, the corona exhibits a distinctive pulsed behavior known as Trichel pulses at voltage levels which slightly or moderately exceed the inception voltage. These pulses are relatively regular in terms of both the frequency of occurrence as well as their magnitude and exhibit a relatively stable behavior over a wide range of voltages. Eventually, the Trichel pulses gradually transition over a voltage range to a steady glow discharge. Raising the voltage further results in sparkover. In contrast with solid and liquid dielectrics, no appreciable space-charge accumulation occurs in gases. Therefore, there is no significant memory effect between subsequent discharges [29].

There are similarities, but also some significant differences between positive and negative corona. In practical applications, it is important to consider how these observations translate to AC voltages and power cables. As mentioned previously, corona is not immediately harmful to power cables, because it does not damage the internal insulation, although corona will be detected by PD measurement instruments. In MV cables, the only part which is typically susceptible to corona is the exposed phase conductor at the termination, if it is damaged or contamination is present, e.g., small metal particles, on the termination. Corona may also occur at the air-insulated switchgear or other equipment to which the cable is connected.

Under AC voltages, the protrusion which presents as a source of corona will be energized both positively and negatively in an intermittent fashion. Under these circumstances, it has been observed that the inception voltage of corona is substantially lower in the negative half-cycle [30]. It has also been determined that positive corona pulses are much larger in magnitude and occur over a narrower segment of phase angles compared to negative corona. Also, considering corona behavior at voltages vastly exceeding the inception voltage is of little practical value in the context of this discussion, because in adequately designed and constructed MV installations the AC voltage will very rarely, if ever, reach anywhere near the voltages required to precipitate glow discharge or sparkover to adjacent conductive objects.

3.2.2 Internal discharge

Generation of PD pulses in voids and cavities is affected by the externally applied electric field and space charges deposited on the boundaries of the void from preceding PD activity. It has been noted that the conductivity of the walls of the PD-inducing defect increases as the PD activity persists, due to chemical and physical alterations of the material. This has a few consequences with regard to subsequent PD activity [31]:

1) The space charge-induced field strength decreases as the charge disperses over a larger area
2) The conductive surface functions as a reservoir of initiatory electrons and the statistical time lag of discharge onset decreases
3) PD activity may discontinue once the surface conductivity is high enough due to insufficient buildup of electric field strength, particularly in prolate cavities
4) Parallel discharges in the same cavity cease to occur

The shape of the PD pulse is also affected by the degree of overvoltage across the cavity in relation to the minimum necessary voltage required to produce a discharge. A small overvoltage results in a Townsend-like discharge (low amplitude and wide) and a higher overvoltage results in a streamer-like discharge (large amplitude and narrow). The latter usually presents with a larger magnitude of charge transfer during the discharge event [32]. In later stages of PD-related degradation, the discharging activity is influenced by crystals of hydrated oxalic acid ($[COOH]_2 \cdot 2H_2O$), which form inside the cavity in addition to other organic compounds containing carboxyl moieties. The PD concentrates at the tips of these crystals and the pulse shape becomes low in amplitude and intermediate in width. Such changes also promote pseudo-glow and pulseless discharge activity [33].

3.2.3 Surface discharge

Surface discharges occur along the interface between a solid or liquid insulating material and air (or some other insulating gas). Components which feature a sudden transition in insulation system geometry, e.g., cable terminations and transformer bushings, are particularly susceptible to surface discharge.

An electric field with a sufficiently high tangential component across the surface of the insulation will precipitate surface discharge. This can occur when there are conductive parts or particles on the insulation surface, or the component has sustained damage in an area exposed to high electric field stress. The interaction between contaminants and moisture on the surface of the insulation can also trigger discharges. Surface discharges become problematic after a prolonged period of persistent activity because the surface of the insulating material will degrade. Some materials are more susceptible to tracking, i.e., the formation of conductive paths on the surface of the dielectric. Tracking contributes to ongoing degradation and worsening of the insulation system component performance. [24]

In case of surface discharge, it is not unusual to observe a large discrepancy between the behavior of discharges during positive and negative half-cycles, which is highly influenced by the availability of initiatory electrons on the electrode. Assuming the electrode which acts as the source of the discharge is connected to the HV electrode, the following behavior is expected [34]. The discharges, which occur during the negative half-cycle, will exhibit an increasing charge value as the voltage reaches the negative peak. Some level of PD should be present during most of the negative half-cycle. There are far fewer PD pulses during the positive half-cycle and they have smaller amplitude as well. Also, the positive PD pulses will primarily occur during the rising portion of the positive half-cycle. The discrepancy between the number and amplitude of pulses occurring during the positive and negative half-cycles increases as the voltage is raised further beyond the inception voltage.

3.3 Partial discharge pulse parameters

As discussed previously, the nature of PD activity is generally pulsed. The research conducted on PD pulses indicates that the actual shape of the current pulse is somewhat Gaussian [35]. The PD current consists of an electronic and an ionic component. As the time required for the translocation of electrons across the discharge volume is very brief, the PD pulses may have a rise time as low as 1 ns. The ion movement is much slower compared to electrons and therefore the PD current pulse features a long, but shallow “tail”, which is more difficult to detect. The measurement instrumentation primarily reacts to the electronic component of PD current. The response of the instrument used to measure PD is typically also a pulse and the shape of the pulse is also influenced by the transfer characteristics of the instrument and the transformation of the pulse shape as a result of propagation from the point of origin to the detector. For computational purposes, the PD pulses are usually characterized by a Gaussian curve, a double exponential wave or in some specific applications, a Dirac delta function. Representations of a mathematically generated PD pulse shape and a real measured PD waveform are provided in Figure 18.

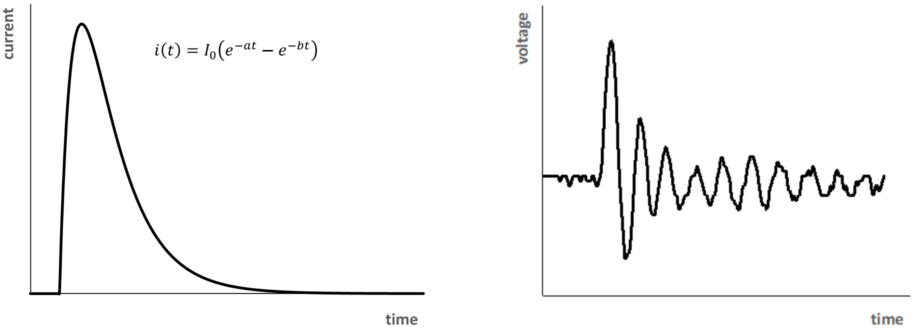

Figure 18. Partial discharge pulse waveforms. Left: Idealized PD current pulse shape (double exponential wave); right: actual PD pulse measured using a high-frequency current transformer.

3.4 General diagnostic approach to partial discharge assessment

The full diagnostic assessment of PD activity in cable insulation (or other HV components) can be subdivided into the following stages:

1) PD measurement
2) PD signal denoising
3) PD location determination
4) PD pattern recognition

A brief description of the main aspects of each of these stages is provided, as well as the challenges associated with them.

3.4.1 Measurement

In practical situations, the electric field inside insulation and cavities is of smaller interest compared to voltage, which is more easily quantifiable. The lowest voltage at which PD can be detected upon increasing the voltage applied to the object under investigation, is called PD inception voltage (PDIV) U_i. The voltage at which PD can no longer be detected after decreasing the voltage from a level at which PD was previously present, is called PD extinction voltage (PDEV) U_e. The measurement of PD has traditionally involved the determination of the apparent charge magnitude of individual discharges. The actual amount of charge displaced during any single discharge is not directly measurable in practice.

A variety of different methods and equipment can be used for PD measurement. PD measurement is based on the detection and quantification of the discharge current and voltage pulses, which are very small in comparison to the parameters of mains electricity. PD apparent charges and pulse peak voltages are usually in the pC and mV range, respectively. The conventional method for detecting and quantifying PD is outlined in IEC 60270 [36]. However, this is mostly limited to off-line testing due to restraints regarding the need for direct galvanic connection of the test equipment to the HV terminals of the test object, the necessity to calibrate the circuit for apparent charge magnitude measurements by injecting a known charge into the test object using a pulse calibrator, and high cost of test equipment.

Other methods of measuring PD involve exploiting the properties, auxiliary effects, and emissions of PD to detect the phenomenon. Most of these methods are considerably less invasive compared to the classic IEC 60270 method. In electrical measurements, the PD signal may be coupled capacitively, inductively or in both modes simultaneously, resulting in the possibility for directional coupling. Examples of hardware which employ these principles and have potential to be used in on-line PD monitoring include high-frequency current transformers (HFCT), ultra-high frequency (UHF) detectors, capacitive couplers (CC), Rogowski coils, Pearson coils, axial magnetic field and sheath interruption sensors, differential electric field sensors and loop antennas [37, 38, 39, 40, 41]. Some detectors can also be incorporated into the construction of cable accessories [42, 43]. The connection to the test object for both IEC 60270-compliant measurement and an HFCT is illustrated in Figure 19.

Other devices used to measure PD include acoustic detectors, optical detectors, and dissolved gas analyzers (in oil-insulated applications) [44]. Excluding chemical assays, methods based on these non-electrical measurement modalities also have some potential for application in XLPE cable monitoring, either independently or in conjunction with electromagnetic sensing.

The major difference between the traditional IEC 60270 measurement method and the other non-conventional methods is related to PD quantification. Reliable representation of apparent charge magnitude is one of the primary objectives of IEC 60270-based measurement systems. The low upper cut-off frequency (up to 500 kHz for wide-band systems) of the detection circuit results in “quasi-integration” of the PD pulse and this enables the apparent charge to be represented with reasonable accuracy. This is useful due to the fact that the amount of damage the insulation will sustain due to any single PD event is considered to be proportional to the amount of charge displaced [23].

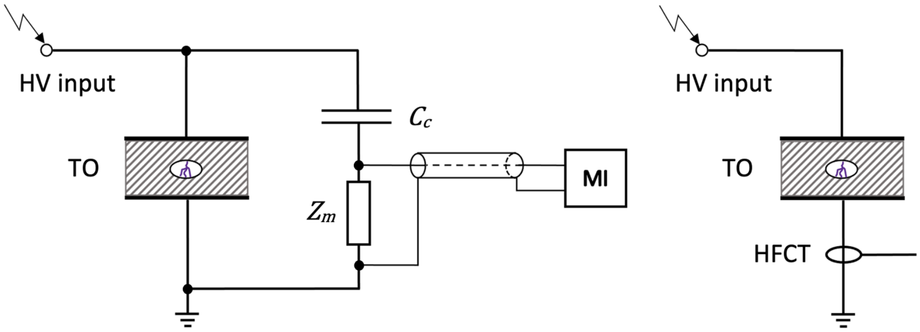

Figure 19. Principle topology of partial discharge measurement. Left: IEC 60270 compliant measurement setup; right: high-frequency current transformer (HFCT) placement around ground terminal of test object. TO – test object, C_c – coupling capacitor, Z_m – measurement impedance, MI – measuring instrument.

The non-conventional methods are usually well suited to detect PD, although quantifying the charge involved in the discharge process is not straightforward. Detectors with a sufficiently wide bandwidth can reproduce the shape of the PD pulse and it can be numerically integrated to produce a quantity which is proportional to the amount of charge transferred, but considerations would have to be made to determine the actual value of the proportionality coefficient, i.e. converting the sensor response to apparent charge in pC [45]. As all PD pulses are slightly different and part of the pulse frequency content will likely reside outside the pass-band of the detector, e.g., an HFCT, this will introduce an additional source of uncertainty into the measurement process.

It has been demonstrated that using the area under the curve of the sensor response will yield an estimate of the apparent charge with a smaller uncertainty than assuming the PD apparent charge is proportional to the peak value of the sensor response, with a variety of different pulse shapes [46]. The capability to examine the pulse shape, however, can be useful for differentiating between PD pulses originating from different sources. Also, the capability to detect the presence of PD is mostly considered to have superior utility than the capability to accurately assess its apparent charge magnitude. Any significant presence of PD within the insulation of extruded power cables has the potential to cause a cable fault over a relatively short timeframe.

An important aspect of measuring PD in power cables, both high and medium voltage, is the limitation of effective scanning length. This is determined by factors such as the type of cable, insulation and semiconducting layer materials, noise level, sensor response and signal-to-noise ratio. Of all the various currently available PD detectors, HFCTs generally possess suitable attributes to be used in cable monitoring. HFCTs usually have a bandwidth from a few hundred kHz to tens of MHz, which may cause pulse distortion due to a high lower cut-off frequency, but still enable the identification and location of PD sources [47].

In power cables, as well as some other types of equipment, the success of PD measurement is strongly affected by travelling wave reflections. This is known to cause superposition errors, which may result in either an additive or subtractive error in the magnitude of the measured PD pulse [22]. The cause of wave reflections is discontinuity of the characteristic impedance of the pulse transmission medium. In power cables, these are usually terminations, joint connections and substantial insulation faults. The relative magnitude of reflection $\mathit{\Gamma}_{12}$ at a discontinuity, where the characteristic impedance changes from Z_1 to Z_2 at the interface between the two media, is described by:

$$\mathit{\Gamma}_{12} = \frac{Z_2 - Z_1}{Z_2 + Z_1} \tag{7}$$

It is apparent that the magnitude of the reflected pulse increases as the disparity between the characteristic impedances increases. Correspondingly, the degree of pulse energy which is transferred across the interface is reduced. In applications where the accuracy of the pulse measurement is important, superposition effects must be accounted for by appropriate calculations or eliminated altogether by using suitable matched impedances which suppress reflections from the opposite cable end [48].

PD cross-talk is also an issue, which is caused by the coupling of PD signals between different conductors, e.g., different phases of the equipment being measured [22]. This may result in the detection of PD activity in phases without an actual PD source. Misrepresentation of cable insulation state *via* PD cross-talk can be surmounted using suitable signal comparison and suppression methods and algorithms to dismiss phantom PD pulses measured in adjacent phases. These may be based on consideration of voltage phase angle (e.g., a negative PD pulse measured during the rising portion of the positive half-period is essentially impossible and its appearance in the measured data may be mediated by cross-talk from another phase or some source of noise) or pulse polarity and detectable time delays [49].

3.4.2 Partial discharge signal denoising

Under real-world conditions, some noise is always present in measurements and the detection of PD is particularly susceptible to sources of electromagnetic interference due to the inherently weak signal PD sources normally emit. Some common sources of noise include: corona from components besides the one under inspection, power tool operation, arc welding, poor electrical contacts, electrostatic precipitators, network switching transients, wireless communications, broadband power line communications and, in general, equipment which produce discharges similar to PD under normal operation [23, 50].

Techniques to facilitate noise rejection include [49, 51]:

- Noise gating, achieved by using an auxiliary noise detection sensor (e.g., antenna) connected to an alternate measurement channel
- Using multiple measurement sensors and arranging them in a way which enables noise cancellation (e.g., balanced differential circuit)
- Frequency-domain noise rejection, i.e., measuring PD in a low-noise frequency band or reducing noise through subsequent signal manipulation

- Rejecting secondary signals from the same source covering alternate propagation paths and resulting in delayed arrival, in case this approach is warranted
- Identifying noise pulses based on discordance with polarity of the energizing voltage, as discussed previously in conjunction with cross-talk

There are also a number of signal processing techniques available for denoising. Some of the main methods used in denoising PD measurements include [23, 50, 52]:

- Fast Fourier transform (FFT), which is particularly effective for identifying sinusoidal noise signals
- Short-time Fourier transform
- Wavelet filtering
- Band-pass filtering
- Notch filtering
- Time *vs* frequency clustering
- Short-time zero-crossing count combined with short-time energy

Of these, wavelet filtering in particular has also been shown to be effective for PD monitoring in on-line situations [53]. In case of wavelet filtering, the Daubechies' mother wavelet is often recognized to be effective. The most appropriate method or combination of methods to denoise PD will be dependent on the number and nature of noise sources present.

3.5 Medium voltage power cable structure

The detection of partial discharges in power cables presents some unique challenges. The typical structure of a modern XLPE-insulated MV power cable is provided in Figure 20. The central conductive core and the main insulation are separated by a semiconducting layer, which is introduced into the structure of the cable to dramatically reduce the inhomogeneity of the electric field inside the insulation, which would otherwise be present due to the irregularity of the conductor surface. Similarly, a semiconducting layer is applied to the outer surface of the insulation to reduce field distortions near the cable screen. The screen usually consists of copper wires evenly distributed across the perimeter of the insulation and a copper tape wound helically on top of these (not shown in the figure) to augment electrical contact between the wires. The cable is covered with a protective outer sheath, typically consisting of PVC, which serves a structural function and also insulates the screen from external conductive objects.

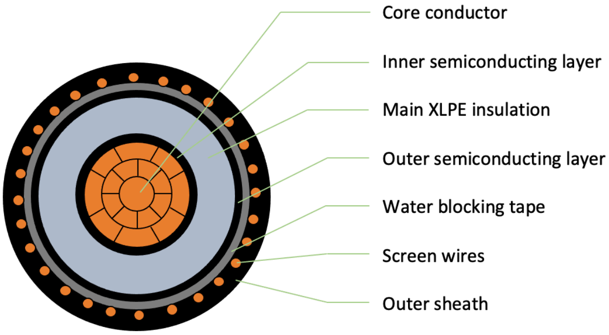

Figure 20. Radial cross-section of a typical XLPE-insulated medium voltage power cable

Some cable types can also include additional protective layers to inhibit water ingress and longitudinal diffusion of moisture within the cable. Excessive aqueous infiltration worsens the insulating properties of XLPE and can trigger the emergence of water treeing. Cables designed for operation in more challenging environments may also include extra layers of armor to augment mechanical resilience.

3.5.1 Partial discharge in power cables

Regarding power cables, online detection of PD has gained increasingly more attention. Based on appropriately conducted cost-benefit analysis, both industrial enterprises and grid utilities can extract significant value from either permanent or rotation-based monitoring of critically important cable circuits [54]. Field experience suggests that the duration of time between detectable PD inception and a subsequent failure is relatively short in case of XLPE insulated cables, usually from a few days to a few months [55]. The time until breakdown is substantially longer for paper-insulated lead coated cables (PILC), typically several years, although continuous discharging activity without breakdown has also been observed [55]. Due to the many economic benefits of using XLPE cables instead of PILC, virtually all new and refurbished general purpose power cables installed in the grid are XLPE insulated and the share of PILC is steadily declining. Consequently, there are obvious benefits to being able to detect, localize and rapidly classify PD activity in power cables. However, there are some practical limitations to measuring and diagnosing PDs in power cables and the reliable interpretation of PD activity can, at present, only be conducted by an experienced specialist. It is also necessary to determine whether the detected PD is indeed caused by a discharging defect, relatively harmless corona or whether it is simply noise.

3.5.2 Determining locations of partial discharge sources

An important aspect of PD diagnostics is the location of PD sources within the studied component. In case of power cables, the issue of localization is simplified by the fact that PD needs to be localized essentially only in one dimension of space, i.e., along the length of the cable. This does not, however, imply that localization is necessarily easy.

In off-line diagnostics of reasonably short cables, time-domain reflectometry (TDR) can be used. This is based on detecting pulse pairs, i.e., the direct pulse travelling from the PD source to the measurement device in one end of the cable and the pulse that has been reflected from the opposite end of the cable.

The difference in arrival time can be measured and the location of the source determined if the velocity of the pulse is known. In XLPE-insulated cables, the pulse velocity v_p is usually in the range of 150…200 m/μs and it is commonly measured prior to the actual PD measurements. The pulse velocity is determined by injecting a calibration pulse at the near end of the cable, detecting the injected original and reflected pulse and applying:

$$v_p = \frac{2L}{\Delta t_{cal}} \tag{8}$$

Where: L – length of cable;
Δt_{cal} – time delay between original and reflected calibration pulse.

The location of a measured PD pulse origin, i.e., the distance of the PD source from the near-end of the cable x can be determined using:

$$x = L - \frac{v_p \Delta t}{2} \tag{9}$$

An important observation concerning (9) is that the interval between pulses is proportional to the distance of the PD source from the far end of the cable. This implies that the original and reflected pulses generated at a source which is sufficiently close to the far end of the cable cannot be resolved.

Using the TDR technique in on-line measurements may not be applicable to long cables, because the magnitude of the reflected pulse is significantly smaller due to the fact that the cable is not disconnected from other equipment at its terminations. The magnitude of the reflected pulse in relation to the incident pulse is determined by the differences of characteristic impedance of the cable and the circuit to which the cable is connected (i.e., the switchgear in a substation), as discussed previously. In off-line tests, practically all of the pulse is reflected, whereas in on-line situations, only a small portion of it might be reflected.

A separate issue in determining PD source location with TDR is the discrimination between pulses originating from the near end and the far end of the cable. Judgement based only on time difference is insufficient, because in both cases, the temporal delay between the 1st and 2nd detected pulse is equal to double the time of pulse transit over the length of the cable, in case the pulses are measured at the cable terminal. Using a high-bandwidth detector which enables the representation of the PD pulse with minimal distortion can, however, aid in distinguishing between pulses originating from the near and far ends. This is discussed in detail in [56] and the three discrimination criteria are based on pulse height, pulse charge and resonance phenomena. The latter two methods also require pulse frequency spectrum analysis and resonance discrimination is probably not applicable to on-line measurements. Pulse height discrimination is more suited to short cables, whereas pulse charge discrimination might be more feasible in case of long cables.

Another approach to achieve location of PD sources on power cables involves time-synchronized measurements at multiple locations, e.g., cable ends or joints. This may also be referred to as arrival time analysis. As the pulse transition time along the cable is very short, in the range of microseconds, the precision of time synchronization is paramount. Using a secondary conductor, e.g., a fiber-optic cable to relay measurements from different sensors to a master device would be ideal from a functional point of view, but in most cases costly and impractical. Synchronization *via* GPS might be feasible, as the error in GPS time is expected to reach up to some tens of ns, although it is variable and affected by a variety of factors, such as antenna positioning, ionospheric delays, satellite visibility and the accuracy of their ephemerides [57]. A time-domain error of 10 ns would result in a PD source location error of around 1.5…2 m. Sources of error related to the hardware of the entire measurement system would require evaluation as well. It has been demonstrated that GPS-synchronization can be used in practice [58]. Achieving synchronized measurements using atomic clocks has also been suggested [59], although the economic feasibility of this approach in practice is dubious and GPS synchronization is, in principle, already utilizing atomic clocks, albeit indirectly. The location of a PD source in case of time-synchronized measurements can be determined based on:

$$x = \frac{L - v_p (t_{II} - t_I)}{2} \tag{10}$$

Where: t_I – time instant the pulse is detected at end 1;
t_{II} – time instant the pulse is detected at end 2.

Another solution to the issue of synchronization has been suggested, which involves using the measurement equipment itself to generate synchronization pulses in the cable under measurement to facilitate communication between devices at either end of the cable [60]. This also enables continuous re-evaluation of pulse propagation velocity, which is somewhat affected by cable temperature. It has been demonstrated that in case of XLPE insulated cables, the propagation velocity has a positive dependence on cable temperature, whereas the propagation velocity decreases with increasing temperature in PILC cables [61]. Amplitude-frequency mapping of measured PD pulses has also been proposed as a method to achieve PD source location [62].

3.5.3 Partial discharge pattern recognition

PD measurement results can be presented in a variety of ways. The most widely recognized and used is the phase-resolved PD pattern (PRPD) plot, on which PD pulses, or other parameters concerning PD, are plotted against the phase angle of the AC voltage cycle. Alternatively, when examining very short time intervals (e.g., under 1 ms) to study PD reflections or pulses occurring in quick succession, PD sensor response time series might be used. Inferring the exact nature of the PD source based just on the pattern of pulses is a significant challenge due to the inherent complexity of PD mechanisms and the multitude of factors which influence PD behavior in any specific case [26]. Some auxiliary parameters used to characterize discharging activity are average discharge current, average discharge power, repetition rate, peak discharge value, quadratic rate [63]. Transforms of PD time-series data, e.g., frequency-domain information, are also often used.

Typically, the process of pattern recognition and assessment formation regarding the number and nature of PD sources inside the equipment under observation would require interpretation by a specialist with significant prior experience in PD diagnostics. To obviate the need for human involvement, several PD analysis and pattern recognition methods have been proposed.

Statistical feature extraction is based on analyzing a large number of PD pulses and determining statistical moments and other parameters to describe the data. Examples of corresponding datasets are pulse count *vs* phase angle or pulse amplitude *vs* phase angle. Parameters, e.g., mean value, variance, skewness, kurtosis, cross-correlation factor, discharge asymmetry and phase asymmetry may be considered as a basis for subsequent analysis. The PD data can also be further processed using various computational methods to extract relevant features and reduce the dimensionality of the data, which can result in a lowered requirement of computational resources [63, 64]. Further processing to yield quantifiable differences in PD activity include mapping techniques such as principal component analysis, discriminant analysis and t-distributed stochastic neighbor embedding [65, 66]. The density-based spatial clustering for applications with noise (DBSCAN) has also been successfully used in PD source discrimination [67].

Numerous methods based on neural networks and machine learning have been developed and applied to PD analysis as well. Others include hidden Markov models, fuzzy logic-based classifiers, self-organizing maps, inductive inference algorithms, support vector machines, rough set theory-based classifiers and sparse representation classifiers [64, 68, 69]. It has also been suggested that applying image processing tools to PD patterns may yield useful results. Examples of these include texture analysis algorithms and fractal feature extraction. These involve making inferences based on features such as fractal dimension (i.e., surface roughness) and lacunarity (i.e., denseness) of the patterns [65]. It is known that PD patterns change over time as the defect develops [70], but the nature of the change is also affected by factors such as ambient temperature, cable load and power quality. Consequently, interpreting the changes in PD patterns remains a challenge [43].

Another approach to study the PD activity is through characterizing the individual pulses in terms of time intervals between discharges (i.e., changes in the instantaneous value of voltage, phase angle, time etc.) This is referred to as voltage difference analysis or pulse sequential analysis. The premise of this approach is the observation that the inception of PD is influenced not only by the externally applied electric field, but also the space charges deposited by preceding discharges. When studying a test object with few PD sources, this approach may yield considerable insight into the nature of the source. [22, 29]

It is also possible to classify PD phenomena by examining pulse shape characteristics, particularly when the measurement system enables sufficiently accurate representation of the pulse waveform. This approach is based on the premise that pulses originating from different sources should exhibit different waveforms, either due to differences in the discharge event itself, propagation-related effects, or both. Features such as peak value, rise time, fall time, width and area-under-the-curve may comprise the basis of such distinctions [65]. Methods such as autocorrelation may be applied to assess the similarity of pulses to determine whether they are related to the same source [69]. Processing waveform data using different transforms, e.g., the Fourier', Wavelet or Karhunen-Loève transform, and extracting appropriate coefficients to describe the pulses can also be used [65].

3.6 Aspects of partial discharge occurrence in cables

The application of PD measurements on power cables has produced practical experience, which can be used for making inferences regarding the state of the insulation of the cable. For example, PILC cables can exhibit a behavior where PD is sparsely occurring within long lengths of the cable. This is usually not a sign of deterioration and could be related to temperature and pressure changes causing fluctuations in the degree of oil impregnation [22]. However, sites of concentrated PD activity typically indicate persistent and potentially harmful defects in the cable. Diffuse PD occurrence is atypical in case of XLPE insulated cables.

Generally, the PD sources are located at the sites of joints and terminations. The installation of these cable accessories is performed under on-site conditions and the assembly quality is highly influenced by workmanship and possible contamination with foreign objects in the sensitive areas exposed to high electric stress. PD activity can, of course, be observed in cable sections remote from joints and terminations, in which case possible causes may include acute injury to the cable by mechanical influences or disintegration of the copper wire screen due to excessive fault currents [71]. The latter may be suspected in case several PD sources are detected which cannot reasonably be associated with cable accessories, after accounting for the uncertainty in source location determination. Destruction of screen wires also introduces further distortion into PD pulse waveforms [72].

A number of other factors influence the characteristics of PD and the patterns also change over the course of aging [65]. It has also been observed that in defected XLPE cable components, the behavior of PD can also be intermittent over time periods of several days [70, 71]. An explanation to why PD may fluctuate in this manner is related to the variation of the dielectric permittivity of the insulating material with temperature, whereas the permittivity of the gas-filled cavity has no appreciable temperature dependence, resulting in a change in the electric field strength within the cavity [29]. This also ensues from (6) and the conjecture is consistent with the observation that the permittivity of XLPE decreases as the temperature increases [73]. It has also been observed that the presence of higher harmonic frequencies in the voltage waveform accelerates electrical tree growth rate, resulting in faster insulation failure [74]. It has also been determined that typical installation defects in MV cable terminations, e.g., protrusions in the semiconducting layer and grooves in the outer surface of the insulation in both the longitudinal and circumferential directions generate PD with distinctly different characteristics [75].

3.6.1 Propagation-related pulse distortion

An important aspect to consider in practical PD measurements is the transmission line behavior of the component under examination. This particularly affects cables, as the distance between the PD source and detection equipment may reach up to several kilometers. The PD pulse waveform becomes significantly distorted due to attenuation and dispersion in the cable. This phenomenon can be explained using the equivalent circuit of the power cable (Figure 21).

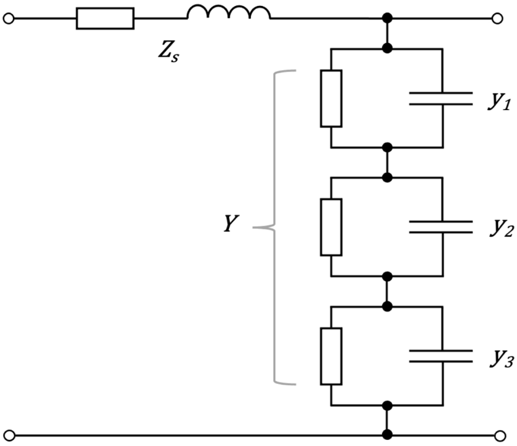

Figure 21. Equivalent circuit model for XLPE insulated power cable at high frequencies

The equivalent circuit for power cables at high frequencies includes the longitudinal impedance and the shunt admittance, similarly to the traditional transmission line model, with some additional components. The longitudinal impedance Z_s accounts for resistive losses and inductance of the core conductor and screen of the cable. Components of the shunt admittance y_1, y_2 and y_3 account for the capacitance and conductivity of the inner semiconducting layer, main XLPE insulation and outer semiconducting layer, respectively. The equivalent shunt admittance Y is derived from:

$$Y = \left(\frac{1}{y_1} + \frac{1}{y_2} + \frac{1}{y_3}\right)^{-1} \tag{11}$$

The propagation constant of the cable γ is:

$$\gamma = \alpha_p + j\beta_p = \sqrt{Z_s Y} \tag{12}$$

Where: α_p – attenuation constant (nepers/m);
β_p – phase constant (radians/m).

Attenuation is caused by dissipation of pulse energy during propagation. This manifests as dielectric losses in the insulation and conduction losses in the conductor, screen, and semiconducting layers. Attenuation increases with frequency and the relative contributions of each structural component of the cable to the overall attenuative effect are frequency-dependent [76]. At frequencies up to approximately 10 MHz, the attenuation is dominated by losses in the conductors, i.e., the phase conductor and screen wires; attenuation at higher frequencies is mainly due to losses in the semiconducting layers and insulation [77].

Dispersion refers to the slightly different speeds at which different frequency components propagate in the cable, resulting in a frequency-dependent phase shift. Measurements indicate that in the frequency range from 0.1 to 100 MHz the phase velocity exhibits a slight upward trend [77]. Other researchers have also shown that the distortion of PD pulses is primarily caused by a lower phase velocity at lower frequencies [47]. In the frequency range up to approximately 100 kHz, the properties of the surrounding ground also have a profound effect on pulse propagation by decreasing the phase velocity in the cable [72]. The combined effect of these phenomena results in the gradual decrease of pulse peak value and an increase in its rise time. The effects of attenuation and dispersion can be accounted for in calculations using the propagation constant γ. However, computational approaches are severely complicated by the fact that the propagation constant of power cables is frequency-dependent, and the properties of the semiconducting layers are difficult to account for.

Failure to consider the transformation of the pulse waveform as it propagates can result in a systemic error in PD source location. The magnitude of the bias in location measurement will depend on which characteristic value of the PD pulse is used to calculate location, i.e., will it be based on the peak value, 50% peak value or an estimated origin time of the pulse (analogous to the virtual origin concept used in lightning impulse voltage measurement). The inaccuracy of information regarding the length of the cable may also be a significant source of error. [78]

Efforts have been made to create computational models to predict the transformation of PD pulse waveforms in conjunction with propagation [79]. These may constitute transmission line models featuring additional elements in the shunt admittance portion of the distributed parameter circuit model to account for the effect of semiconductive layers of the power cable [76]. A sufficiently accurate model may enable the compensation of attenuation and dispersion to yield a more accurate representation of the PD waveform at its origin. The propagation constant may also be extracted from the FFT-based analysis of TDR measurements on a cable, but the accuracy of this approach is limited to frequencies up to approximately 30 MHz [47].

In modern XLPE-insulated cables, electrical properties of the semiconducting layers covering both the cable conductor and insulation impart a significant effect on pulse propagation characteristics, particularly the dispersive nature of the cable. Early efforts at modelling the pulse behavior revealed that neglecting to account for the effects of semiconducting layers results in disagreement between expected and experimentally gathered results [80]. The conductivity of the semiconducting layers in particular influences the phase velocity [81]. The insulating material itself is also important, e.g., the older oil-paper insulated cables, which are characterized by higher dielectric losses compared to XLPE cables, also exhibit stronger attenuation and dispersion of the PD pulses [23].

The transformation of PD pulses during propagation can be predicted analytically based on the geometry of the cable and the properties of its constituent materials. The accuracy of this approach will, however, be limited by the accuracy of information regarding the materials, e.g., complex permittivity of the semiconducting layers, as this can change significantly between cables from different manufacturers and the corresponding data are not readily available. The measurement of complex permittivity also requires sophisticated equipment and careful consideration of test sample preparation, and it has also been shown that this parameter is both temperature and pressure dependent [76]. Reasonable accuracy can be achieved with an approximate model which is based on a linear approximation of the propagation constant at frequencies exceeding 1 MHz [82].

A number of other factors also influence pulse propagation. For example, aging of insulation materials has similarly been shown to impart an effect on propagation characteristics. A higher dissipation factor (tan δ) will result in stronger attenuation, regardless of frequency [81]. It has also been suggested that water ingress will affect the propagation characteristics of cables due to the substantial relative permittivity of water ($\varepsilon_r \approx 80$, at room temperature). The magnitude of this effect would be difficult to quantify because the extent of water infiltration cannot be reliably deduced, and it can be inhomogeneous both in terms of the extent of the cable affected as well as the degree of water saturation [72]. This problem is more likely to affect older types of cables, as modern XLPE cables usually incorporate considerable structural defense features to avert water infiltration, both in the radial and longitudinal directions.

The effect of cable joints on pulse propagation should also be considered. Simulation results suggest that the degree of reflection which occurs at joints increases with frequency [83], but as higher frequencies are rapidly attenuated during propagation regardless, the effect on PD measurements performed at cable terminations is likely insignificant.

The PD detection sensitivity is deemed optimal if the signal-to-noise ratio of the detection device is the highest. This requirement is generally fulfilled if the bandwidth of the PD detector matches the frequency content of the PD pulse. In practice, this implies that in case of cables, the PD detection bandwidth should be inversely dependent on the expected distance to the PD source being measured. A bandwidth which is too high may introduce substantially more noise into the measurements, while a bandwidth which is too narrow will result in a significant loss of pulse frequency spectrum information. Considering the nature of PD detection in power cables, HFCTs are usually a feasible compromise. The detection characteristics of HFCTs can be manipulated, to an extent, by altering design features such as the winding turns ratio and ferrite core complex permeability. [47]

Simulation studies have suggested that PD detection over shorter lengths of cable, below approximately 1 km, is more effective using high-bandwidth detectors. Over longer lengths, the difference between the sensitivity of conventional IEC 60270-compliant detectors and UWB detectors diminishes. However, the measured pulse peak value will always be higher in case of UWB detection, as the IEC 60270 frequency band is a subset of the ultra-wide band. [84]

The nature of the PD source will also affect the degree of pulse distortion. For example, a longer rise time Townsend-like pulse will contain fewer high-frequency components and will therefore experience less distortion as it propagates through the cable compared to a shorter rise-time pulse caused by a streamer-like discharge [78].

3.7 Aspects of partial discharge pulse behavior

Considering cavities inside power cable insulation, it has been observed that PD activity is more pronounced during the negative half-cycle. This behavior can be explained by the fact that the electric field inside the cavity is stronger at the side closer to the phase conductor and the negatively charged interface between the cavity and solid insulation is the origin of the initiatory electron which triggers the PD [85]. It is reasonable to assume the degree of discrepancy in behavior between positive and negative half-cycles increases with the size of the cavity and the relative position of the cavity inside the insulation.

Advancements in understanding of PD mechanisms have aided in producing reliable models to predict characteristics of PD activity in solid insulation. As an extension, these insights can also be exploited for the analysis of PD in power cables. Modeling has been shown to enable predicting the behavior of PD inside a spherical cavity with a remarkable degree of accuracy under different voltage magnitudes and frequencies [86]. Models which are used to predict the behavior of PD incorporate, besides the geometry of the PD defect and surrounding media, parameters which inherently determine the triggering of discharges [87, 88]: inception electric field, residual electric field, charge deposited onto the void-dielectric interface, thermal trapping and de-trapping of electrons on the cavity surface, natural radiation as a source of free electrons and statistical operators to mimic the probabilistic nature of PD. Although modeling efforts have been successful, there are still limitations in the fundamental understanding of PD processes in voids, which do not, at present, permit the development of a model which relies on a fully mechanistic physical description of the PD process [87]. However, a sufficiently accurate model may be used to aid in interpreting PD measurement results and making detailed assumptions regarding the shape, position and other attributes of the PD source.

3.8 Testing the accuracy of PD source location using time-domain reflectometry

To assess the accuracy of PD source identification in power cables, an experiment was devised on a 20 kV cable containing artificially created defects [III]. The test setup used for measuring PDs is depicted in Figure 22. For the measurement of wave propagation velocity, a PD calibrator was temporarily connected in a de-energized state as described in the figure. During the PD measurements, the cable was energized using a variable HV source, and the PDIV of the cable was determined to be 13.5 kV (phase-to ground). In order to increase the PD activity level and obtain sufficient discharges from both defects, the applied voltage was raised to 20 kV prior to taking PD measurements.

The cable terminations are designated as End 1 and End 2, with the measurement equipment connected at End 1. This involved connecting a coupling capacitor (1 nF) at End 1 of the cable in series with the measuring impedance of a commercial IEC 60270-compliant PD measuring system. The 20 kV single-phase XLPE-insulated MV cable with length L = 199.3 m remained open-circuited at End 2. The cable contained two insulation defects, a knife cut at a mechanically measured distance of s_1 = 2.4 m from End 1 and a hole with an approximate diameter of 2 mm drilled into the cable such that it penetrated the sheath and outer semiconducting layer into the XLPE insulation, at a mechanically measured distance of s_2 = 27.8 m from End 1.

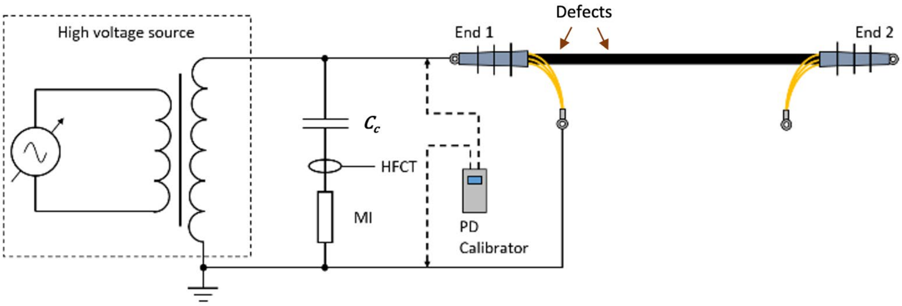

Figure 22. Principal schematic depicting the test setup for partial discharge measurement in an open-ended medium voltage power cable in a laboratory environment. C_c – coupling capacitor; HFCT – high frequency current transformer; MI – measuring impedance of commercial PD measurement system.

The parameters of the HFCT used in the tests are:

- Transfer ratio 1:10
- Bandwidth 0.5 to 80 MHz (−3 dB)

The HFCT secondary was connected via coaxial cable to a digital storage oscilloscope (DSO) and terminated using a 50 Ω impedance. In addition to the equipment deployed for recording the waveforms of PD pulses, a commercial PD measuring system was used for simultaneously monitoring other parameters, such as PD apparent charge magnitude, repetition rate etc. The measuring impedance was contained within a quadrupole, which effectively functions as a voltage divider in combination with the coupling capacitor and the signal acquired from the quadrupole was also used to record the applied voltage waveform using the DSO. An example of the captured PD waveform data is shown in Figure 24. The data were recorded at a sampling rate of 200 MS/s (5 ns per sample) and further analysis was performed using MATLAB.

To determine the pulse velocity prior to measurement, calibration was performed by injecting a pulse into the cable at the near end using a dedicated pulse calibrator. The calibration measurement is provided in Figure 23. Applying TDR principles, the apparent pulse velocity is determined using (8) and found to obtain a value of v_p = 174.5 m/µs.

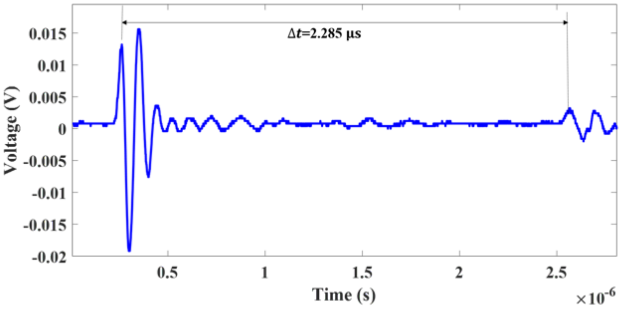

Figure 23. Original and reflected pulses measured in the tested cable post injection with partial discharge calibrator

Several measurements were recorded in order to analyze the PD activity. The measurements were recorded at the upper memory limit of the DSO (1,000,000 samples) and the sampling rate 200 MS/s was chosen such that it enables sufficiently accurate representation of the PD waveform. This amounts to a length of 5 ms per acquisition, i.e., one quarter-cycle of the 50 Hz AC cycle. As some noise is always present when measuring PD, the waveforms were also denoised using the discrete wavelet transform (DWT) technique. The effect of denoising is illustrated in Figure 24.

For analyzing the individual PD pulses in the time domain, two PD signals have been chosen as shown in Figure 24. These PD signals have been identified based on the behavior post initial pulse, which includes reflections and contains information regarding the distances at which the sources are positioned. Figure 25 depicts a recording of PD from the source closest to the cable near-end termination, denominated “PD type 1”, presenting with two reflections at certain intervals following the first (original) PD pulse. A PD pulse from the second, slightly more distant source, denominated “PD type 2” is depicted in Figure 27, where three clearly recognizable pulses and one semi-distinguishable pulse are observed following the original PD pulse. Considering the apparent behavior, further investigation is made based on TDR principles. At this point, two basic inferences can be drawn. Firstly, PD activity is present on the cable, which indicates there is at least one insulation defect from which pulses are emitted. Secondly, two types of reflection behaviors indicate the presence of two PD sources at different locations. Further analysis will elucidate the nature of the PD activity in more detail.

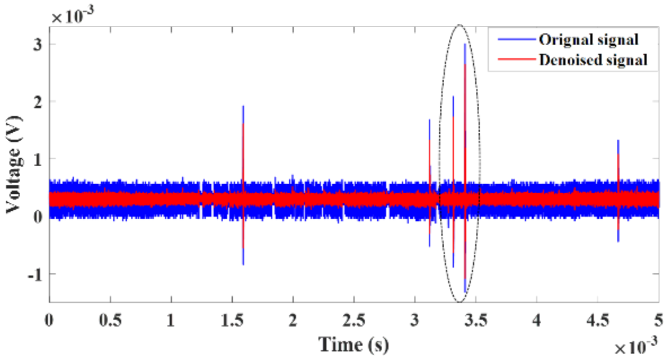

Figure 24. Example of partial discharge data recorded over one quarter-cycle of AC voltage, raw signal and denoised signal (wavelet filter)

3.8.1 Partial discharge type 1

From Figure 25, it can be observed that Pulse 1 or the original pulse appears at $t_1 = 0$ µs, Pulse 2 appears at $t_2 = 2.255$ µs while Pulse 3 appears at $t_3 = 4.540$ µs. Considering the length of the cable (two-way propagation length) is 398.6 m and the propagation velocity is 174.5 m/µs, it can be assumed that any pulse appearing within the time frame 2.285 µs, which is the time required for the pulse to travel twice the length of the cable, after Pulse 1 can be the 1st reflection of the pulse originating from the PD source, which has reflected from the opposite end of the cable. The time difference between Pulse 1 and Pulse 2 is $\Delta t_{12} = 2.255$ µs. Applying (9), the defect location can be determined as $x_1 = 2.6$ m.

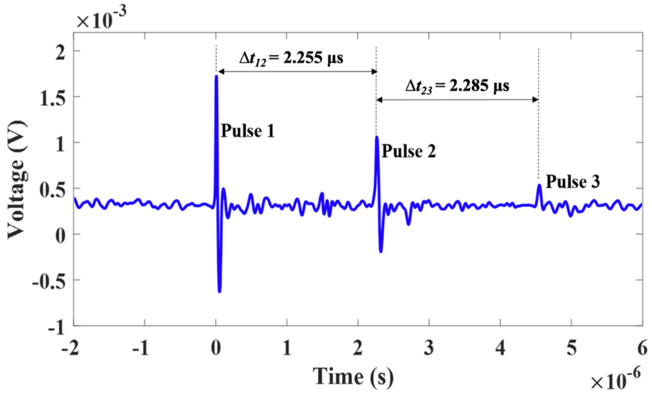

Figure 25. Original pulse and reflections recorded from 1st partial discharge source

It can also be observed that Pulse 3 appears after a time difference Δt_{23} = 2.285 µs after the second pulse. To examine the cause of this behaviour, it is beneficial to construct a lattice diagram (Figure 26) to illustrate the pulse transition across the cable. The peak of Pulse 1 detected at End 1 is chosen as the origin of the time axis.

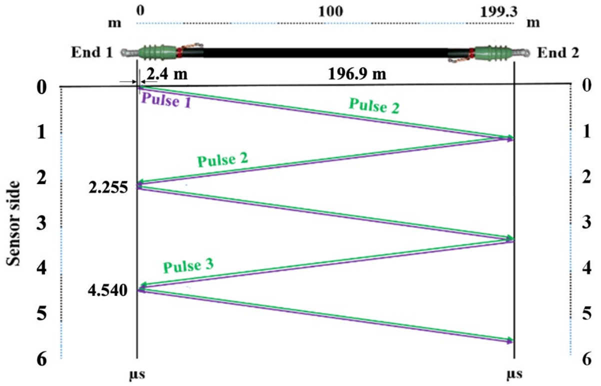

Figure 26. Lattice diagram illustrating the propagation of pulses from partial discharge source 1 in the cable

Considering that the PD defect is located at a manually measured distance of s_1 = 2.4 m from end 1, the PD occurs at its source and generates two pulses (Purple and Green) which simultaneously propagate towards either end of the cable. In an arbitrary reference timeframe, the Purple pulse covering the distance of 2.4 m reaches the HFCT at t = 0 µs as Pulse 1, while towards the other end of the cable, the Green pulse propagates and is reflected from End 2, continues its propagation towards End 1 and is detected by the HFCT as Pulse 2, at t_2 = 2.255 µs. The time interval 2.255 µs corresponds to a distance of 393.5 m. After having been registered and reflected from End 1, pulse Green again travels towards End 2, reflects and reaches End 1 (as Pulse 3), where it is recorded once again.

When Pulse 1 (Purple) is measured by the HFCT at instant t_1 = 0 µs, it also reflects from End 1 and travels towards End 2. Having reflected from End 2, it travels towards End 1. At this instant, both the Purple and Green pulses are travelling towards End 1 with Purple following Green at a distance of 4.8 m and reaching End 1 at a time of approximately

2.285 µs. The difference of the time of arrival is approximately 0.03 µs between the two pulses, which is too small to be resolved and these are detected as a single pulse. In addition, comparing the amplitude of the PD pulses after each reflection, significant attenuation can be observed, and after Pulse 3, the travelling waves are practically undetectable.

3.8.2 Partial discharge type 2

The second type of PD signals are illustrated in Figure 27. The first (original) PD signal Pulse 1 (pulse Purple in in the lattice diagram depicted on Figure 28) is detected at t_1 = 0 µs and its first reflection Pulse 2 (pulse Green) is recorded at t_2 = 1.970 µs. Similarly, the subsequent reflections Pulse 3 and Pulse 4 are registered at times t_3 = 2.280 µs and t_4 = 4.255 µs, respectively. A final reflection, Pulse 5, can also be distinguished at t_5 = 4.565 µs, although this is borderline. As analysed previously for PD type 1, the first pulse and the first reflection are used to determine the location of the PD-producing defect, while the remaining reflections carry information regarding the propagation behaviour of the PD pulses between the cable ends. The difference of arrival time between Pulse 1 and Pulse 2 is Δt_{12} = 1.970 µs. Applying (9), the defect location can be determined as x_2 = 27.4 m.

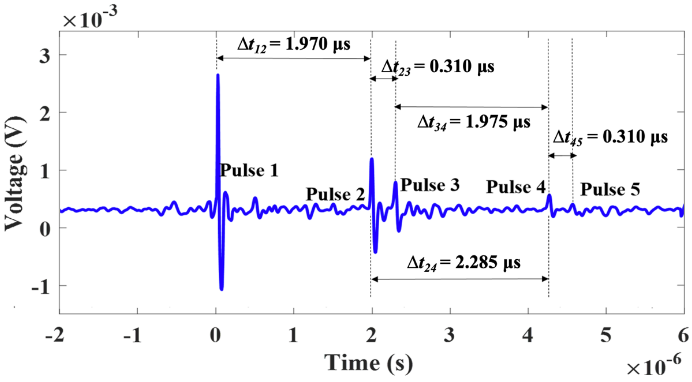

Figure 27. Original pulse and reflections recorded from 2nd partial discharge source

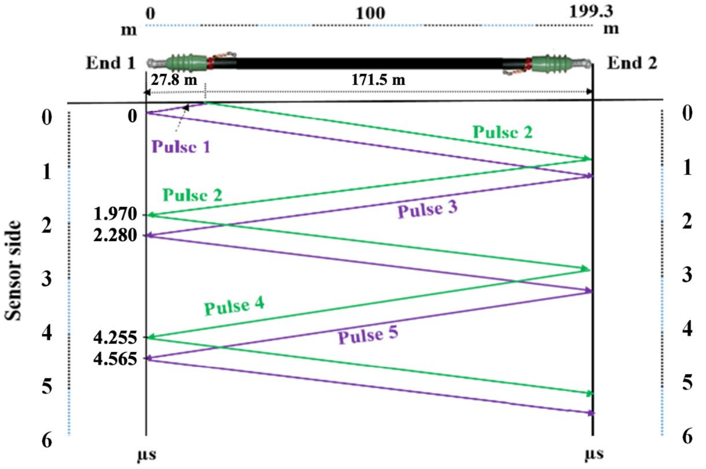

Figure 28. Lattice diagram illustrating the propagation of pulses from partial discharge source 2 in the cable

Due to greater distance of the defect from the measurement end compared to PD type 1, the two travelling pulses are spaced further apart and can be distinguished in the recorded waveform. Generated at the defect site (manually measured at 27.8 m from End 1), Pulse 1 (Purple) reaches the measuring instrument at $t = 0$, while simultaneously pulse Green is travelling towards End 2. Pulse Purple is reflected from End 1 and starts to propagate towards End 2, following pulse Green at a distance of approximately 55.6 m (2×27.8 m). After being reflected from End 2, both reach End 1 and are recorded at $t_2 = 1.970$ µs and $t_3 = 2.280$ µs, respectively. Similarly, continuing after their reflections from End 1 and returning after reflection from End 2, the pulses are recorded again as Pulse 4 and Pulse 5 at $t_4 = 4.255$ µs and $t_5 = 4.565$ µs, respectively. The lattice diagram illustrates the propagation behaviour of PD type 2 and depicts the mechanically measured location of the PD defect at 27.8 m from End 1 of the cable.

3.8.3 Defect location accuracy and discussion

The location of both PD defects has been determined and they appear to be located at a distance of 24.8 m from each other ($x_2 - x_1$), based on the TDR analysis of their individual pulses. Comparing both signals of PD type 1 and PD type 2 in a time reference where the original (first) pulses are simultaneous, it can be observed that the time difference of the reflected pulses (0.285 µs) reaffirms the distance between both faults on the cable as shown in Figure 29.

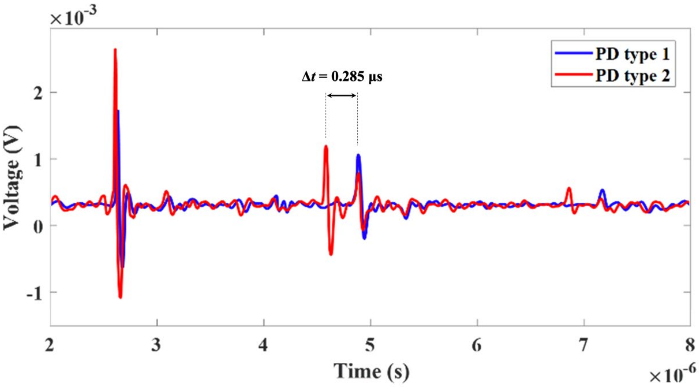

Figure 29. Signals from sources PD type 1 and PD type 2 overlaid on each other

With dual confirmation of the locations of the PD defects, the TDR findings can be compared to the actual location of the defects which caused the PD. As mentioned previously, the MV cable used in this experimental investigation has two defects. The locations of both defects have been manually measured at $s_1 = 2.4$ m and $s_2 = 27.8$ m, while the experimentally inferred distances are $x_1 = 2.6$ m and $x_2 = 27.4$ m. The difference in these location estimates is:

$$\Delta = x - s \tag{13}$$

The difference of the manually measured locations and the locations inferred using TDR therefore produce a difference of $\Delta_1 = +0.2$ m and $\Delta_2 = -0.4$ m. This indicates a good match between the actual and TDR-based locations of the PD defects. An error below 1 m is not practically significant.

There are some sources of uncertainty, which contribute to the mismatch in defect location measurement: the effective length of the cable, taking into account the termination parts and also the finite signal sampling rate have an effect. Although the distances of the defect points from the cable end were measured meticulously, these are still subject to various measurement errors. The manually measured distances were determined using the sequential numeric meter markings inscribed on the cable sheath by the manufacturer and a tape measure was used to determine the distance of the cable lugs and the defect locations from the nearest distance marker. The cable ends were unrolled from a cable drum; therefore, some residual curvature was also present. To account for these factors, the manually measured locations are presented with a conservative accuracy of 0.1 m.

The measurements were recorded using a sampling period of 5 ns. This translates to a spatial resolution of approximately 0.872 m corresponding to one sample, considering the pulse velocity. This also implies that it is in practice not possible to distinguish defects at a very small distance from each other, at least not without using other means in addition to TDR.

Another important aspect to note is the time delay between subsequent reflections. Consider the time delay between Pulse 1 and Pulse 3 or Pulse 2 and Pulse 4 in Figure 27. These are Δt_{13} = 2.280 µs and Δt_{24} = 2.285 µs, respectively. Comparing these to the time delay recorded with the calibration pulse (Figure 25), it is apparent that these match almost perfectly. This raises the question whether or not calibration is necessary at all, because the subsequent reflections can be exploited to determine the pulse propagation velocity. Although the PD pulse experiences attenuation and dispersion as it propagates across the cable, as discussed in the literature, the shift in the measured peak location of the pulse is apparently not significant enough to cause a noticeable error in PD source location and the apparent pulse velocity in the cable remains effectively constant over the duration of its propagation along the cable. Apparently, the necessity to perform calibration for the purpose of pulse velocity determination is therefore dependent on the length of the cable. The subsequent, or even the first reflections and original inbound PD pulses may be attenuated too strongly for detection before reaching the measuring instrument in case the distance is too great. The specific structural parameters of the tested cable also have an influence on the results, further validation of these findings with measurements on different types of cables of various lengths should be considered.

4 Differentiating partial discharge sources based on pulse characteristics and phase-resolved patterns

To investigate the problem of PD source separation, three distinct PD sources were studied in a laboratory environment, each of which represents a PD subtype, as shown in Figure 30. The sources were energized, one at a time, with 50 Hz AC voltage and the PD pulses were measured, at a voltage slightly above the PDIV, using a HFCT [IV]. The PD activity was recorded using a digital storage oscilloscope (DSO) with a bandwidth of 80 MHz at a sampling rate of 250 MS/s. The sources of PD and the voltage levels associated with these were:

- corona discharge – a pin-plane electrode configuration, HV is applied to the pin (PDIV 11 kV; PDs measured at 12 kV)
- internal discharge – a small incision was made into the outer sheath of a MV power cable segment, approximately 3 m long, which penetrates into the insulation (PDIV 6.5 kV; PDs measured at 8 kV)
- surface discharge – a damaged cable termination (PDIV 8 kV; PDs measured at 10 kV)

A principal schematic of the test setup is provided in Figure 31.

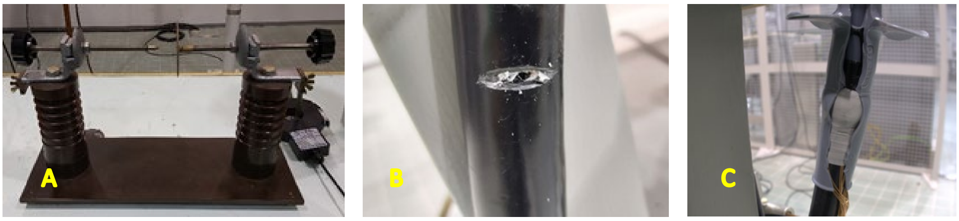

Figure 30. Partial discharge sources used in the tests to distinguish different types of PD: A) corona discharge, B) internal discharge, C) surface discharge

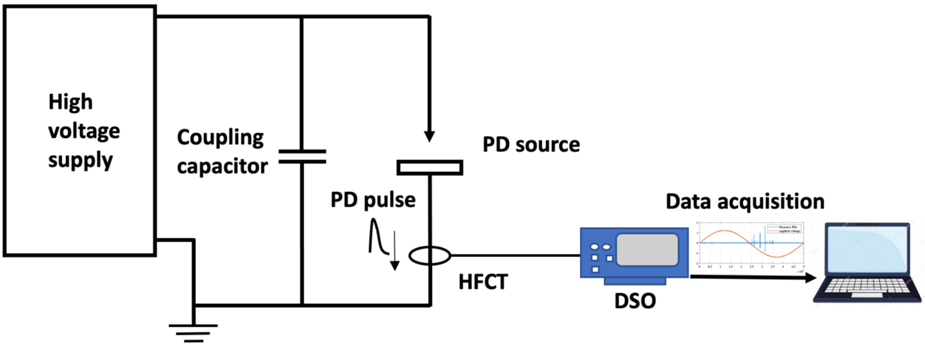

Figure 31. General schematic of test setup for measuring partial discharge pulses. HFCT – high frequency current transformer, DSO – digital storage oscilloscope

4.1 Data processing and partial discharge related parameters

The measured data were processed in MATLAB to extract a series of characteristic quantities to represent each type of PD source. Software-based data processing included the following stages:

- PD data denoising
- pulse identification and quantification
- accumulating pulse parameters extracted from full-cycle PD data into data arrays to describe PD activity during the positive and negative half-cycles
- calculating characteristic parameters for half-cycles of both polarity
- plotting the graphs for PRPD and pulse waveforms

From the measured data, the PD-related parameters were calculated. Based on these, the sources are compared and the utility of the calculated parameters for distinguishing between different types of PD sources is evaluated:

- pulse count n
- maximum peak pulse value p_{max}
- minimum peak pulse value p_{min}
- mean peak pulse value μ_p
- normalized standard deviation of pulse peak value σ_{pn}

$$\sigma_{pn} = \frac{\sigma_p}{\mu_p} \tag{14}$$

- first pulse time t_f (the smallest discharge epoch observed during any half-cycle of either positive or negative polarity)
- last pulse time t_l (the largest discharge epoch observed during any half-cycle of either positive or negative polarity)
- phase span of PD activity t_{PD}

$$t_{PD} = t_l - t_f \tag{15}$$

- maximum pulse width w_{max}
- minimum pulse width w_{min}
- mean pulse width μ_w
- pulse width standard deviation σ_w
- pulse width span w_{span}

$$w_{span} = w_{max} - w_{min} \tag{16}$$

- maximum pulse interval (intervals are calculated only for half-cycles during which at least two pulses occurred) τ_{max}
- minimum pulse interval τ_{min}
- mean pulse interval μ_τ

- pulse interval standard deviation σ_τ
- pulse interval normalized standard deviation $\sigma_{\tau n}$

$$\sigma_{\tau n} = \frac{\sigma_\tau}{\mu_\tau} \tag{17}$$

- maximum voltage difference between pulses Δu_{max} (the difference of the instantaneous value of the energizing voltage during subsequent PD pulses; voltage differences are considered for half-cycles during which at least two pulses occurred. The absolute values of voltage differences are considered, due to the possibility of the parameter attaining both positive and negative values depending on whether the pulses occur before or after the peak of the half-cycle).
- minimum voltage difference between pulses Δu_{min}
- mean voltage difference between pulses $\mu_{\Delta u}$
- normalized standard deviation of the voltage difference between pulses $\sigma_{\Delta un}$; here also the absolute values of voltage differences are used to calculate the standard deviation.

$$\sigma_{\Delta un} = \frac{\sigma_{\Delta u}}{\mu_{\Delta u}} \tag{18}$$

- correlation coefficient of pulses r; the Pearson correlation coefficient is calculated for the pulses with the smallest and largest width and for both polarities of pulses. Samples captured from 200 ns before the pulse peak to 800 ns after the peak are included in the calculation. Pulses originating from the same source are, in general, expected to present with a similar shape, which is the reason this parameter is evaluated.

$$r = \frac{\operatorname{cov}(P_1, P_2)}{\sigma_{P_1}\sigma_{P_2}} = \frac{\sum_{i=1}^{k}\left(P_{1_i} - \overline{P_1}\right)\left(P_{2_i} - \overline{P_2}\right)}{\sqrt{\sum_{i=1}^{k}\left(P_{1_i} - \overline{P_1}\right)^2}\sqrt{\sum_{i=1}^{k}\left(P_{2_i} - \overline{P_2}\right)^2}} \tag{19}$$

Where: P_1 – sampled waveform of 1st pulse;
P_2 – sampled waveform of 2nd pulse;
P_{1_i}– discrete samples of 1st pulse waveform;
P_{2_i}– discrete samples of 2nd pulse waveform;
$\overline{P_1}$ – sample mean of 1st pulse waveform;
$\overline{P_2}$ – sample mean of 2nd pulse waveform;
σ_{P_1}– standard deviation of 1st pulse waveform;
σ_{P_2}– standard deviation of 2nd pulse waveform;
k– total number of samples per waveform.

- interval – peak value ratio normalized standard deviation; this parameter is associated with the effect of space charges on PD activity. For every two consecutive pulses occurring during the rising portion of every half-cycle at times t_{i-1} and t_i, the first with a peak value of p_{i-1}, the parameter I_i is calculated according to (20). To characterize the statistical spread of I_i, the mean value μ_I, standard deviation σ_I, and normalized standard deviation σ_{In} are also calculated.

$$I_i = \frac{t_i - t_{i-1}}{p_{i-1}} \tag{20}$$

$$\sigma_{In} = \frac{\sigma_I}{\mu_I} \tag{21}$$

- voltage difference – peak value ratio normalized standard deviation; this parameter is also associated with the effect of space charges on PD activity. For every two consecutive pulses occurring during the rising portion of every half-cycle at instantaneous voltage values of u_{i-1} and u_i, the first of which has a peak value of p_{i-1}, the parameter V_i is calculated according to (22). To characterize the statistical spread of V_i, the mean value μ_V, standard deviation σ_V and normalized standard deviation σ_{Vn} are also calculated. The quantities used to calculate the pulse interval and voltage difference ratios to the preceding pulse peak value are graphically depicted in Figure 32.

$$V_i = \frac{u_i - u_{i-1}}{p_{i-1}} \tag{22}$$

$$\sigma_{Vn} = \frac{\sigma_V}{\mu_V} \tag{23}$$

In this discussion, the pulse width refers to the width of the pulse at half of the peak value. The values of all of the aforementioned parameters were determined for PD activity for both the positive and negative half-cycle of the applied voltage using each source. In addition, the positive-to-negative half-cycle ratio was calculated for each parameter, i.e., the parameter value corresponding to the positive half-cycle was divided by the value corresponding to the negative half-cycle for determining the asymmetry of PD behavior between the positive and negative half-cycles with regard to the parameter in question.

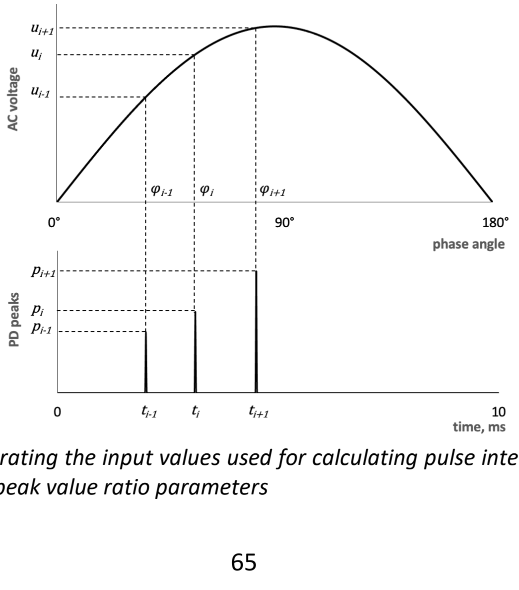

Figure 32. Graphic illustrating the input values used for calculating pulse interval-peak value ratio and voltage difference-peak value ratio parameters

4.2 Partial discharge measurement results and discussion

The PRPD patterns of each of the PD sources are presented in Figure 33. Additionally, the negative polarity pulses with the maximum and minimum width at half value for every PD source are also provided in Figure 34. Table 5 contains the full range of calculated parameters describing the PD activity of each source. The results are based on the PD recorded over 7 full AC voltage cycles.

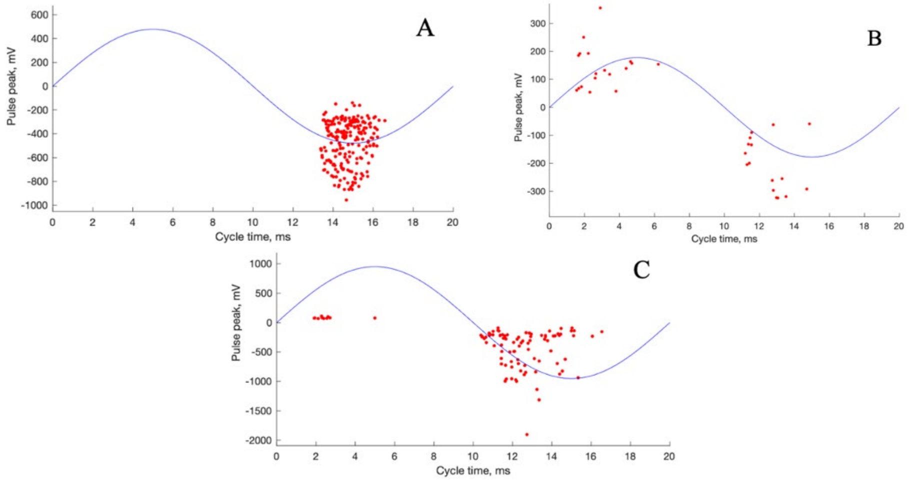

Figure 33. Phase-resolved partial discharge patterns for each of the PD sources: A) corona discharge, B) internal discharge, C) surface discharge

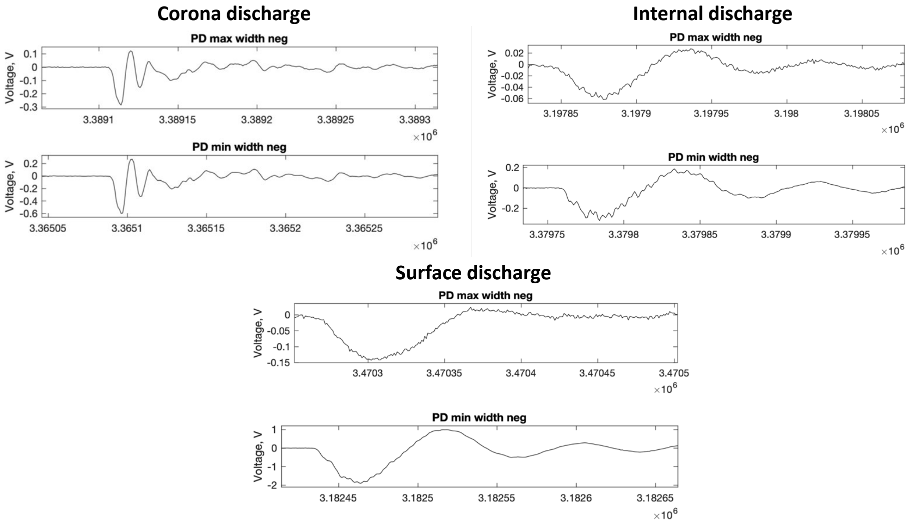

Figure 34. Negative pulses with maximum and minimum width recorded with the different partial discharge sources

The results of the tests indicate that there are numerous parameters which may be used to distinguish between different types of PD sources. While the behavior of PD is somewhat different in any real-world scenario, the features of PD activity are inherently linked to the mechanism which produces it. The behavior of PD sources is also influenced by the degree to which the energizing voltage exceeds the inception voltage, e.g., higher voltages can also invoke corona discharge during the positive half-cycle. The presented measurements were collected at voltages which are representative of the difference in behavior of PD sources. The parameters which provided the strongest indication of difference between the sources are discussed as follows (also marked in bold in Table 5).

Table 5. Parameters characterizing partial discharge in the three types of sources, for positive and negative half-cycles and their ratio (SD – standard deviation)

	Corona	**Internal**			**Surface**		
Parameters	**neg**	**pos**	**neg**	**pos /neg**	**pos**	**neg**	**pos/neg**
pulse count	209	18	16	1.13	10	92	0.11
max peak (mV)	956	355	324	1.10	111	1902	0.06
min peak (mV)	139	54	59	0.91	68	90	0.76
mean peak (mV)	472	143	201	0.71	82	432	0.19
normalized SD peak	0.39	0.53	0.48	1.12	0.16	0.76	0.21
first pulse time (ms)	3.39	1.56	1.19	1.31	1.91	0.39	4.88
last pulse time (ms)	6.59	6.22	4.86	1.28	5.00	6.54	0.76
phase span (ms)	3.20	4.67	3.67	1.27	3.08	6.15	0.50
pulse width max (ns)	36	164	164	1.00	148	236	0.63
pulse width min (ns)	32	104	116	0.90	132	144	0.92
pulse width mean (ns)	32	142	139	1.02	140	160	0.88
pulse width SD (ns)	1.0	13.6	12.1	1.12	5.1	12.1	0.42
pulse width span (ns)	4	60	48	1.25	16	92	0.17
max interval (ms)	0.37	3.57	1.97	1.82	2.61	1.52	1.72
min interval (ms)	0.04	0.34	1.37	0.25	0.60	0.01	73.5
mean interval (ms)	0.09	1.56	1.67	0.93	1.27	0.40	3.22
pulse interval SD (ms)	0.05	0.88	0.20	4.37	1.15	0.27	4.29
normalized SD interval	0.49	0.57	0.12	4.67	0.91	0.68	1.33
max voltage difference (kV)	0.36	5.44	6.01	0.91	4.50	2.53	1.78
min voltage difference (kV)	∼0	1.08	2.54	0.42	1.93	0.03	57.8
mean voltage difference (kV)	0.09	3.48	4.85	0.72	2.83	0.94	3.00
normalized SD voltage difference	0.97	0.41	0.24	1.69	0.51	0.61	0.84
correlation of pulse waveforms	0.98	0.96	0.97	0.99	0.99	0.64	1.54
normalized SD interval-peak ratio	0.56	0.40	0.60	0.66	0.93	0.86	1.08
normalized SD voltage diff.-peak ratio	0.99	0.45	0.46	0.99	0.54	0.87	0.62

4.2.1 Pulse count

Corona and surface discharge indicated strong asymmetry between pulse counts over the positive and negative half-cycles. If the voltage is low enough, there might even be a complete absence of pulses during the positive half-cycle, as is the case with corona discharge in this test. In case of internal discharge, the pulse counts are similar during both half-cycles, as might be expected.

4.2.2 Maximum peak value of the pulse

In case of internal discharge, the peak value is approximately equal during both the positive and negative half-cycles. In case of surface discharge, the maximum value is significantly smaller during the positive half-cycle compared to the negative half-cycle. In case of corona, higher pulse peaks are expected during the positive half-cycle.

4.2.3 Mean peak value of the pulse

Similarly to the maximum peak pulse value, the asymmetry of mean peak value is substantially larger in case of surface discharge compared to internal discharge. In case corona discharges occur during both the positive and negative half-cycles, it is again expected to see much larger peaks during the positive half-cycle.

4.2.4 Phase span

The phase span of internal discharges is similar for both half-cycles. In case of both corona and surface discharges, the phase span is notably smaller or non-existent for the positive half-cycle. This can be explained with the increased supply of electrons during the negative half-cycle.

4.2.5 Pulse width parameters

The width of PD pulses is closely related to the discharge mechanism. Provided that detection equipment with a suitably high bandwidth is used, as is the case in this study, it is possible to distinguish PD pulses from different sources based on pulse width. The detector properties and transmission line characteristics will also have an impact on the pulse shape and consequently, the measured pulse waveform is always somewhat distorted. Regardless, the measured pulses exhibit distinctly different width characteristics, which can be exploited for identification of different PD sources.

The width of negative corona pulses was significantly smaller than that of the pulses from other sources, providing a reliable criterion to identify the existence of this type of discharge. From Table 5, it is apparent that there was no overlap between the pulse width ranges of corona and the other two PD sources. Also, there was small variability in the width of corona pulses. The width of internal and surface discharge pulses was similar, although in case of internal discharges, the maximum pulse width was equal for both polarities. This is anticipated, as the process of internal discharge is inherently curtailed by the cavity size in which it occurs. The data also suggest that the maximum and mean pulse widths of surface discharge are notably larger during the negative half-cycle.

It should also be noted that the accuracy of data regarding pulse widths is somewhat diminished due to the finite sampling rate. However, this effect does not reach an extent at which it would invalidate the aforementioned inferences.

4.2.6 Pulse interval parameters

The time interval between pulses can also provide information regarding the PD sources, as this is affected by the space charges deposited at the source from previous PD activity, or, particularly in case of corona discharge, lack thereof. As expected, the mean interval is smallest for corona and largest for internal PD. In case of surface PD, the mean interval is significantly smaller during the negative half-cycle, as can be predicted based on the notably larger pulse count. Also, the mean interval of internal PD is approximately equal for both polarities, as anticipated.

4.2.7 Voltage difference parameters

As expected, the smallest variability in the applied voltage differences between subsequent pulses is observed with internal discharge, also the maximum voltage difference between pulses during the same half-cycle is approximately equal for both polarities. This is also reflected upon consideration of the magnitude of the preceding pulse (last row of Table 5), as that value was lower in comparison to corona and surface discharge.

4.2.8 Correlation of pulse shape at maximum and minimum pulse widths

The Pearson correlation coefficient was relatively high (> 0.95) in most cases, as is to be expected in case there is only one active PD source and the pulses are generated under consistent circumstances. The only exception to this was the negative half-cycle of the surface discharge with a correlation of 0.64. This reflects the large difference in the maximum and minimum pulse widths, which can also be observed in Figure 34. Apparently, surface discharges can produce a larger variety of pulse widths, possibly due to the less constrained discharge propagation conditions at the surface of the insulation.

4.3 Applicability of the parameter-based approach in distinguishing PD sources

From these data, it can be inferred that there are numerous possibilities to distinguish different types of PD sources. In simple cases, with only one source, it may not be particularly difficult to make an accurate assessment of the type and nature of the PD source. With multiple simultaneous active sources however, the diagnosis can be challenging and with the availability of several relevant metrics, arrival to an accurate interpretation can be simplified. Exploiting as many of the previously discussed parameters in the analysis of PD activity, in an appropriate manner, can aid in the diagnosis process. Some parameters, e.g., pulse width, can provide a strong indication regarding the presence of corona. Others, e.g., pulse interval parameters, can provide suggestive indications, but not always a conclusive diagnosis. The nature of the equipment being tested, e.g., cable, transformer, or GIS, and their typical defects should also be considered. Data from other researchers suggest that the surface discharge pattern can be similar to what was observed in the experiment [34], or it can also mimic the phase pattern of internal discharge [89]. Subsequent experiments also corroborated the variability of surface discharge patterns.

Another important observation which stemmed from the analysis of PD activity, is the complexity in choosing initial parameters for post-processing of measured data. In order to facilitate any analysis of individual PD pulses, these must first be identified from the measurement results. As described previously, this can be challenging when there is substantial noise present. In these measurements, the level of background noise was low enough not to pose a serious problem and the thresholding method was used to distinguish PD pulses. The other facet of this problem is related to the interval between PD pulses. As it is necessary to avoid identifying pulse reflections and the oscillations of the detector post excitation by an authentic PD pulse as further original PD pulses, a “dead time” parameter was introduced. This specifies a time interval of quiescence following a PD pulse peak, during which any peaks which might otherwise be accounted for as pulses, are discarded from inclusion into subsequent data processing. The implementation of these pulse identification parameters is illustrated in Figure 35.

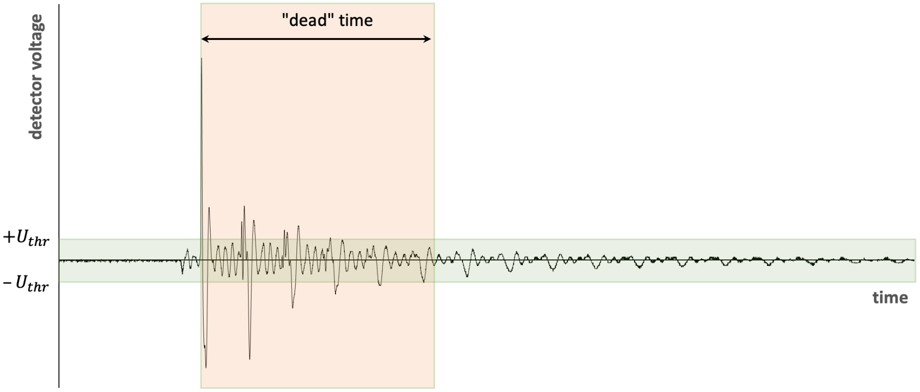

Figure 35. Measured partial discharge activity including one authentic PD pulse, oscillations of detection equipment, and pulse reflections. Shaded areas represent pulse rejection zones across the voltage and time domains. U_{thr} *– PD pulse detection threshold voltage.*

It is apparent that the choice of values for the threshold voltage and dead time parameters have a profound impact on any analysis regarding PD activity, which succeeds the pulse identification stage. If either parameter is assigned a value which is too low, these will be ineffective. If the values are excessively high, this can result in extensive omission of authentic PD pulses from the resulting dataset, followed by a potentially erroneous interpretation regarding the nature of recorded PD activity. Therefore, for any PD dataset, there is a mean range of optimal values for each of these parameters, which produces the highest number of actual PD pulses while discarding the highest number of noise and inauthentic PD pulses. Identifying values which approximate these optima can require multiple iterations along with significant time and involvement by the person performing the analysis.

There are, of course, other potential modalities to approach this problem of pulse discrimination. The threshold and dead time parameters do not necessarily have to remain static across the entire dataset. It might also be feasible to assign a lower threshold value and apply an algorithm to discriminate PD from noise on a pulse-to-pulse basis. Often the noise pulses can be highly regular in terms of their intervals and peak values, particularly when generated as a result of the operation of a power electronic device and can be distinguished based on these attributes.

4.4 Intermediate summary

Several PD-related parameters were calculated based on measurements performed on three different PD sources, each of which represented a distinct type of PD: corona discharge, internal discharge, and surface discharge. The values of these parameters were calculated for both the positive and negative half-cycle and the asymmetry of the parameters was also elucidated by determining the positive half-cycle value relative to the negative half-cycle value. The parameters which provided the most significant degree of difference between the sources and can be used in distinguishing multiple simultaneous PD sources, are:

- pulse count
- peak values (maximum, mean and standard deviation)

- phase of PD pulses (first pulse, last pulse, phase span)
- pulse width (minimum, maximum, mean standard deviation, span)
- sequential pulse intervals
- sequential pulse voltage differences
- correlation between pulse waveforms

Utilizing these parameters in the analysis of PD activity can provide numerous approaches to identify simultaneous active PD sources and component defects. The parameters could also be used for the development of computer-aided PD recognition algorithms. Further work can involve developing these methods and testing their feasibility for on-site implementation.

Conclusion

Partial discharge (PD) is a significant challenge for modern power grids. This thesis discusses some important implications of PD concerning covered conductors (CCs) and power cables.

PD causes degradation of CC overhead lines and some relevant aspects of the process which determine the rapidity of progression to breakdown of the insulation were studied. It was found that in comparison with cross-linked polyethylene (XLPE), an insulating cover consisting of regular polyethylene (PE), or varieties thereof, appears to exhibit higher resilience under the influence of a strong electric field and PD activity. Although PE and XLPE are very similar materials, there are some plausible factors which can contribute to the superior performance of PE. These include the absence of additives in the insulation formula used to chemically mediate the cross-linking process, and the absence of water, which forms as a by-product of the cross-linking reaction. The variability of insulation quality across different manufacturers also appears to influence the results of durability tests to a significant degree. However, the confidence of the XLPE *vs* PE comparison is somewhat limited due to high variability in test results and further investigation regarding this topic is warranted.

Further tests conducted to elucidate the nuances which affect the failure time of CCs under electric stress revealed that the amount of total surface area exposed to the strong electric field appears to correlate well with decreased withstand time. The peak electric field strength appeared to be positively correlated with a longer withstand time of the insulation. This apparent paradox can, however, be explained by the self-limiting effect of strong electric fields. These generate PDs and space charges in the air surrounding the solid polymeric insulation and at the interface of the two media, counteracting the electric field imposed by electrode potentials. While this does have an effect on the effective field strength, a substantial amount of corrosive substances is also produced. PD byproducts create chemical stress in the insulation, which starts to degrade. The results suggest that the dominant factors which determine the time-to-failure of CC insulation are (a) the presence of weaker spots in the insulation and (b) the intensity of PD activity in the immediate vicinity of the insulation.

As the adoption rate of CCs increases, it might be useful to improve the resilience of CC OHLs in the future by introducing requirements for the manufactured conductors to be subjected to a standardized test to verify that these can withstand contact with a grounded object for a predetermined amount of time, e.g., 60 days. This could provide reassurance to electrical utilities and improve grid reliability. The feasibility and expedience of this approach should be further evaluated by the relevant technical authorities, and, if found to be reasonable, the test conditions specified, e.g., general setup, energizing voltage and atmospheric parameter tolerances.

The tests investigating the location accuracy of PD in medium voltage (MV) power cables indicate that use of high-frequency current transformers (HFCTs) can achieve a level of accuracy which is adequate for locating PD sources. In sufficiently short cables, the calibration process used to determine pulse propagation velocity might not be necessary, in case subsequent pulse reflections of actual PD pulses are not excessively attenuated and can be detected. The time delay between these reflections can also be used to determine pulse velocity in the cable with a sufficient degree of accuracy. The primary factor which limits the accuracy of PD source detection under controlled laboratory conditions appears to be the sampling rate of measurement equipment.

There are some aspects related to on-line monitoring, which may cause some additional uncertainty in PD measurements. It is necessary to utilize pulse propagation velocity in the PD source location process and the most reliable method to determine this parameter is to measure it immediately prior to the measurement of PD. The velocity of high-frequency pulses in cables is dependent on several parameters, notably temperature, and can therefore vary depending on ambient ground conditions and cable load. The accuracy of PD source location can therefore be enhanced if the velocity of pulse frequency components is more accurately determined. Provided that different manufactures use different formulations for producing the semiconducting layers of the cable, which have a profound impact on pulse propagation characteristics, this relationship is difficult to determine analytically, perhaps insurmountably so for practical implementation. It may be prudent to require manufacturers to measure and report the pulse propagation characteristics of their cables, i.e., $\gamma(f)$ or $v_p(T)$ under a specific set of predefined conditions, including different temperatures, in the future. This would enable compensation of location errors due to the variability of pulse velocity during on-line monitoring through computational means, improving the diagnostic process.

The results from PD differentiation experiments indicate that there are some key features which can be useful for discriminating PD sources. Pulse width is one of these, as it appears to be very useful in detecting the presence of negative corona discharge. Intervals between subsequent PD pulses can also be exploited to distinguish sources and negative corona exhibits a very particular behavior in terms of pulse intervals. These observations imply that it should be possible to reliably recognize the presence of corona discharges in measured data, at least during the negative half-cycle. As corona can often be considered harmless, these pulses can be omitted from further analysis, after which classification efforts should focus on the identification and discrimination of internal discharge and surface discharge sources. There may, of course, be instances where the aforementioned general principles do not apply and further investigations to delineate such circumstances should be performed. For example, pulse shapes may become excessively distorted after propagation through a long cable, to an extent that they may lose a significant degree of their characteristic pulse shape. The gathered data also reaffirmed some prior knowledge regarding the general attributes of different types of PD, e.g., their phase-resolved pattern, pulse counts and half-cycle asymmetry characteristics.

Another significant challenge which was revealed is the difficulty in automating PD analysis. Due to the presence of noise, pulse reflections, and oscillations of the PD sensor output, it is necessary to omit these non-authentic PD pulses dispersed throughout the gathered data from analysis directed towards interpretation of the nature of PD sources. This can be achieved, e.g., by implementing a minimum detection threshold for PD pulses (e.g., 10 mV) and specifying a time period of dormancy (e.g., 10 μs) immediately following an identified PD pulse, during which the pulses which may be present in initially measured data are discarded from the dataset subjected to further analysis. If the values of the threshold and dormancy parameters are excessively low, they will become ineffective in filtering out the undesirable pulses. If the values are too high, however, this can result in the omission of a substantial number of genuine PD pulses, leading to an erroneous conclusion regarding the extent or nature of the PD activity. A method to optimize the selection process of these initial post-processing parameters should be created, or some alternative perspectives regarding this problem could be tested, e.g., an approach based on machine learning.

In summary, the main findings of the thesis, briefly reiterated, are:

- PE is, on average, a more durable insulation material for use in MV CC overhead lines, from the perspective of electrical stress
- In case of a round conductive object in contact with a CC, the rate of progression to insulation breakdown is positively dependent on the curvature radius of the object
- The time period until breakdown occurrence is primarily determined by the size of the insulation area exposed to elevated electrical stress and the intensity of PD activity
- In short MV power cables, the accuracy of PD source location with time-domain reflectometry using HFCTs is sufficient for practical applications and does not require pulse calibration prior to measurement
- Corona, internal and surface discharge can be effectively distinguished by utilizing parameters to describe their phase-resolved patterns and individual pulse parameters

Future work

The findings of this thesis have elucidated some possible directions for further research. Unresolved questions regarding the performance of MV CCs include further clarifying whether or not PE actually is effectively more resilient than XLPE under electric stress. Designing an experiment with a sufficiently high number of test samples might detect a statistically and practically significant difference between the durability of the two materials under electrical stress. Investigating approaches to improve the resilience of both PE and XLPE under combined electrical, mechanical, and chemical stress might enable the development of more robust CC insulation. For example, the feasibility of including additives which confer antioxidant capacity into the insulation formula could be studied. It might also prove beneficial to investigate the degree to which parameters of the trees, e.g., species, age, moisture, etc., which come into contact with CCs have an effect on survival time characteristics, as well as the dependence of survival time on mechanical contact pressure.

Other suggestions include the development of PD pattern recognition algorithms and on-line monitoring systems. The rapid identification of PD problems would aid electric utilities in maintaining their grid, accelerating repair and refurbishment operations, and improving reliability. Efforts should be made to surmount the previously discussed difficulties concerning PD analysis. The ultimate objective would be to design a system capable of monitoring and assessing PD on-line autonomously, which would equal or surpass the performance of a human expert in interpretation of PD activity.

List of figures

Figure 1. Radial cross-section of a typical medium voltage covered conductor with two layers of insulating material 17
Figure 2. Macromolecular structure of different types of polyethylene: A) LDPE, B) HDPE, C) XLPE 19
Figure 3. Principle schematic illustrating grounded copper wire winding placement on covered conductor surface during voltage stress tests 23
Figure 4. Principle schematic depicting the general arrangement and connections of the test setup for covered conductor insulation durability testing 24
Figure 5. Photograph of grounded copper wire winding around covered conductor (left). The discoloration of insulation caused by prolonged surface discharges at the edges of the winding is evident. Photograph of winding acquired in a darkened room using a 30 second shutter delay (right) reveals notable surface discharge activity........ 25
Figure 6. FEM simulation of electric field strength in covered conductor insulation and surrounding air at test voltage instantaneous peak value 19.8 kV (cross-section along the longitudinal axis of the conductor). The x-axis is provided in reference to the values presented in Figure 7. 26
Figure 7. Modelled electric field strength at different depths in the insulation and air across the grounded copper wire winding at test voltage instantaneous peak value (19.8 kV). 26
Figure 8. Electric durability test results for different covered conductors. The columns represent the three puncture times of grounding points ranked from shortest to longest and the mean. 27
Figure 9. Principle schematic of grounding electrode types used in the study of covered conductor durability. A – 5 mm round wire, B – 25 mm round pipe; C – 125 mm round pipe; D – aluminium tape; E – copper wire winding. 30
Figure 10. Withstand times of individual grounding points and overall mean withstand times of electrode types in sequence of increasing durability. Mean withstand time is not provided for electrode types regarding which some grounding locations did not puncture over the duration of the test........ 31
Figure 11. Kaplan-Meier plot for the survival rate of all tested electrode configurations during withstand testing of the XLPE-insulated conductor 33
Figure 12. Estimated two-parameter Weibull cumulative distribution functions describing the failure rates of the 125 mm round conductor, 25 mm round conductor and copper wire winding electrodes. Dashed lines represent cumulative distribution function curves corresponding to 95% confidence interval boundaries for scale parameter α... 34
Figure 13. Electric field strength (FEM model) at the highest stressed sites of the different electrode types used: A) aluminium tape; B) copper wire winding; C) 5 mm round conductor 36
Figure 14. Modelled electric field strength at test voltage instantaneous peak value (19.8 kV) directly above the surface of the insulation for different electrode types. The locations corresponding to the highest electric stress are aligned with the origin of the x-axis (zoomed-in view). 36
Figure 15. Modelled electric field strength at test voltage instantaneous peak value (19.8 kV) directly above the surface of the insulation for different electrode types. The locations corresponding to the highest electric stress are aligned with the origin of the x-axis (wide view). 37

Figure 16. Electric field strength inside solid insulating material and gas-filled void in insulation 39
Figure 17. Types of partial discharge in an insulation system: A) corona discharge, B) internal discharge, C) surface discharge 41
Figure 18. Partial discharge pulse waveforms. Left: Idealized PD current pulse shape (double exponential wave); right: actual PD pulse measured using a high-frequency current transformer. 43
Figure 19. Principle topology of partial discharge measurement. Left: IEC 60270 compliant measurement setup; right: high-frequency current transformer (HFCT) placement around ground terminal of test object. TO – test object, C_c – coupling capacitor, Z_m – measurement impedance, MI – measuring instrument. 45
Figure 20. Radial cross-section of a typical XLPE-insulated medium voltage power cable .. 47
Figure 21. Equivalent circuit model for XLPE insulated power cable at high frequencies .. 52
Figure 22. Principal schematic depicting the test setup for partial discharge measurement in an open-ended medium voltage power cable in a laboratory environment. C_c – coupling capacitor; HFCT – high frequency current transformer; MI – measuring impedance of commercial PD measurement system. 56
Figure 23. Original and reflected pulses measured in the tested cable post injection with partial discharge calibrator 56
Figure 24. Example of partial discharge data recorded over one quarter-cycle of AC voltage, raw signal and denoised signal (wavelet filter) 57
Figure 25. Original pulse and reflections recorded from 1st partial discharge source 58
Figure 26. Lattice diagram illustrating the propagation of pulses from partial discharge source 1 in the cable 58
Figure 27. Original pulse and reflections recorded from 2nd partial discharge source ... 59
Figure 28. Lattice diagram illustrating the propagation of pulses from partial discharge source 2 in the cable 59
Figure 29. Signals from sources PD type 1 and PD type 2 overlaid on each other 60
Figure 30. Partial discharge sources used in the tests to distinguish different types of PD: A) corona discharge, B) internal discharge, C) surface discharge 62
Figure 31. General schematic of test setup for measuring partial discharge pulses. HFCT – high frequency current transformer, DSO – digital storage oscilloscope 62
Figure 32. Graphic illustrating the input values used for calculating pulse interval-peak value ratio and voltage difference-peak value ratio parameters 65
Figure 33. Phase-resolved partial discharge patterns for each of the PD sources: A) corona discharge, B) internal discharge, C) surface discharge 66
Figure 34. Negative pulses with maximum and minimum width recorded with the different partial discharge sources 66
Figure 35. Measured partial discharge activity including one authentic PD pulse, oscillations of detection equipment, and pulse reflections. Shaded areas represent pulse rejection zones across the voltage and time domains. U_{thr} – PD pulse detection threshold voltage 70

List of tables

Table 1. Insulation composition and presence of semiconducting layer on the studied conductors 23
Table 2. Tentative ranking of different grounding electrodes based on expected covered conductor insulation puncture time characteristics (in order of decreasing expected puncture time) 31
Table 3. Estimated Weibull distribution parameters of the three electrode types which produced failures at all grounding locations, with 95% confidence intervals 33
Table 4. Results of log-rank tests to evaluate the difference in durability between different electrode types 35
Table 5. Parameters characterizing partial discharge in the three types of sources, for positive and negative half-cycles and their ratio (SD – standard deviation).......... 67

References

[1] J. B. Wareing, “Covered Conductor Systems for Distribution,” EA Technology, 2005.

[2] A. Kasparans, M. Budahs and J. Rozenkrons, “20 kV Insulated Overhead Lines Overvoltage Protection Problems in Latvia’s Distribution Network,” in *Electric Power Quality and Supply Reliability Conference*, Viimsi, Estonia, 2006.

[3] M. Lehtonen, “Fault Rates of Different Types of Medium Voltage Power Lines in Different Environments,” in *Electric Power Quality and Supply Reliability Conference*, Kuressaare, Estonia, 2010.

[4] Y. Ojala, T. Leskinen, M. Lahtinen and A. Hinkkuri, “110 kV Overhead Transmission Line With Covered Conductors,” in *CIGRE Session*, Paris, 1998.

[5] R. Bravo, E. Pham, A. Luy, J. Rorabaugh and E. Hutchinson, “12kV Covered Conductor Testing,” in *IEEE/PES Transmission and Distribution Conference and Exposition (T&D)*, Chicago, IL, USA, 2020.

[6] G. C. Silva, F. Piazza and M. Munaro, “Field Behavior on Polymer-Covered Overhead Conductors Submitted to Natural Aging on Diverse Weather and Geographic Conditions in Brazil,” *IEEE Transactions on Power Delivery,* vol. 24, no. 3, 2009.

[7] F. Nishimura, L. D. Cicarelli, M. Coelho, B. Trager and M. R. Soares, “Covered Cable Comparative Testing: HDPE and XLPE Evaluation,” in *IEEE/PES Transmission and Distribution Conference and Exposition*, Atlanta, 2001.

[8] A. M. Nóbrega, M. L. B. Martinez and A. A. A. d. Queiroz, “Investigation and Analysis of Electrical Aging of XLPE Insulation for Medium Voltage Covered Conductors,” *IEEE Transactions on Dielectrics and Electrical Insulation,* vol. 20, no. 2, 2013.

[9] T. Leskinen and V. Lovrenčić, “Finnish and Slovene Experience of Covered Conductor Overhead Lines,” in *CIGRE Session*, Paris, 2004.

[10] W. Panosch, K. Schongrundner and K. Kominek, “20 kV Overhead Lines with Covered Conductors,” in *International Conference and Exhibition on Electricity Distribution*, Amsterdam, 2001.

[11] G. Eduful and K. N. Asante, “In Search of Electric Power Reliability in Forested Terrain with Covered Conductors: the ECG Experience,” in *IEEE 4th International Conference on Adaptive Science & Technology (ICAST)*, Kumasi, Ghana, 2012.

[12] M. Isa, “Partial Discharge Location Technique for Covered-Conductor Overhead Distribution Lines,” Aalto University School of Electrical Engineering, Espoo, Finland, 2013.

[13] P. Pakonen, “Detection of Incipient Tree Faults on High Voltage Covered Conductor Lines,” Tampere University of Technology, Tampere, Finland, 2007.

[14] Y. Mecheri, M. Nedjar, A. Lamure, M. Aufray and C. Drouet, “Influence of Moisture on the Electrical Properties of XLPE Insulation,” in *Annual Report Conference on Electrical Insulation and Dielectric Phenomena (CEIDP)*, West Lafayette, IN, USA, 2010.

[15] F. M. Defandorf, “Electrical Resistance to the Earth of a Live Tree,” *Transactions of the American Institute of Electrical Engineers. Part III: Power Apparatus and Systems,* vol. 75, no. 3, 1956.

[16] H. Lehtinen, I. Lehtinen and A. Hinkkuri, “Research on Covered Medium-voltage Overhead Lines in Finland,” in *International Conference on Electricity Distribution (CIRED)*, Brighton, UK, 1989.

[17] J. Vehanen and P. Hyvönen, “Diagnosis of Medium Voltage Covered Conductors (in Finnish: Päällystetyn keskijänniteavojohdon kunnon diagnosointi),” Espoo, 2003.

[18] S. Mišák, Š. Hamacek, P. Bilík, M. Hofinek and P. Petvaldský, “Problems Associated with Covered Conductor Fault Detection,” in *11th International Conference on Electrical Power Quality and Utilisation*, Lisbon, 2011.

[19] P. Pakonen, “Characteristics of Partial Discharges of Trees in Contact with Covered Conductor Lines,” *IEEE Transactions on Dielectrics and Electrical Insulation,* vol. 15, no. 6, 2008.

[20] E. A. Feilat, “Lifetime Assessment of Electrical Insulation,” in *Electric Field*, IntechOpen, 2018.

[21] “IEC 50397-1:2006 Covered conductors for overhead lines and the related accessories for rated voltages above 1 kV AC and not exceeding 36 kV AC. Part 1: Covered conductors”.

[22] CIGRE, “Knowledge Rules for Partial Discharge Diagnosis in Service,” 2003.

[23] G. C. Stone, “Partial Discharge Diagnostics and Electrical Equipment Insulation Condition Assessment,” *IEEE Transactions on Dielectrics and Electrical Insulation,* vol. 12, no. 5, pp. 891-903, 2005.

[24] R. Arora and W. Mosch, High Voltage and Electrical Insulation Engineering, Hoboken, New Jersey: John Wiley & Sons, Inc., 2011.

[25] R. Bartnikas, “Partial Discharges: Their Mechanism, Detection and Measurement,” *IEEE Transactions on Dielectrics and Electrical Insulation,* vol. 9, no. 5, pp. 763-808, 2002.

[26] R. J. Van Brunt, “Physics and Chemistry of Partial Discharge and Corona: Recent Advances and Future Challenges,” *IEEE Transactions on Dielectrics and Electrical Insulation,* vol. 1, no. 5, pp. 761-784, 1994.

[27] A. Pedersen, G. C. Grichton and I. W. McAllister, “The Theory and Measurement of Partial Discharge Transients,” *IEEE Transactions on Electrical Insulation,* vol. 26, no. 3, pp. 487-497, 1991.

[28] E. Kuffel and W. S. Zaengl, High Voltage Engineering Fundamentals, Pergamon Press, 1984.

[29] D. Benzerouk, “Pulse Sequence Analysis and Pulse Shape Analysis: Methods to Analyze Partial Discharge Processes,” University of Siegen, 2008.

[30] “IEEE Guide for Conducting Corona Tests on Hardware for Overhead Transmission Lines and Substations,” IEEE, New York, 2017.

[31] P. H. F. Morshuis, “Degradation of Solid Dielectrics due to Internal Partial Discharge: Some Thoughts on Progress Made and Where to Go Now,” *IEEE Transactions on Dielectrics and Electrical Insulation,* vol. 12, no. 5, pp. 905-913, 2005.

[32] J. C. Devins, “The Physics of Partial Discharges in Solid Dielectrics,” in *Conference on Electrical Insulation & Dielectric Phenomena*, Claymont, DE, USA, 1984.

[33] P. H. F. Morshuis, “Partial Discharge Mechanisms,” Delft University Press, Delft, Netherlands, 1993.

[34] H. Illias, T. S. Yuan, A. H. A. Bakar, H. Mokhlis, G. Chen and P. L. Lewin, “Partial Discharge Patterns in High Voltage Insulation,” in *IEEE International Conference on Power and Energy*, Kota Kinabalu Sabah, Malaysia, 2012.

[35] S. A. Boggs and G. C. Stone, “Fundamental Limitations in the Measurement of Corona and Partial Discharge,” *IEEE Transactions on Electrical Insulation,* Vols. EI-17, no. 2, 1982.

[36] “IEC 60270:2000 High-voltage test techniques – Partial discharge measurements”.

[37] M. Hashmi, S. Hänninen and M. Lehtonen, “Intelligent Fault Diagnosis for On-line Condition Monitoring in Smart Distribution Networks,” in *IEEE International Conference on Condition Monitoring and Diagnosis*, Bali, Indonesia, 2012.

[38] G. A. Hussain, M. Shafiq, L. Kumpulainen, F. Mahmood and M. Lehtonen, “Performance Evaluation of Noise Reduction Method During On-line Monitoring of MV Switchgear for PD Measurements by Non-intrusive Sensors,” *Electrical Power and Energy Systems,* vol. 64, pp. 596-607, 2015.

[39] M. Muhr, T. Strehl, E. Gulski, K. Feser, E. Gockenbach, W. Hauschild and E. Lemke, “Sensors and Sensing Used for Non-conventional PD Detection,” in *CIGRE*, 2006.

[40] CIGRE, “Partial Discharge Detection in Installed Extruded Cable System,” 2001.

[41] M. Shafiq, M. Lehtonen, G. A. Hussain and L. Kütt, “Performance Evaluation of PD Monitoring Technique Integrated Into Medium Voltage Cable Network for Smart Condition Assessment,” in *Electric Power Quality and Supply Reliability Conference*, Rakvere, Estonia, 2014.

[42] R.-N. Wu and C.-K. Chang, “The Use of Partial Discharges as an Online Monitoring System for Underground Cable Joints,” *IEEE Transactions on Power Delivery,* vol. 26, no. 3, pp. 1585-1591, 2011.

[43] P. L. Lewin, J. Steele-Davies, S. M. Rowland, V. M. Catterson, C. Johnstone and C. Walton, “The State of the Art of Condition Monitoring: Where Do We Go from Here?,” in *Insucon 2013: 12th International Electrical Insulation Conference*, Stafford, UK, 2013.

[44] M. M. Yaacob, M. A. Alsaedi, J. R. Rashed, A. M. Dakil and S. F. Atyah, “Review on Partial Discharge Detection Techniques Related to High Voltage Power Equipment Using Different Sensors,” *Photonic Sensors,* vol. 4, no. 4, pp. 325-337, 2014.

[45] E. Gulski, E. Lemke, M. Gamlin, E. Gockenbach, W. Hauschild and E. Pultrum, “Experiences in Partial Discharge Detection in Distribution Power Cable Systems,” *Electra,* June 2003.

[46] A. Rodrigo, P. Liovera, V. Fuster and A. Quijano, “Calibration Constant and Associated Uncertainty of High Frequency Current Transformers for Off-line or On-line Partial Discharge Measurement in High Voltage Insulated Cables,” in *CIGRE Session*, Paris, 2014.

[47] M. Tozzi, “Partial Discharges in Power Distribution Electrical Systems: Pulse Propagation Models and Detection Optimization,” University of Bologna, 2010.

[48] “IEC 60885-3:2015 Electrical test methods for electric cables- Part 3: Test methods for partial discharge measurements on lengths of extuded power cables”.

[49] B. T. Phung, Z. Liu, T. R. Blackburn, G. Burgess, P. McMullan, H. Zhang and A. Zagari, "On-Line Monitoring of MV and HV Distribution Cables using VHF Partial Discharge Detection," in *CIGRE Session*, Paris, 2008.

[50] B. T. Phung, Z. Liu, T. Blackburn, G. Burgess, P. McMullan and H. Zhang, "Diagnostic Testing and On-line Condition Monitoring of Cable Systems Based on Partial Discharge Measurements," in *CIGRE Session*, 2014.

[51] B. Fruth and D. Gross, "Interpretation of Digital Partial Discharge Measurements," in *IEE Colloquium on PD Display Systems and Analytical Software*, London, UK, 1996.

[52] S. Sriram, S. Nitin, K. M. M. Prabhu and M. J. Bastiaans, "Signal Denoising Techniques for Partial Discharge Measurements," *IEEE Transactions on Dielectrics and Electrical Insulation,* vol. 12, no. 6, pp. 1182-1191, 2005.

[53] F. Garnacho, Sánchez-Uran, M., J. Ortego, J. Moreno, F. Álvarez, J. L. Vallejo, B. Losada and J. Gonzalo, "Partial Discharge Monitoring System for High Voltage Cables," in *CIGRE*, 2010.

[54] L. Renforth, R. MacKinlay and M. Seltzer-Grant, "Deployment of Distribution Online Partial Discharge Monitoring Devices on Medium Voltage Electricity Networks," in *20th International Conference on Electricity Distribution*, Prague, Czech Republic, 2009.

[55] F. Steennis, P. Wagenaars, P. van der Wielen, P. Wouters, Y. Li, T. Broersma, D. Harmsen and P. Bleeker, "Guarding MV Cables On-line: With Travelling Wave Based Temperature Monitoring, Fault Location, PD Location and PD Related Remaining Life Aspects," *IEEE Transactions on Dielectrics and Electrical Insulation,* vol. 23, no. 3, pp. 1562-1569, 2016.

[56] A. R. Mor, P. H. F. Morshuis, P. Llovera, V. Fuster and A. Quijano, "Localization Techniques of Partial Discharges at Cable Ends in Off-line Single-Sided Partial Discharge Cable Measurements," *IEEE Transactions on Dielectrics and Electrical Insulation,* vol. 23, no. 1, pp. 428-434, 2017.

[57] W. Lewandowski, G. Petit and C. Thomas, "Precision and Accuracy of GPS Time Transfer," *IEEE Transactions on Instrumentation and Measurement,* vol. 42, no. 2, pp. 474-479, 1993.

[58] B. Li, H. Li, X. Zeng, W. He and X. Zeng, "Novel Time Synchronization Method based on Duo-Satellite Triggering for Double-Ended PD Location in MV Cables," in *1st International Conference on Electrical Materials and Power Equipment*, Xi'an, China, 2017.

[59] M. Motoyama, S. Ohtsuka, H. Suzuki and K. Abe, "Partial Discharge Localization Method of Power Cable using High-precision Synchronization by Atomic Clocks," in *International Conference on Condition Monitoring and Diagnosis*, Beijing, China, 2008.

[60] P. C. J. M. van der Wielen, J. Veen, P. A. A. F. Wouters and E. F. Steennis, "Time-base Alignment of PD Signals Measured at Multiple Cable Ends," in *Proceedings of the 2004 IEEE International Conference on Solid Dielectrics*, Toulouse, France, 2004.

[61] Y. Li, P. A. A. F. Wouters, P. Wagenaars, J. M. van der Wielen and E. F. Steennis, "Temperature Dependent Signal Propagation Velocity: Possible Indicator for MV Cable Dynamic Rating," *IEEE Transactions on Dielectrics and Electrical Insulation,* vol. 22, no. 2, pp. 665-672, 2015.

[62] A. Cavallini, G. C. Montanari and F. Puletti, “A Novel Method to Locate PD in Polymeric Cable Systems Based on Amplitude-frequency (AF) Map,” *IEEE Transactions on Dielectrics and Electrical Insulation,* vol. 14, no. 3, pp. 726-734, 2007.

[63] N. C. Sachoo, M. M. A. Salama and R. Bartnikas, “Trends in Partial Discharge Pattern Classification: A Survey,” *IEEE Transactions on Dielectrics and Electrical Insulation,* vol. 12, no. 2, pp. 248-264, 2005.

[64] W. J. K. Raymond, H. A. Illias, A. H. A. Bakar and H. Mokhlis, “Partial Discharge Classifications: Review of Recent Progress,” *Measurement,* vol. 68, pp. 164-181, 2015.

[65] A. Krivda, “Automated Recognition of Partial Discharges,” *IEEE Transactions on Dielectrics and Electrical Insulation,* vol. 2, no. 5, pp. 796-821, 1995.

[66] M. Wu, H. Cao, C. Jianneng, H.-L. Nguyen, J. B. Gomes and S. P. Krishnaswamy, “An Overview of State-of-the-Art Partial Discharge Analysis Techniques for Condition Monitoring,” *IEEE Electrical Insulation Magazine,* vol. 31, no. 6, pp. 22-35, 2015.

[67] L. Hao, P. Lewin, D. Swaffield and C. Walton, “A New Method for Automatic Multiple Partial Discharge Classification,” in *XVII International Symposium on High Voltage Engineering*, Hannover, Germany, 2011.

[68] T. K. Abdel-Galil, R. M. Sharkawy, M. M. A. Salama and R. Bartnikas, “Partial Discharge Pulse Pattern Recognition Using an Inductive Inference Algorithm,” *IEEE Transactions on Dielectrics and Electrical Insulation,* vol. 12, no. 2, pp. 320-327, 2005.

[69] S. Biswas, D. Dey, B. Chatterjee and S. Chakravorti, “An Approach Based on Rough Set Theory for Identification of Single and Multiple Partial Discharge Source,” *Electrical Power and Energy Systems,* vol. 46, pp. 163-174, 2013.

[70] P. C. J. M. van der Wielen and E. F. Steennis, “On-Line PD Monitoring System for MV Cable Connections with Weak Spot Location,” in *2008 IEEE Power and Energy Society General Meeting - Conversion and Delivery of Electrical Energy in the 21st Century*, Pittsburgh, PA, USA, 2008.

[71] A. N. Cuppen, E. F. Steennis and P. C. J. M. van der Wielen, “Partial Discharge Trends in Medium Voltage Cables Measured While In-service with PDOL,” in *IEEE PES Transmission and Distribution Conference and Exposition*, 2010.

[72] J. P. Steiner and P. H. Reynolds, “Estimating the Location of Partial Discharges in Cables,” *IEEE Transactions on Electrical Insulation,* vol. 27, no. 1, pp. 44-59, 1992.

[73] O. E. Gouda and Z. Matter, “Effect of the Temperature Rise on the XLPE Dielectric Properties,” in *Proceedings of the 35th Midwest Symposium on Circuits and Systems*, Washington, DC, USA, 1992.

[74] R. Sarathi, K. H. Oza and L. G. Pavan Kumar, “Electrical Treeing in XLPE Cable Insulation Under Harmonic AC voltages,” *IEEE Transactions on Dielectrics and Electrical Insulation,* vol. 22, no. 6, pp. 3177-3185, 2015.

[75] D. A. Fynes-Clinton, D. R. Cornish and C. Nyamupangedengu, “Partial Discharge Patterns of Typical Installation Defects in MV Power Cable Terminations,” in *19th International Symposium on High Voltage Engineering*, Pilsen, Czech Republic, 2015.

[76] G. Mugala, “Influence of the Semi-conducting Screens on the Wave Propagation Characteristics of Medium Voltage Extruded Cables,” Royal Institute of Technology, Stockholm, Sweden, 2003.

[77] G. Mugala, R. Eriksson and P. Pettersson, “Dependence of XLPE Insulated Power Cable Wave Propagation Characteristics on Design Parameters,” *IEEE Transactions on Dielectrics and Electrical Insulation,* vol. 14, no. 2, pp. 393-399, 2007.

[78] F. H. Kreuger, M. G. Wezelenburg, A. G. Wiemer and W. A. Sonneveld, “Partial Discharge. XVIII. Errors in the Location of Partial Discharges in High Voltage Solid Dielectric Cables,” *IEEE Electrical Insulation Magazine,* vol. 9, no. 6, pp. 15-24, 1993.

[79] R. Paludo, G. C. Silva and V. S. Filho, “The Study of Semiconductor Layer Effect on Underground Cables with Time Domain Reflectometry (TDR),” *IOSR Journal of Electrical and Electronics Engineering,* vol. 7, no. 6, pp. 1-7, 2013.

[80] G. C. Stone and S. A. Boggs, “Propagation of Partial Discharge Pulses in Shielded Power Cable,” in *Conference on Electrical Insulation & Dielectric Phenomena*, Amherst, MA, USA, 1982.

[81] H. N. J. O, *Propagation of High Frequency Partial Discharge Signal in Power Cables,* University of New South Wales, 2009.

[82] M. Tozzi, A. Cavallini, G. C. Montanari and G. Burbui, “PD Detection in Extruded Power Cables: An Approximate Propagation Model,” *IEEE Transactions on Dielectrics and Electrical Insulation,* vol. 15, no. 3, pp. 832-840, 2008.

[83] M. Mahdipour, A. Akibari and P. Werle, “Cable Joints Effect in Partial Discharge Signal Propagation,” in *20th International Symposium on High Voltage Engineering*, Buenos Aires, Argentina, 2017.

[84] S. Chandrasekar, A. Cavallini, G. C. Montanari and F. Puletti, “Bandwidth and Sensitivity Issues in PD Detection in Power Cables,” *IEEE Transactions on Dielectrics and Electrical Insulation,* vol. 14, no. 3, pp. 735-743, 2007.

[85] H. A. Illias, M. E. Othman, M. A. Tunio, A. H. A. Bakar, H. Mokhlis, G. Chen and P. L. Lewin, “Measurement and Simulation of Partial Discharge Activity Within a Void Cavity in a Polymeric Power Cable Model,” in *IEEE International Conference on Solid Dielectrics*, Bologna, Italy, 2013.

[86] H. Illias, G. Chen and P. L. Lewin, “Partial Discharge Behavior Within a Spherical Cavity in a Solid Dielectric Material as a Function of Frequency and Amplitude of the Applied Voltage,” *IEEE Transactions on Dielectrics and Electrical Insulation,* vol. 18, no. 2, pp. 432-443, 2011.

[87] G. Callender and P. L. Lewin, “Modeling Partial Discharge Phenomena,” *IEEE Electrical Insulation Magazine,* vol. 36, no. 2, pp. 29-36, 2020.

[88] G. Ala, R. Candela, P. Romano and F. Viola, “Simplified Hybrid PD Model in Voids,” in *8th IEEE Symposium on Diagnostics for Electrical Machines, Power Electronics & Drives*, 2011.

[89] O. Kozák and J. Pihera, “Partial Discharge Analysis and Simulation Using the Consecutive Pulses Correlation Method,” *Energies,* vol. 14, no. 9, 2021.

Acknowledgements

Several people have contributed in some way or another into this thesis coming to fruition and to them I owe thanks.

I would like to express my gratitude, first and foremost, to my supervisors Paul Taklaja and Ivo Palu for their efforts and guidance, which have helped me navigate the PhD chapter of my educational journey. I am also very grateful to my colleagues and co-authors, with whom it is always a pleasure to conduct research and, every once in a while, withdraw from the business end of things to enjoy some leisurely activities, or simply enrich the day with the occasional jest. I would especially like to thank Muhammad Shafiq for his contribution to the work we have done, and Kaur Tuttelberg, who helped primarily with computer modelling.

I would also like to acknowledge everybody at the university who have moulded it into a fabulous institution, especially those who work hard and help keep the show going, yet mostly operate outside the limelight.

I am thankful to the companies we have collaborated with and who have trusted us to help them solve challenging real-world problems, while also inspiring interesting avenues of research.

I am grateful to SA Archimedes, for supporting my participation at scientific conferences. This work was also supported by the Estonian Research Council’s grant PSG632 “Aging Behaviour of Medium Voltage Cables under Smart Grid Operation”.

Last, but not least, I am also very grateful to my family and friends, who have been supportive of my various endeavours, while also helping nudge me along the path towards the completion of my studies.

Abstract
Insulation durability and measurement of partial discharge

This work addresses issues associated with medium voltage (MV) covered conductor (CC) durability, partial discharge (PD) measurement and classification. The thesis was motivated by the problems faced by contemporary electrical utilities and recent trends in high voltage engineering. The main methodologies utilized in the research included conducting laboratory tests on various CCs, MV power cables, and artificially created PD sources, analysing gathered data using regular and advanced data processing software (e.g., MATLAB) and performing computations of electric field shape using the finite element method (FEM).

Distribution grid utilities often deploy CCs in MV power lines to increase their reliability. However, trees often fall on overhead power lines and can cause faults after a period of time due to overstressing the insulation and subsequent breakdown of the insulating layer. Aspects of this process are investigated to gain a better understanding of the factors which influence the durability of CCs under these circumstances, including the choice of CC material and shape of the object in contact with the CC. As a result of laboratory studies, it was found that insulation based on cross-linked polyethylene (XLPE) tends to be less resilient compared to varieties of regular polyethylene. It was also determined that CCs with a higher number of insulating layers tended to exhibit inferior durability compared to single-layer conductors of equivalent thickness. However, the confidence which can be assigned to these findings is relatively low due to the high variability in observed withstand times. It was determined that in case the conductor is in contact with a round object, the time until breakdown appears to be inversely correlated with the curvature radius of the object. The results indicate that it is the total area of the stressed insulation and intensity of PD activity affecting it, rather than the electric field strength, which predicts a reduced time until insulation breakdown.

PDs were also investigated from the perspective of MV power cables, with a focus on the accuracy of PD source location using time-domain reflectometry and classification to identify the type of PD (corona, internal, or surface discharge) using high-frequency current transformers (HFCT) instead of more traditional methods to measure PD. It was found that the accuracy of PD source location in a cable, when using a HFCT for measurement, is satisfactory for practical applications, being primarily limited by the sampling rate of the measurement equipment or other external factors. Although it is known that power cables behave as a lossy transmission line in case of high-frequency signals, the combined effect of attenuation and dispersion experienced by the travelling waves was not observed to be significant enough to introduce a substantial error into the estimation of pulse propagation velocity or PD source location.

The issue of PD classification was addressed by performing measurements on three different PD sources, each representing a primary subtype of the phenomenon. Several different parameters were calculated to evaluate their usefulness for differentiating PD sources. It was found that aspects such as PD pulse width, pulse intervals and similarity between pulse waveforms indicate the highest degree of usefulness in discriminating PD sources. The identified parameters can be exploited in the development of advanced algorithms designed to perform computer-aided PD recognition and interpretation tasks. It was also determined that a successful approach to autonomous PD analysis must include functionality to distinguish authentic PD signals in measured data from oscillations of the PD detection sensor, pulse reflections and various sources of noise.

Lühikokkuvõte
Isolatsiooni vastupidavus ja osalahenduste mõõtmine

Antud töös käsitletakse kaetud keskpingejuhtmete vastupidavuse, elektriliste osalahenduste (OL) mõõtmise ja klassifitseerimisega seonduvaid probleeme. Töö oli ajendatud elektrivõrguettevõtete tänapäevastest väljakutsetest ja kõrgepingetehnika valdkonna viimase aja suundumustest. Põhilised metoodikad, mida antud töö tulemuste saavutamiseks kasutati, on: kaetud keskpingejuhtmete, keskpingekaablite ning kunstlikult tekitatud OL allikatega teostatud laboratoorsed katsed, mõõteandmete analüüs kasutades tavapäraseid ja edasiarenenud andmetöötluse tarkvarapakette (nt MATLAB) ja elektriväljade kuju arvutuslik modelleerimine kasutades lõplike elementide meetodit.

Jaotusvõrguettevõtted kasutavad tihti kaetud juhtmeid keskpinge õhuliinides, peamiselt võrgu töökindluse suurendamise eesmärgil. Samas langevad murdunud puud tihti õhuliinidele ja võivad teatud aja möödudes tekitada isoleerkatte koormamise tõttu selles läbilöögi, mille tagajärjel tekib tehniline rike. Selle protsessi kiirust määravaid aspekte uuritakse antud töös, parandamaks arusaama nüanssidest, mis mõjutavad isolatsiooni vastupidavust taolistes oludes, sh käsitletakse isoleermaterjali valikut ja juhtmega kontaktis oleva juhtiva objekti kuju. Laboratoorsete uuringute tulemusena leiti, et ristsillatud polüetüleen (XLPE) on madalama vastupidavusega võrreldes tavalise polüetüleeni erimitega. Tulemustest nähtus ka mitmekihilise isolatsiooni madalam vastupidavus võrreldes samaväärse paksusega ühekihilise isolatsiooniga, kuigi nende leidude usaldusväärsus on madal katseobjektide kestvusaegade suure varieeruvuse tõttu. Tulemused viitavad ka isolatsiooni vastupidavusaja pöördvõrdelisele sõltuvusele juhtmega kohtaktis oleva objekti kõverusraadiusest. Katseandmetest saab järeldada, et isoleerkatte vastupidavusaega vähendavad eelkõige kõrgendatud elektriväljaga koormatud piirkonna suurus ja seda mõjutavate OL-te intensiivsus, mitte niivõrd elektrivälja tugevus.

OL-i uuriti ka keskpinge jõukaablitega seonduvalt, eelkõige keskendudes OL allika asukoha määramise täpsusele reflektomeetria kaudu ja OL tüübi määramisele (koroonalahendus, sisemine OL või pindlahendus) kasutades mõõtesensorina kõrgsagedusvoolutrafot (KSVT) traditsiooniliste OL mõõtemeetodite asemel. Leiti, et OL allika asukoha määramise täpsus KSVT-ga on rahuldav praktikas rakendamiseks ja seda piiravad eelkõige mõõtmise ajaline resolutsioon või muud välised faktorid. Kuigi on teada, et kõrgsageduslike signaalide seisukohast käitub jõukaabel nagu kadudega ülekandeliin, ei leitud, et pulsside levimisel nendele mõjuv sumbumine ja dispersioon avaldaks märgatavat efekti pulsi kiiruse mõõtmisel või OL allika asukoha määramisel.

OL allikate klassifitseerimise probleemi käsitlemiseks teostati OL mõõtmised kolmel erineval OL allikal, mis esindasid OL peamiseid alaliike. Mõõteandmete põhjal arvutati mitu erinevat parameetrit ja hinnati nende otstarbekust allikatüübi eristamiseks. Leiti, et OL pulsside laiused, intervallid ja korrelatsioonitegurite kaudu väljendatav sarnasus on kõige parema kasutatavuspotentsiaaliga OL allikate diferentseerimiseks. Nimetatud parameetreid saab ära kasutada algoritmide koostamiseks, mis võimaldavad arvutipõhist tuge OL tuvastamise ja tõlgendamisega seonduvate ülesannete täitmiseks. Tuvastati ka tõsiasi, et eduka autonoomse OL analüüsi teostamiseks on tingimata vajalik mõõteandmetes tõhusalt eristada autentseid OL pulsse mõõtesensori järelvõngetest, peegeldunud pulssidest ja erinevatest mürasignaalidest.

Appendix 1

Publication I

Kiitam, I.; Taklaja, P.; Tuttelberg, K. (2018). Voltage Withstand Properties of the Insulation of Different Types of Medium Voltage Covered Overhead Line Conductors. 19th International Scientific Conference Electric Power Engineering (EPE), Brno, Czech Republic. IEEE, 18–21.

Voltage Withstand Properties of the Insulation of Different Types of Medium Voltage Covered Overhead Line Conductors

Ivar Kiitam, Paul Taklaja, Kaur Tuttelberg
Department of Electrical Power Engineering and Mechatronics
Tallinn University of Technology
Tallinn, Estonia
ivar.kiitam@ttu.ee

***Abstract*— Using covered conductors in overhead lines has become a widespread practice for increasing the reliability of distribution grids. To determine the ability to withstand prolonged voltage stress of different insulating materials, 10 different types of covered conductors with a rated voltage of 20 kV were tested by placing grounded copper wire electrodes on the outer surface of the conductor. In the tests, 3 grounding points were applied to each tested conductor. The conductors were energized to a standard testing voltage of 14 kV and the accumulative time until puncture of the insulation was measured. Some conductors showed a high variability of withstand times, possibly due to presence of weak spots in the insulation. On average, conductors insulated with PE performed best in the tests, PE/XLPE combined insulation was second best and XLPE insulated conductors exhibited the shortest withstand times.**

Keywords*— *covered conductors; voltage withstand; insulation durability; XLPE insulation; PE insulation

I. INTRODUCTION

An important development in enhancing the reliability of distribution grids is the increasing use of covered conductors in overhead lines. Covered conductors inhibit the occurrence of earth faults and short circuits as well as increases the level of safety in case of line malfunctions. The risk of electric shock for persons and animals is significantly reduced in case of structural failure of the line. Using covered conductors also enables a longer permissible time for clearing any trees that have fallen on the conductor after storms and other extreme weather incidents. It is beneficial for grid operators due to more efficient allocation of personnel and resources when restoring normal grid condition as well as the possibility to introduce longer overhead line inspection timespans. A grid utility was interested in the properties of various covered conductors and a variety of tests were conducted to evaluate them and investigate the aforementioned benefits in comparison to bare conductors. In the experience of electrical utilities from different European countries, employing covered conductors has improved grid reliability in various aspects of line performance. However, additional problems related to overvoltage protection and aeolian vibration have been observed [1] [2].

Different materials are used for insulating the covered conductors. The most widely applied materials include different types of polyethylene, both high- and low-density polyethylene (HDPE, LDPE) and cross-linked polyethylene (XLPE). The covered conductor usually contains a semiconducting layer surrounding the central conductor to reduce electric stress on the insulation. The semiconducting layer produces a round cross-section of the conductive parts of the covered conductor, effectively increasing the conductor radius and lowering the electric field intensity in the insulating outer layer or layers.

In operation, the danger for insulation breakdown is highest when a grounded conductive object is in direct contact with the insulating layer. This creates a strong concentration of electric stress which rapidly degrades the insulation. This situation can occur if a fallen tree comes into contact with the conductor. Another negative aspect concerning this situation is the conductor friction created by movement of the tree under windy conditions. The abrasive effect would erode the insulating layer at a rate which is dependent on the specific circumstances of the tree-conductor contact.

Several factors affect the timespan before insulation breakdown of the covered conductor occurs. These include the quality and thickness of the insulating material, operating voltage of the power line, species and age of tree in contact with the line, contact force and abrasivity of the tree bark, as well as the resistance to ground, which effects the magnitude of leakage current. Previous research carried out on covered PAS type conductors in Finland has also shown that small holes may appear in the insulation when the line is energized, creating potential weak spots in the insulation [3]. A tree coming into contact with this kind of weak spot could cause insulation failure over a very short duration of time. For utilities employing covered conductors it is beneficial to determine which insulating materials perform best and are most durable in use. To investigate some important aspects of covered conductor performance, a number of different tests were carried out in the high voltage and mechanical labs.

In total, 10 different types of covered conductors from various manufacturers were tested. Tests carried out on conductors were restricted to two basic types, which indicate the covered conductors' durability under voltage stress and rate of

This research was supported by the European Union from the European Regional Development Fund

978-1-5386-4612-0/18/$31.00 ©2018 IEEE

wear due to contact friction with wood. The aim of the electric and tribologic tests was to determine the duration covered conductors could withstand continuous AC voltage stress and mechanical wear. This paper discusses only the results of the electric tests. Another goal of the tests was to determine whether the types of polyethylene (PE, LDPE/HDPE and XLPE) have any significant differences in performance i.e. if any material could be conclusively considered superior to the others for field operation purposes. A supplementary research objective was to verify the results of preceding studies, which have concluded that a combined insulating layer consisting of HDPE and LDPE tends to perform better than a single layer XLPE coating [4].

The tested conductors featured variable insulation materials, insulation thickness and conductor cross-section. The rated voltage of all examined conductors was 20 kV. Although the insulation thickness for all conductors was 2.3 mm specified according to standard [5], some deviations were observed when samples of the studied conductors were examined under microscope. The minimum insulating layer thickness ranged from 2.06 mm to 2.58 mm. The tested conductors had similar conductor cross-section areas, ranging from 50 to 99 mm^2. The main parameters of the tested covered conductors are presented in Table 1. In order not to disclose any manufacturers and specific makes of conductor, the test objects are simply referred to as conductors No. 1 to 10.

TABLE I. MAIN CHARACTERISTICS OF TESTED CONDUCTORS

Conductor No.	Insulating material (inner layer/outer layer in case of two layers)	Semiconducting layer
1	PE	Yes
2	XLPE	Yes
3	PE	Yes
4	LDPE/HDPE	Yes
5	XLPE	Yes
6	XLPE	Yes
7	XLPE/PE	Yes
8	LDPE/HDPE	Yes
9	LDPE/HDPE	Yes
10	XLPE	No

II. VOLTAGE DURABILITY TESTS

In order to simulate the voltage stress that affects the covered conductor insulation when in contact with a grounded conducting object, a test setup according to standard [5] (Annex B: Measurement of the leakage current) was constructed. The standard describes this kind of setup for leakage current measurement, but it was chosen as a suitable setup for voltage withstand testing purposes. While conforming to most requirements specified in the standard, the requirement of immersing the tested conductors in water over a 24-hour period prior to testing was omitted and the conductors were effectively dry throughout the test. A copper wire winding was wound tightly around the tested conductors. Although wood is significantly less conductive than most metals, it is much more conductive than the insulating material. Therefore, for practical considerations, copper wire is a good material for simulating the electric field produced in the insulation. For comparison, a total of 3 such windings were applied to each tested conductor. Because the tested conductor samples were quite short, no more testing points could be prepared. This amounts to a total of 30 grounding points applied to the 10 tested conductors.

The basic test setup, including the winding placement was also implemented according to standard [5], Annex B. The copper wire diameter is 2 ± 0.05 mm and the winding length across the insulation surface is 100 mm. The ends of the winding were placed at least 450 mm from the edge of the insulating layer and other windings to minimize the mutual effect they have on the resulting electric field shape. The windings were grounded to create the difference in potential across the insulation and the resulting voltage stress. The principle setup of grounding points on the conductor is depicted on Fig.1

The conductors were energized to a voltage level specified in [5], equal to 0.7 times the conductor rated voltage. This resulted in a test voltage of 14 kV. The objective of the test was to determine the accumulative time before the insulation punctured. Previous tests have shown that testing at a higher voltage level (24 kV) can result in breakdown of the conductor insulation within 5 minutes of voltage application, with a higher susceptibility to puncture in case the conductor has already aged in service. Conductors that have not been used in grid operation do not puncture quite as fast [6]. Considering this, it was estimated that the insulation on tested conductors would puncture within some hours or days of constant voltage application.

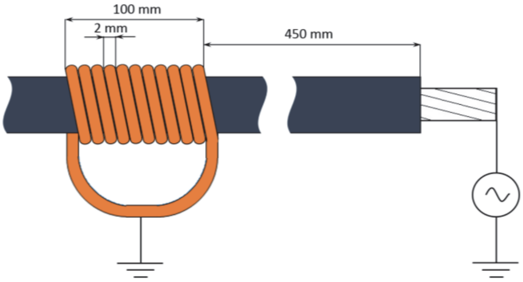

Fig. 1. Principle schematic of copper wire winding placement on covered conductor in voltage stress tests

The resulting electric field that occurs around the grounded winding affects the insulating layer by starting to rapidly degrade it. The strong electric field causes breakdown and decomposition of air surrounding the insulation, resulting in partial discharges. After a period of a few days the effect becomes apparent on the insulating layer, causing noticeable discoloration near the edges of and under the grounded copper winding. Decomposition products also oxidize the copper wire, after a few weeks the copper starts to develop a grayish coating, which can be observed near the outermost turns of the winding presented in Fig. 2.

The partial discharges can be best observed when the test laboratory is darkened. Even in this case they are faintly discernable and can barely be detected visually. In Fig. 3 the photograph of partial discharges taken in the dark is acquired using a 30 second shutter time. Apparently, the partial discharges are most intense at the edges of the winding, although test results showed that the vast majority of locations where puncture occurred remained somewhere under the winding, not at the edges of it.

Initially it was assumed that the electric field is strongest at the edges of the winding due to the edge effect. Computer

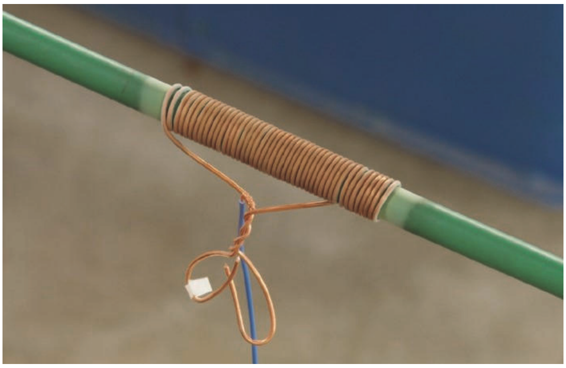

Fig. 2. Example of a test object, which consists of a grounded copper wire wound around a covered conductor. Discoloration of the insulation surface and copper around the edges of the winding are evident.

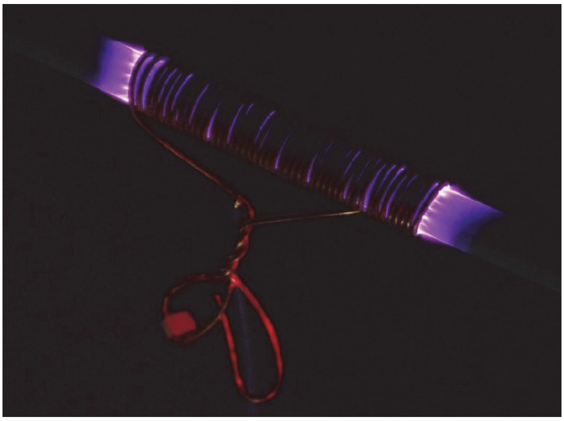

Fig. 3. Energized test object in the dark. Photograph acquired using a 30 second shutter time.

simulation using the finite element method (FEM) presented in Fig. 4 indicates that the electric field in the surface layers of the insulation is strongest under the outermost turn of the winding and starts to periodically decrease and increase towards the center of the winding. In the inner layer of the insulation, electric field strength increases to its largest value 2…3 turns from the ends of the winding and essentially remains constant (Fig. 5). The relative permittivity of the insulation was equal to 2.3 in the simulation. The results of modelling the electric field around the grounded winding indicate that the electric field strength is sufficiently high in the air surrounding the winding to initialize breakdown and partial discharges (exceeding 3 kV/mm). The visually observed discharge activity is consistent with the results of the simulation.

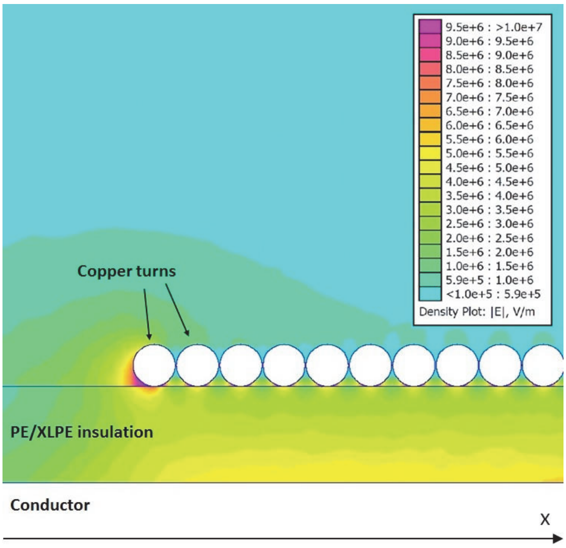
9.5e+6 : >1.0e+7
9.0e+6 : 9.5e+6
8.5e+6 : 9.0e+6
8.0e+6 : 8.5e+6
7.5e+6 : 8.0e+6
7.0e+6 : 7.5e+6
6.5e+6 : 7.0e+6
6.0e+6 : 6.5e+6
5.5e+6 : 6.0e+6
5.0e+6 : 5.5e+6
4.5e+6 : 5.0e+6
4.0e+6 : 4.5e+6
3.5e+6 : 4.0e+6
3.0e+6 : 3.5e+6
2.5e+6 : 3.0e+6
2.0e+6 : 2.5e+6
1.5e+6 : 2.0e+6
1.0e+6 : 1.5e+6
5.9e+5 : 1.0e+6
<1.0e+5 : 5.9e+5
Density Plot: |E|, V/m
Copper turns
PE/XLPE insulation
Conductor
x

Fig. 4. FEM simulation of electric field strength in covered conductor insulation and surrounding air. The x-axis is given in reference to the values respresented in Fig. 5.

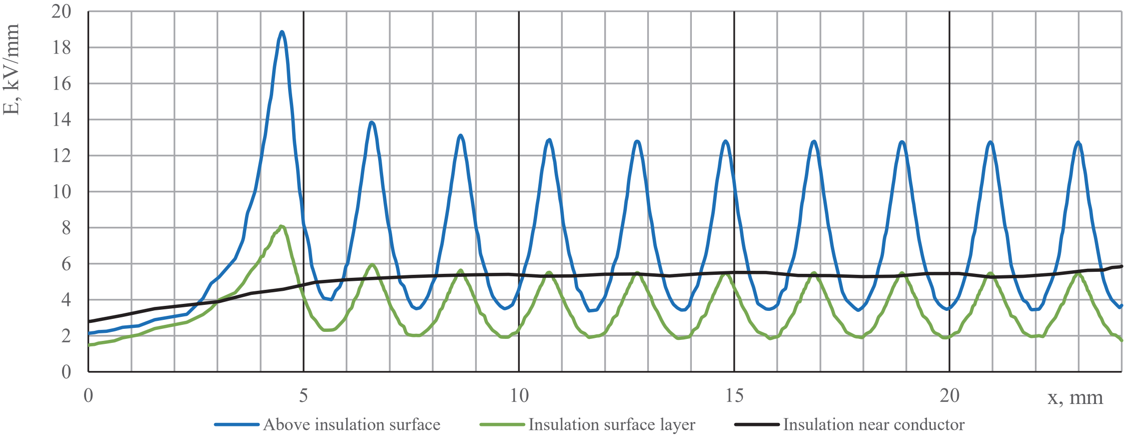

Fig. 5. Electric field strength in layers of insulation and air across the grounded winding at voltage amplitude value (19.8 kV).

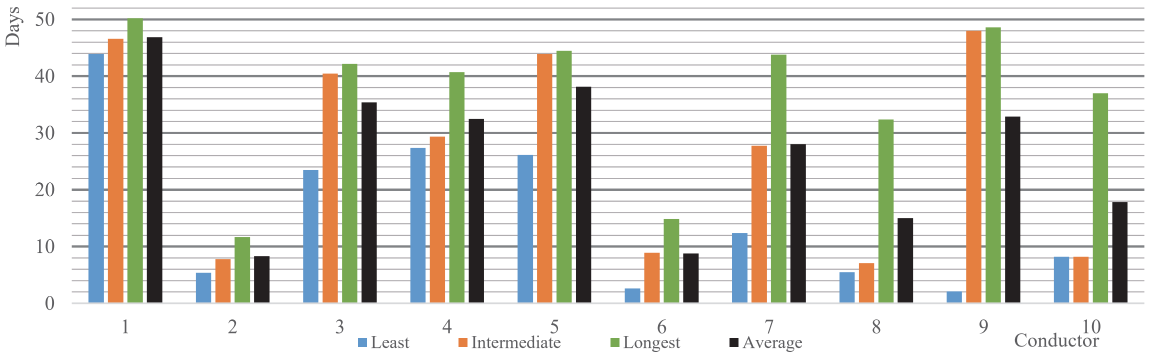

Fig. 6. Voltage durability test results for different covered conductors. The columns represent the 3 different puncture times of grounding points (shortest, intermediate ja longest duration) as well as the average puncture time of the tested conductor considering all 3 grounding points.

III. TEST RESULTS AND ANALYSIS

The overall results of the voltage durability test are provided in Fig. 6. In the graph, the values represent the time in days for puncture to occur in each of the 3 grounded windings. It is notable how different the results are for the same type of conductor considering some of the test samples. For example, the minimum time for conductor No. 9 to puncture is 2.1 days and the maximum time is 48.6 days. The third location broke down at 48 days, so the average durability is 32 days. The ratio of maximum and minimum puncture times is approximately 24, making this a highly durable conductor when considering the average or maximum puncture times, but a very nondurable conductor when considering the minimum puncture time. Similarly large discrepancies between minimum and maximum puncture times are recorded for conductors 6, 7, 8 and 10. For conductors 1, 2, 3, 4 and 5 the relative difference in withstand durations for grounding points is relatively small.

This kind of large variability in the test results may indicate inconsistencies in insulation quality along the conductor length. The existence of weak spots is possibly a side effect of inadequate manufacturing quality. The large variability in breakdown times can not be attributed to the type of material used, because in case of both XLPE and PE insulated conductors there were occurrences of large and small variability in breakdown times. The variability of workmanship of individual copper wire windings might also have a notable influence on the test results.

Another peculiar outcome is that although the electric field across the insulating layer should be strongest at the edge of the winding, only one tested grounding point out of 30 was punctured from the edge of the winding. A possible reason is that due to partial discharges occurring under the copper winding, air becomes conductive and it evens out the electric field in the exterior of the insulation. The actual electric field intensity in the insulation at peak voltage value may be considerably less variable than presented in Fig. 5.

When considering the total average of the different insulation materials, the time until puncture amounted to:

- 32.5 days for PE insulated conductors
- 18.3 days for XLPE insulated conductors
- 28.0 days for PE/XLPE insulated conductor

It is also notable that conductor No. 10, which lacked a semiconductive layer under the XLPE insulation, actually performed quite well relative to other XLPE insulated conductors. The high variability in withstand times indicates that there are other relevant factors besides the insulation material itself, which influence the ability of covered conductors to perform under continuous AC voltage stress. The variable manufacturing quality of the conductive layer is a possible issue in this case. Also, the number of test objects used in this study is rather small, a larger number of grounding points per conductor would enable the production of more reliable inferences. At present there is no theoretical explanation to the superior performance of PE. It is possible that the manufacturing process enables the production of a more consistent insulating layer compared to XLPE.

IV. CONCLUSIONS AND FUTURE WORK

The test results indicate that PE is a superior material for employing in covered medium voltage conductors. The voltage withstand time for XLPE insulated conductors was 56% of the withstand time for PE insulated conductors on average and the conductor with a combined XLPE/PE insulation withstood 86% of the average withstand time of PE insulation. To further support the results of this study, analogous tests could be conducted with a larger number of test samples. Varying the shape of the grounding electrode could also provide interesting results, because the shape of the electrodes can be altered to better resemble parts of actual trees.

REFERENCES

[1] T. Leskinen and V. Lovrenčić, “Finnish and Slovene experience of covered conductor overhead lines”, CIGRE Session 2004, B2-207

[2] W. Panosch, K. Schongrundner and K. Kominek, “20 kV overhead lines with covered conductors”, International Conference and Exhibition on Electricity Distribution, 2001. Part 1: Contributions. CIRED. (IEEE Conf. Publ No. 482)

[3] J. Vehanen and P. Hyvönen, “Diagnosis of medium voltage covered conductors” (*Päällystetyn keskijänniteavojohdon kunnon diagnosointi*), Espoo, 2003

[4] F. Nishimura, L. D. Cicarelli, M. Coelho, B. Trager and M. R. Soares, “Covered cable comparative testing: HDPE and XLPE evaluation”, IEEE/PES Transmission and Distribution Conference and Exposition, Atlanta, 2001

[5] EN 50397-1:2006 “Covered conductors for overhead lines and the related accessories for rated voltages above 1 kV AC and not exceeding 36 kV AC Part1: Covered conductors”

[6] A. Kasparans, M. Budahs and J. Rozenkrons, “20 kV insulated overhead lines overvoltage protection problems in Latvia’s distribution network” Electric Power Quality and Supply Reliability Conference, Viimsi, Estonia, 2006

Appendix 2

Publication II

Kiitam, I.; Taklaja, P.; Tuttelberg, K. (2018). Effect of Electrode Shape on Medium Voltage Covered Conductor Insulation Durability Under Electric Stress. IEEE 59th International Scientific Conference on Power and Electrical Engineering of Riga Technical University (RTUCON). IEEE, 1–6.

Effect of Electrode Shape on Medium Voltage Covered Conductor Insulation Durability Under Electric Stress

Ivar Kiitam, Paul Taklaja, Kaur Tuttelberg
Department of Electrical Power Engineering and Mechatronics
Tallinn University of Technology
Tallinn, Estonia
ivar.kiitam@ttu.ee

***Abstract*— Covered power line conductors aid in maintaining normal operation in case of objects coming into contact with phase conductors. An electric test was conducted where various types of grounded electrodes were brought into contact with the insulating layer of the covered conductor. The conductor was energized and the cumulative time was measured until insulation breakdown occurred at the contact point of each of the grounding electrodes. Five different types of electrodes were used. Three of these were round in shape and were used for simulating tree branches with different diameter. One electrode was a copper wire winding specified in covered conductor testing standard and one was aluminum tape. A total of 10 electrodes of each shape were used for better estimation of the variability of breakdown time. The average breakdown times of each type of electrode were notably different but also the variability of breakdown times in case of electrodes of the same type was quite substantial.**

Keywords— covered conductors; insulation withstand; electric stress; insulation breakdown; electrode shape

I. INTRODUCTION

A primary interest of distribution grid utilities worldwide is to keep the reliability of their power lines as high as possible in order to reduce the number and duration of power outages for consumers. A typical problem for distribution grids in more densely forested areas of the world are trees falling on power lines, resulting in an earth fault in case the grid operates with an insulated neutral. This requires a rapid response from the utility, to remove the fallen tree and restore normal operation.

One of the main constructional measures used to increase reliability of medium voltage overhead lines in such instances is using covered conductors (CCs). These conductors feature a layer of insulating material on the surface of the metallic phase conductor. Various materials are used for the insulation, most commonly regular polyethylene (PE) and cross-linked polyethylene (XLPE). In some cases, the insulating cover consists of two layers of different materials (e.g. HDPE and LDPE), which generally outperforms single-layer XLPE insulation [1]. Usually there is a semiconductive layer between the insulation and conductor, which aids in maintaining a more even electric field in the insulation.

The share of overhead lines employing CCs in medium voltage grids has generally increased over time. Currently the share of CC lines in 6…20 kV power grid in Estonia is approximately 5.4% of all power lines and 8% of overhead lines. Although constructing power lines using CCs is somewhat more expensive [2] than using bare conductors, they do usually improve safety and reliability of the grid. Using CCs can mitigate earth fault or short circuit incidents due to the absence of a conducting path between the phase conductor and ground. This would provide utilities a substantially longer period of time to survey the grid, locate and remove any fallen trees from the power lines. Failing to remove the trees fast enough causes further issues for the utility. The fallen tree can lean against the conductor with substantial force. During windy weather conditions, it causes considerable wear of the insulating layer due to mechanical friction. In some forested areas initial employment of CCs has actually led to a decline in grid reliability [3].

Another issue with fallen trees is the increased electric stress in and around the insulation near the contact area between the tree and conductor. For more efficient asset management, it is important to know the approximate duration conductors can withstand concentrated electric stress due to fallen trees or other objects. To study this problem, it is necessary to examine closely how the shape of the object in contact with the conductor affects the insulation withstand time.

In case of trees falling on the conductor, the concentration of electric field is dependent on the shape of the branch or trunk, which is in contact with the conductor. Although wood is generally a poor conductor of electricity in comparison to most metals, its resistivity is still magnitudes smaller than the resistivity of the insulating layer materials [4],[5]. As a result, the electric field concentration is significant in the insulation and surrounding air. It is supposed that in case of a smaller branch the electric field is stronger due to its smaller radius, resulting in a higher electric field intensity on the surface of the

---

This research was supported by the European Union from the European Regional Development Fund.

branch and in the air directly near the point of contact. This should cause the insulation to puncture after a shorter period of time than in comparison with contact with a branch of a larger diameter. Generally it is expected that the insulation should endure at least two weeks of contact with a tree branch [6]. The rate of deterioration of insulation should increase over the duration of contact and be visually observable through changes in the appearance of the conductor insulation. Previous tests employing partial discharge measurements have indicated an increase in PD activity after prolonged contact with a grounded conductive object [7].

II. TEST SETUP

In order to verify this hypothesis and quantify the ability of CCs to withstand electric stress, a test setup was constructed which included grounded conductors in contact with the XLPE insulation of a typical medium voltage CC used in distribution grid construction. In the test, five sections of a covered medium voltage conductor were energized to a voltage of 14 kV. The conductor parameters:

- XLPE insulated with semiconducting layer;
- Conductor cross-section 70 mm^2;
- Conductor diameter 9.7 mm;
- Overall diameter 14.9 mm;
- Insulation thickness 2.3 mm;
- Semiconductive layer minimum thickness 0.3 mm;
- Rated voltage 20 kV.

Each section included 10 locations where a grounded conductor of a specific shape was placed in direct contact with the insulating layer. The shape of the grounded conductor was different in each of the five sections, amounting to a total of 50 grounding points. The distance between grounding points or the minimal distance between parts of adjacent grounding electrodes was 450 mm. This was to minimize the mutual effect of ground electrodes on the electric field of each grounding location.

Three of the five conductors were round (metal pipes or wire) intended to simulate tree branches of different sizes. The diameter of the round conductors was 125 mm, 25 mm and 5 mm. This results in an electric field similar to what a tree branch in contact with a CC would produce, although other authors have reasoned that different parts of a tree are not necessarily equipotential under these kinds of circumstances [8]. The surface of the round conductors was polished prior to applying them to the surface of the insulation to minimize effects of field concentrations around protrusions. The round conductors were secured to the insulation surface using zip ties. Minimal tightening strength was used upon application of zip ties as the purpose of using them was to mitigate possible displacement of the ground conductor relative to the CC. This was necessary to prevent changes of the area of insulation affected by the electric field. Excessive tightening of the zip ties would result in increased mechanical stress and possible deformation of the insulation at the point of contact. Without a possibility to accurately measure the contact pressure, minimal application of force was opted for.

The fourth type of conductor was a copper wire 2 mm in diameter wound densely around the covered conductor with a total coil length of 100 mm. This electrode shape and wire diameter is in accordance with standard [9] (Annex B: Measurement of the Leakage Current), which specifies insulation testing conditions of CCs. Although the standard on which it is based specifies this configuration for leakage current measurements, it is also applicable for the purpose of insulation durability testing and has been used in previous tests to determine withstand properties of materials used in CCs [10].

The fifth type of grounding conductor was an aluminium tape wound tightly around the conductor. The width of the tape was 100 mm. In theory, this kind of grounding point would produce a strong electric field around the edges of the tape, contributing to a rapid degradation of insulation in that area. It is similar to the winding type electrode, although it is expected to produce a more uniform electric field in the insulation directly under the tape. Discharges would mostly occur only near the edges of the electrode. The principle schematic of the grounding points with different electrode types is presented in Fig. 1.

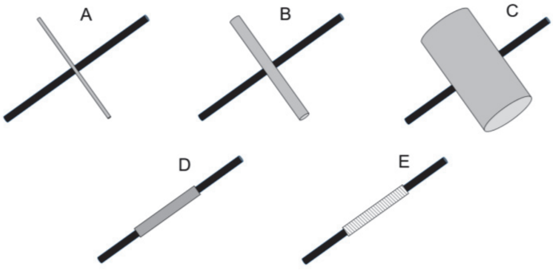

Fig. 1. Principle schematic of used grounding electrodes. A- 5 mm round wire, B- 25 mm round pipe; C- 125 mm round pipe; D- aluminium tape; E- copper wire winding

In the test, the medium voltage CCs were energized to 14 kV (0.7*rated voltage of CC according to [9]) that approximately corresponds to the maximum phase-to-ground voltage level (24/√3 kV) in 20 kV grid under normal circumstances. The test voltage was applied using a high voltage test transformer fed by a programmable AC power source, which outputs a practically pure sine wave. The test voltage was free of distortions and higher harmonic frequencies that may be present in the voltage waveform of mains power supply. The test voltage was continuously applied to the conductors until a breakdown occurred in one of the grounding points, causing a short circuit and tripping of the power supply. After insulation failure, the grounding point was disconnected and the conductors re-energized. The performance of the grounding points was quantified by the cumulative amount of time the CC was energized before the insulation breakdown occurred.

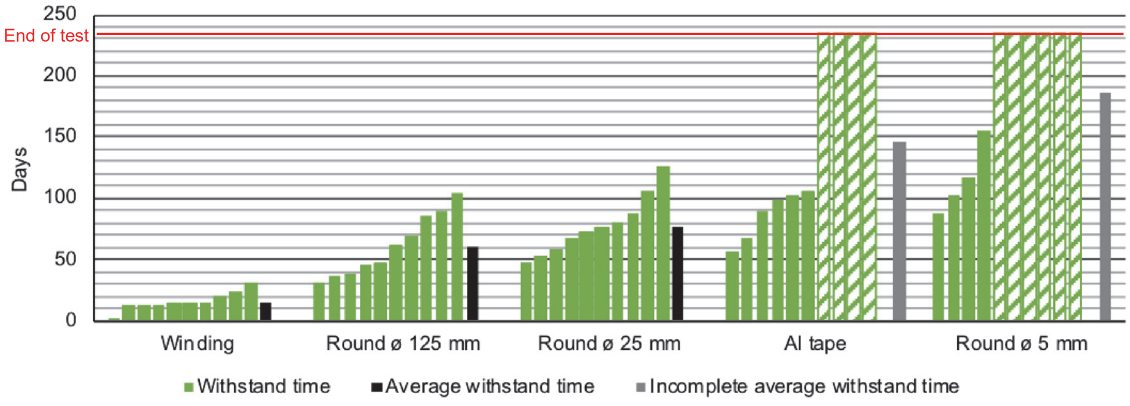

Fig. 2. Withstand times of individual grounding points and averages of electrode types in sequence of increasing durability. Incomplete average withstand time is provided for electrode types in case of which some grounding locations did not puncture.

III. TEST RESULTS

The average amount of time the various types of grounding points withstood the voltage stress differed significantly. The test was eventually discontinued due to practical considerations, because some grounding points withstood in excess of 7 months of accumulated electric stress. Over the test period, breakdown occurred in all of the 10 grounding points in case of three of the five different types of grounding electrodes. Some grounding points with the aluminium tape and 5 mm round conductor did not suffer breakdown over the duration of the experiment and the estimates for breakdown average time are therefore not directly comparable to the other three electrode types.

The test results are presented in Fig. 2. Based on the results, the sequence of insulation durability for different grounding electrodes can be inferred and the ranking based on breakdown times is presented in Table I. It should be noted that the first breakdown of a wound electrode grounding point occurred after only a very brief period of electric stress application, approximately 12 hours. Other grounding points of the same type punctured after 13 to 31 days of electric stress, which suggests the insulation at the first punctured location was abnormally fragile. However, this outlying result does not have a significant impact of the main conclusions of this study.

The ranking of the insulation durability for different ground electrodes is the same regardless of which breakdown time characteristic it is based on. The minimum, maximum and average breakdown times all increase in the following sequence: winding, 125 mm round and 25 mm round electrode. Although some of the grounding points of the aluminum tape and 5 mm round conductors did not puncture over the duration of the test, it can be deduced with a fair degree of certainty that the latter ranks higher due to the following considerations:

- The minimum puncture time for the 5 mm round electrode is higher than that of the Al tape electrode;
- The incomplete average withstand time based only on the grounding points that punctured over the duration of the test is higher in case of the 5 mm round electrode;
- The number of grounding points that punctured is lower in case of the 5 mm round electrode compared to the Al tape electrode.

The test results in general showed a notable variation in the amount of time before breakdown of the different grounding points of the same type. This might imply that there is significant variation of the insulation layer quality over the length of the conductor with a number of weak spots present.

TABLE I. RANKING OF COVERED CONDUCTOR INSULATION DURABILITY FOR DIFFERENT TYPES OF GROUNDING ELECTRODES

Grounding electrode type	**Insulation durability rank (in order of increasing time)**	**Grounding point breakdown time characteristics (days)**		
		Min	**Max**	**Average**
Winding	1	0,5	23	16
Round ø 125 mm	2	32	89	61
Round ø 25 mm	3	47	106	77
Aluminium tape	4	56	N/A	146*
Round ø 5 mm	5	88	N/A	187*

* Incomplete average, some of the grounding points did not puncture

The results also showed that the average time until breakdown was shorter for the round grounding conductors with a larger diameter. This is in contradiction with the initial hypothesis that a smaller diameter of the grounding conductor would cause a breakdown faster due to higher electric field intensity. This can be explained by the notion that a larger diameter would result in a wider area of high electric stress in the insulation and there is a higher probability for the inclusion of weak spots in the stressed area of the insulation. Also, the puncture sometimes occurred some mm away from the point of contact between the CC insulation and round electrode.

The average time until breakdown was smallest in case of the copper winding grounding points. The electric stress in this instance was elevated due to high discharge activity in the air between the copper windings and insulation surface. This possibly generated oxidizing gases in significant amounts, which contributed to the rapid degradation of the insulating layer. The highly stressed area was also significantly larger than in case of the round electrodes due to the field concentration at each turn, the width of the winding and the fact that the entire circumference of the CC was affected. Furthermore, only two of the punctures occurred at the outermost turns of the winding, the remaining eight occurred under the inner turns, where the electric field was not as strong according to simulations (Fig-s. 4, 6, 7).

The performance of the aluminium tape grounding points exhibited unexpected characteristics as well. The time until breakdown was rather long on average despite the highest simulated electric stress (Fig. 6) and all the punctures occurred at the edge of the electrode. In addition, the area of increased electric stress was continuous along the surface of the conductor, so weak spots should have caused breakdown in the insulation under the aluminium tape considerably faster. This, contrary to observations made in conjunction with other grounding points, implies the absence of weak spots in the insulating layer.

IV. ELECTRIC FIELD SIMULATIONS

In order to study the electric field at the grounding locations, a number of field simulations using the finite element method (FEM) were performed. The field strength at test voltage amplitude value (19.8 kV) is presented for the Al tape electrode, copper winding electrode and 5 mm round electrode in Fig.-s 3, 4 and 5, respectively. The field for only the outermost turns of the winding is presented, because it is known from previous simulations that the field intensity is highest at the edges of the winding [10].

For simpler comparison of the electric fields of different electrodes, the field strength in the air directly above the insulation across the grounding electrodes is presented in Fig.-s 6 and 7. The location of highest electric stress is chosen as the 0 coordinate of distance. In Fig. 6, a close-up of the field strength in the area of highest stress is provided, whereas a more general overview is presented in Fig. 7.

From these figures, it is apparent that the electric stress is highest in case of the Al tape electrode, although in a very narrow area. Electric field intensity is second highest at the wound electrode, which has a smaller maximum value, but a wider area of high electric stress. Under each turn is a point of contact and the peak values are only slightly smaller than under the outermost turn. The large overall area of high electric stress is apparently the main reason why this type of electrode caused puncture of the insulation over the shortest period of time. The three round electrodes exhibit a smaller value of maximum field intensity in the sequence of increasing diameter, but also a wider area of elevated electric stress as the diameter increases. This is clearly visible in Fig. 7.

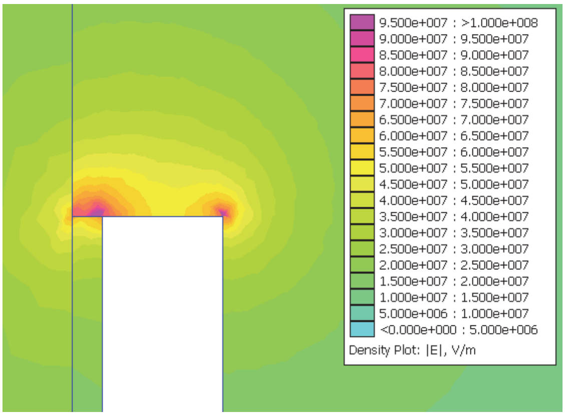

Fig. 3. Electric field strength around the edge of the aluminium tape electrode. The presence of adhesive is taken into account.

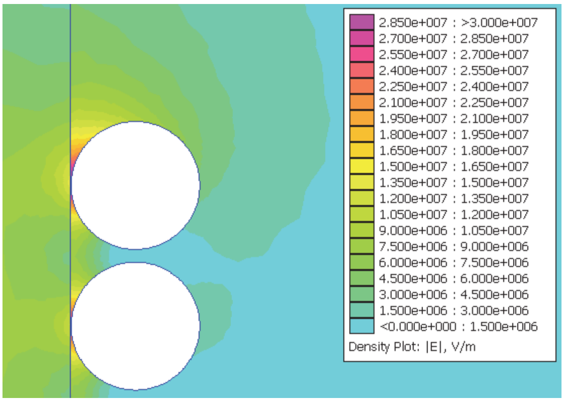

Fig. 4. Electric field strength around the outermost turns of the wound copper wire electrode.

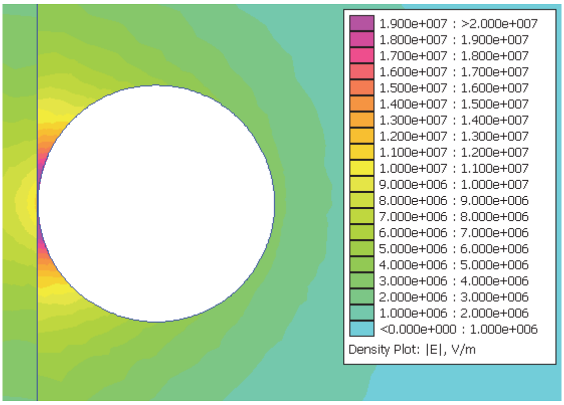

Fig. 5. Electric field strength around the 5 mm diameter round electrode at the point of contact with the CC insulation. Field shape is similar for the remaining electrodes with a larger diameter.

These field simulations remain somewhat indicative, because after the field is strong enough to initiate discharge activity in the air surrounding the electrode, they have an impact on the shape of the field due to the emergence of conductive paths in the air. However, before any discharges occur in any given AC half-cycle, the field should be proportional to the presented field intensity values and therefore the areas in which the simulated electric stress is higher suffer a higher overall time of elevated stress.

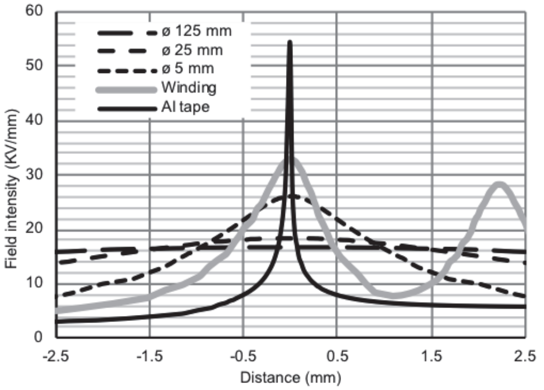

Fig. 6. Electric field intensity in the air directly above the surface of the insulation for different electrode types at the location of highest electric stress (narrow view)

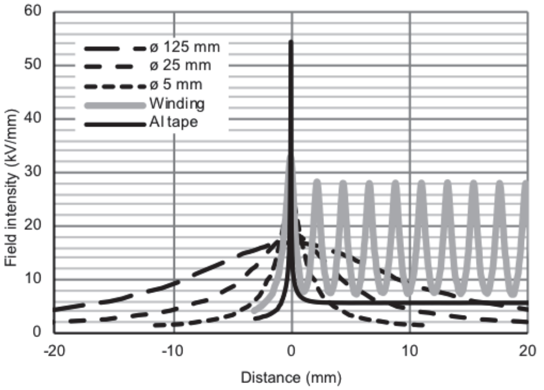

Fig. 7. Electric field intensity in the air directly above the surface of the insulation for different electrode types at the location of highest electric stress (wide view)

V. CONCLUSIONS

The performed tests showed that the electric stress caused by contact with an object which has a substantially higher electrical conductivity compared to the insulating material of the CC, causes puncture of the insulation over a timespan which ranges from hours to months under normal operating voltage, depending on the shape of the object. If the object is round, a larger diameter causes breakdown faster, possibly because a wider area of insulation is stressed and there is a higher probability of weak spots in that area. A smaller diameter electrode will cause a stronger electric field, but in a narrow area, and will possibly cause puncture after a longer period of time in most cases. The size of the total area under stress is apparently more significant than the strength of the electric field under the test conditions. In case of the wound electrode, there was a combination of high electric stress and a large area of insulation under influence, which resulted in punctures over a much shorter duration than in case of other tested electrodes.

However, in case the electrode is flat and has a long contact area with the CC insulation, the intensity of the electric field is important. In case of the Al tape, the CC was effectively in contact with an electrode of infinite diameter, but all the punctures occurred at the edges of the tape, where the field was strongest.

Four of the tested electrode types did not cause puncture in the insulation faster than after two weeks for any single test point. Four of the winding electrode testing points punctured within two weeks, one of which punctured within 12 hours. This electrode shape, however, is not very representative of the objects that could come into contact with actual CCs in the grid. It can be used to simulate worst-case electric stresses in tests, because the electrode has caused the shortest insulation withstand times.

For practical considerations, distribution grid operators should be most concerned by larger diameter trees and branches falling onto power lines using CCs. In addition to the faster occurrence of breakdown due to purely electrical effects, larger branches also have a more significant mechanical impact on the CC, which also contributes to the wear of insulation. Because of the high potential variability of breakdown time depending on the insulation strength at the point of contact, it would be prudent to remove any objects from CC power lines with minimal delay.

REFERENCES

[1] F. Nishimura, L. D. Cicarelli, M. Coelho, B. Trager and M. R. Soares, “Covered cable comparative testing: HDPE and XLPE evaluation”, *IEEE/PES Transmission and Distribution Conference and Exposition*, Atlanta, 2001

[2] A. Kasparans, M. Budahs and J. Rozenkrons, “20 kV insulated overhead lines overvoltage protection problems in Latvia’s distribution network” *Electric Power Quality and Supply Reliability Conference*, Viimsi, Estonia, 2006

[3] G. Eduful and K. N. Asante, "In search of electric power reliability in forested terrain with covered conductors the ECG experience," *2012 IEEE 4th International Conference on Adaptive Science & Technology (ICAST)*, Kumasi, 2012, pp. 149-153.

[4] Y. Mecheri, M. Nedjar, A. Lamure, M. Aufray, C. Drouet, “Influence of Moisture on the Electrical Properties of XLPE Insulation”, *2010 Annual Report Conference on Electrical Insulation and Dielectric Phenomena (CEIDP)* . pp. 1-4. ISSN 0084-9162

[5] F. M. Defandorf, “Electrical Resistance to the Earth of a Live Tree” *Transactions of the American Institute of Electrical Engineers. Part III: Power Apparatus and Systems*, vol. 75, no. 3, Jan. 1956.

[6] J. Vehanen and P. Hyvönen, “Diagnosis of medium voltage covered conductors” (*Päällystetyn keskijänniteavojohdon kunnon diagnosointi*), Espoo, 2003

[7] S. Mišák, Š. Hamacek, P. Bilík, M. Hofinek and P. Petvaldský, "Problems associated with covered conductor fault detection," *11th*

International Conference on Electrical Power Quality and Utilisation, Lisbon, 2011, pp. 1-5.

[8] P. Pakonen, "Characteristics of partial discharges caused by trees in contact with covered conductor lines," in *IEEE Transactions on Dielectrics and Electrical Insulation*, vol. 15, no. 6, pp. 1626-1633, December 2008.

[9] EN 50397-1:2006 “Covered conductors for overhead lines and the related accessories for rated voltages above 1 kV AC and not exceeding 36 kV AC Part 1: Covered conductors”

[10] I. Kiitam, P. Taklaja and K. Tuttelberg, “Voltage Withstand Properties of the Insulation of Different Types of Medium Voltage Covered Overhead Line Conductors”, *19th International Scientific Conference on Electric Power Engineering (EPE)*, 16-18 May, 2018, Brno, Czech Republic. Brno University of Technology, 2018.

BIOGRAPHIES

Ivar Kiitam was born in Tallinn, Estonia in 1992. He received his BSc and MSc degrees in electrical power engineering from Tallinn University of Technology (TTÜ) in 2014 and 2017, respectively. He is currently a PhD student at Department of Electrical Power Engineering and Mechatronics in TTÜ. His main research interests include medium voltage power cable and covered conductor insulation diagnostics.

Paul Taklaja received the MSc and PhD degrees in electrical power engineering in 2007 and 2012, respectively, from Tallinn University of Technology. He is currently working as senior lecturer at the Department of Electrical Power Engineering and Mechatronics in the Tallinn University of Technology. His research interests include essentially high voltage engineering issues.

Kaur Tuttelberg (Student Member ’14) was born in Rakvere, Estonia in 1990. He received the BSc and MSc degrees in electrical power engineering from Tallinn University of Technology (TTÜ), Tallinn, Estonia, in 2012 and 2014, respectively, with the last year of studies carried out at KTH Royal Institute of Technology, Stockholm, Sweden. He received his PhD from Tallinn University of Technology in 2018. At the moment he is working as a researcher at the Department of Electrical Power Engineering and Mechatronics of TTÜ. His current research focuses on the development of monitoring applications for power systems and their elements.

Appendix 3

Publication III

Shafiq, M.; Kiitam, I.; Taklaja, P.; Kütt, L.; Kauhaniemi, K.; Palu, I. (2019). Identification and Location of PD Defects in Medium voltage Underground Power Cables Using High Frequency Current Transformer. IEEE Access, 7, 103608−103618.

IEEE Access
Multidisciplinary ⋮ Rapid Review ⋮ Open Access Journal

Received June 17, 2019, accepted July 11, 2019, date of publication July 24, 2019, date of current version August 13, 2019.

Digital Object Identifier 10.1109/ACCESS.2019.2930704

Identification and Location of PD Defects in Medium voltage Underground Power Cables Using High Frequency Current Transformer

**MUHAMMAD SHAFIQ[1], IVAR KIITAM[2], PAUL TAKLAJA[2], LAURI KÜTT[2],
KIMMO KAUHANIEMI[1], AND IVO PALU[2], (Member, IEEE)**
[1]School of Technology and Innovations, Electrical Engineering, University of Vaasa, 65200 Vaasa, Finland
[2]Department of Electrical Power Engineering and Mechatronics, Tallinn University of Technology, 19086 Tallinn, Estonia

Corresponding author: Muhammad Shafiq (muhammad.shafiq@uwasa.fi)

This work was supported by the Project Smart Condition Monitoring of Power Grid, funded by the Academy of Finland, under Grant No. 309412.

ABSTRACT Fault location is an important diagnostic task in condition monitoring of underground medium voltage cables. Available solutions are well capable of determining the location of a single partial discharge (PD) defect on a cable section. In case several PD defects are active simultaneously along a cable section, the interpretation of the measured data becomes complex to identify the presence of more than one PD sources. In this paper, experimental investigation of two PD defects/sources at different locations on a medium voltage (MV) cable section is presented. A high frequency current transformer is used for single end PD measurements. Time domain reflectometry-based in-depth study of the reflected pulses provides the most valuable information to identify the presence of PD sources which further leads to the location of the individual PD sources. In this paper, the proposed solution is presented for two PD sources, however, the same methodology can be extended to locate multiple PD sources on the cable.

INDEX TERMS Cable insulation, power distribution lines, partial discharges, time domain analysis, sensors, condition monitoring.

I. INTRODUCTION

Overhead power lines are highly vulnerable to various external and climatic factors, such as faults initiated by accidents, adverse weather conditions and natural disasters. Unfortunately, extreme weather events, including hurricanes, storms, snow, and floods usually cause significant damage every year. The operation of overhead power lines is severely affected by this. To minimize the occurrence of faults in the future, several initiatives have been made around the world to replace overhead lines with underground power cables. For example, studies made by Consolidated Edison, Inc. and Florida Public Service Commission have suggested converting the overhead lines to underground cables and provided estimated costs in the range of billions of dollars to accomplish this conversion for New York and Florida [1]. Similarly, in Europe, underground cabling has been adopted as a preferred solution for a reliable and secure means of power distribution [2]. In Finland, the replacement of underground cable installations in distribution network is in progress; reaching an estimated 70% installation in 2023; the target is to complete the replacement by 2028 [3].

This trend is likely to continue, as the security of supply is a top priority for grid utilities and underground installations will significantly reduce the frequency of power outages compared to overhead lines in a vast majority of operating conditions. However the aging, operational stresses, and abnormal situations in the installed underground distribution cables is a looming issue. Therefore, upgrades in the condition monitoring of power cables are needed to pre-emptively avoid fault occurrences in expensive cable installations and the associated critical infrastructure.

Dielectric insulation is one of the most critical components in power equipment, ranging from low voltage to high voltage applications. In all the major network components such as power transformers, cables, switchgear, machines, etc. the purpose of the insulation materials (which can be in either solid, liquid or gaseous state), is to electrically separate the

The associate editor coordinating the review of this manuscript and approving it for publication was Taha Selim Ustun.

This work is licensed under a Creative Commons Attribution 4.0 License. For more information, see http://creativecommons.org/licenses/by/4.0/

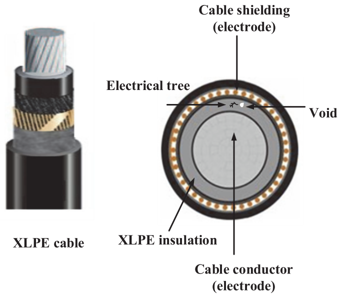

FIGURE 1. Insulation defects depicted in the MV cable insulation.

energized conductors of different phases from each other and from earth. However, when the insulation material has some defects (cracks, voids, or cavities) as depicted in Fig. 1, the dielectric strength of the defective part decreases, which causes the occurrence of partial discharges (PD). PD activity within solid insulation is initiated in the defective locations under suitably high electric field stress. PD activity progresses in time and may lead to the development of carbonized paths inside the insulation, so-called 'electric trees', which tend to expand and after a certain amount of time lead to insulation failure if not attended to in a timely manner.

Although PD activity is a gradual process of degradation and it may follow a certain pattern to failure, however an event of elevated stress may lead to an accelerated rate of degradation and cause sudden failure [4]. To prevent the unexpected outages, PD-based online condition monitoring is an effective tool to observe the PD profile of the most failure-prone grid components. Cables are of particular interest in this regard as the most vulnerable components of the electric grid regarding insulation faults [5], [6]. Cable repairs are time-consuming and accurate fault location is not always straightforward.

PD is accompanied by electromagnetic activity, which can be used to identify its occurrence. In case of cables, the PD pulse emitted from the defect site propagates along the cable line and can be monitored using appropriate sensors and suitable techniques. Over the past few decades, there has been increasing interest in improving the available monitoring and diagnostic solutions. A lot of work has been done in order to improve the detection and location of the PD defects. However, most of the efforts are aimed at detecting and locating the presence of a single PD defect on the section of a cable.

An ample amount of research has been conducted on the investigation of multiple PD faults initiated by different types of PD sources [7]–[10] in different power components. The developed techniques are used to detect and identify the presence of multiple PD sources which may present as corona, discharges in dielectric liquids, surface discharges or internal discharges using phase-resolved PD (PRPD) patterns. These types of discharges can be identified based on PRPD analysis because each type of PD activity appears during certain phase angles of the voltage cycle. However, when two PD sources of same type are active simultaneously, they will appear at the same phase location and identification of these sources is generally not possible by PRPD analysis. It is important to investigate the individual PD signals to analyze the presence of single or multiple PD-causing defects of the same type.

Antenna and acoustic sensor based techniques have been used for the location of multiple PDs of the same type using PD pulse analysis in the substation equipment such as power transformers, switchgear, and similar types of enclosed system components. These techniques are often, however, not effective when investigating cables. The fact that the cable may span over several kilometers renders the methods based on measurements using multiple antenna and acoustic sensors unfavorable [11]–[13]. A detailed explanation of the capabilities of sensors specific to the type of power equipment has been discussed in detail in [14].

The location of single PD faults in power cables has been traditionally accomplished using the time domain reflectometry (TDR) method [15]. However, its application to multiple PD sources in a single cable has rarely been considered thus far. The TDR technique is usually implemented using one-end measurements (single sensor) or two-ends measurements (two sensors). Both of these methodologies are based on observing the time of arrival (ToA) of the original PD pulse arriving at the sensors, its subsequent reflected pulses arriving at the sensors, the wave propagation speed, and the total length of the cable. However, when two or more PD sources are active simultaneously on a cable section, the sensor(s) at the end(s) of the cable record the emitted (original) PD signals indiscriminately together with the reflected pulses propagating along the line. This makes the implementation of location techniques a complex task. These recorded signals have to be separated from one another in order to correctly recognize each PD source.

Recently, the work presented in [16] describes how to detect the presence of multiple PD sources along the cable section using power spectral separation. The use of this technique can provide adequate results. However, its implementation needs high expertise in signal processing techniques and prior knowledge and assumptions regarding the number of PD sources to aid the experts in making the correct evaluation. Therefore, there is need to keep developing the conventional and speedy techniques.

This paper proposes a simple approach based on time domain analysis for identification and separation of PD pulses from different sources, configuring the number of PD sources, and the location of the PD sources in power cables. The work is based on experimental investigations carried out in a laboratory environment using a high frequency current transformer (HFCT) sensor and single-end measurement. TDR based analysis is used to localize the PD signals.

II. TIME DOMAIN REFLECTOMETRY (TDR) BASED FAULT LOCATION

When PD activity is initiated, PD occurs at particular phase angles over the power frequency voltage cycles.

The amplitude and polarity of these PD pulses depend on characteristics of the PD source, the instantaneous value of the applied voltage, and its polarity. PD presents at a certain repetition rate. The PD initiates an electric pulse, which propagates towards both ends of the cable. The signals are reflected from one end of the cable and propagate towards the other end. When using single end measurement, the signal which first reaches the measurement sensor (HFCT in this case) is designated as the original pulse and the signal reaching the sensor after reflection from the far end is designated as the reflected pulse. The time difference between the original and the reflected pulse can be used to determine the location of the PD source using TDR.

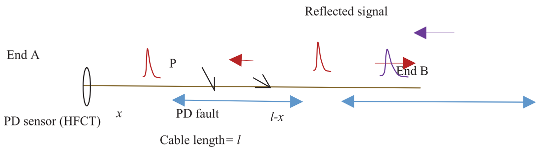

FIGURE 2. PD pulses and their reflections propagating in the cable.

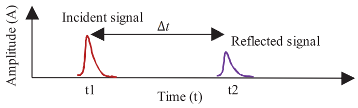

FIGURE 3. Output of PD sensor illustrating time difference of arrival between incident (original) and reflected PD pulse.

As illustrated in Fig. 2, the PD pulse generated from P starts to travel towards End 1 of the cable with length l and is recorded with the HFCT (installed at End 1) at a distance x from point P at time t_1. Simultaneously, the other PD pulse from P starts to travel towards End 2 of the cable by first covering the distance l-x. It is reflected from End 2 and reaches End 1 after also covering the distance l and is eventually recorded by the same HFCT sensor at time t_2 as shown in Fig. 3. Considering the wave propagation speed in the cable v, the time t_1 at which the first PD pulse reaches the HFCT can be expressed as:

$$t_1 = \frac{x}{v} \tag{1}$$

Covering the direct distance (l-x) towards End 2 and 'reflected distance' l, the time t_2 can be expressed as:

$$t_2 = \frac{l + (l - x)}{v} \tag{2}$$

The time difference of arrival Δt between the pulses is determined as:

$$\Delta t = t_2 - t_1 \tag{3}$$

$$\Delta t = \frac{l + (l - x)}{v} - \frac{x}{v} \tag{4}$$

The distance x of PD source at point P from End 1 can be calculated as:

$$x = l - \frac{\Delta t v}{2} \tag{5}$$

III. PRACTICAL CONSIDERATIONS REGARDING REFLECTION OF PD SIGNALS ON A CABLE

While using TDR based fault location methods, it is important to consider the measurement arrangements, i.e. the length of the cable being tested, the response of the measurement sensors, data acquisition system (DAS) and apply this knowledge when interpreting the data. In this section, practical issues regarding cable length and the capabilities of the measuring sensor are discussed briefly while DAS and data interpretation will be discussed in the following sections.

A. CABLE LENGTH

A PD signal has a certain pulse width P_w, which ranges from a few nanoseconds to microseconds. Based on the wave propagation velocity and the length of the cable, the reflected pulse arrives at the sensor after a certain time difference and is captured by the sensor. It is very important to capture the complete reflected PD pulse, particularly the first part of the pulse. The first peak of the pulse can be considered more reliable for determining the time difference of arrival between the pulses. If the cable length is not sufficient to cause a suitably long time delay between the original and reflected pulse, the reflected pulse will arrive at the measuring sensor during the time interval when the original pulse is being captured. This will cause superposition of the reflected pulse and the original pulse, which causes ambiguity and in many cases it is impossible to reliably distinguish or separate the two pulses in the obtained signals.

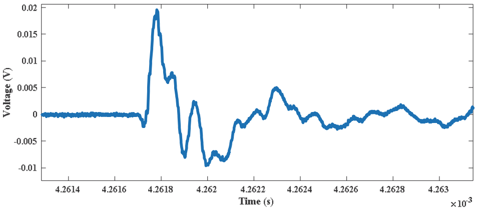

FIGURE 4. Experimentally measured PD signal (pulse).

In Fig. 4, a PD pulse measured on a medium voltage (MV) cable of 10 m length is presented, in which the wave propagation velocity has been measured at 1.54 × 10^8 m/s. Performing TDR on such a short length of cable may not be useful, because the PD pulse width is approximately 0.142 μs (see Fig. 3), while the reflection appears after a short time, 0.064 μs. The pulses have been superimposed and the reflected pulse cannot be distinguished from the original pulse as illustrated in Fig. 4. The PD pulses undergo multiple reflections, but due to attenuation, the subsequent reflections may not have a high enough amplitude to be measured. In Fig. 5, no reflections can be identified even until 20 μs

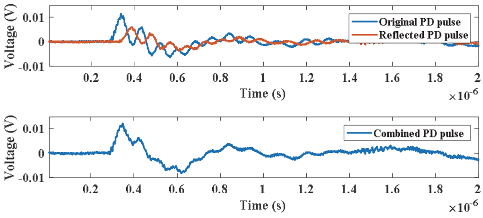

FIGURE 5. PD signal superposition due to short cable length; top- individual waveforms of original and reflected pulse, bottom- the resultant waveform of original and reflected pulse.

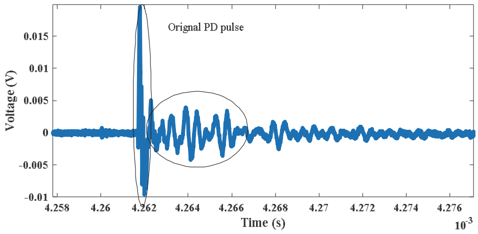

FIGURE 6. Experimentally measured PD signal with post-pulse oscillations.

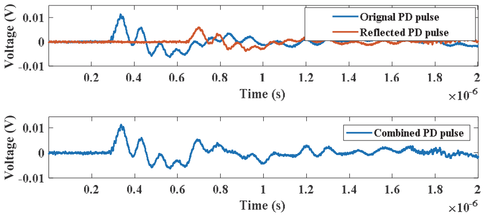

FIGURE 7. Effect of the longer oscillation due to sensor's response; top-individual wave shape of original and reflected signal, bottom- the resultant waveform of original and reflected pulse.

has passed, while a measurement done on a longer cable of 200 m in length would present the first reflection after approximately 2 μs.

For the sake of argument, it can be stated that for a reliable location diagnostic the minimum cable length should be approximately 25 m or more. However, even cables in this length category can experience problems with PD source location diagnostics. This is caused by problems associated with the response characteristics of the measurement sensor.

B. MEASUREMENT SENSOR

A sensor with suitable sensitivity and bandwidth is important for measurement of PD that leads to a reliable location diagnostic in MV cables. Based on their geometrical design and materials used, the cable and HFCT sensor possess intrinsic RLC parameters (resistance, inductance, and capacitance) [14], [17], [18], which affect the waveform of the measured signals.

Oscillations may appear in the sensor output following the PD pulse and are damped after a certain period of time as shown in Fig. 6. It can be seen that the oscillations remain quite significant until the time interval of 12 μs after the appearance of the first PD pulse. Therefore, ideally the study of reflected PD pulses will be reliable if they appear after the oscillatory part. If the sensors have better sensitivity, the amplitude of the measured reflected wave is high enough that the pulse can be identified even if it appears during the oscillatory part. However, a sensor with higher bandwidth has reduced oscillatory time that leads to better measuring performance.

IV. EXPERIMENTAL SETUP FOR FAULT LOCATION ON MV CABLES

Considering the real cases in the MV network, the usual length of cables is in the range of hundreds of meters up to some kilometers. This is sufficiently long for reflections to be easily seen during real world diagnostic measurements. In this study, an experimental investigation is performed at High Voltage laboratory in Tallinn University of Technology. A 20 kV single phase MV cable, type HXCMK with a conductor cross-section of 35 mm^2 and 199.3 m in length, is used for the investigation. The investigation is performed in two stages.

1) Determining the wave propagation velocity of the cable,
2) PD measurement at AC voltage (50 Hz).

A. WAVE PROPAGATION VELOCITY OF THE CABLE

Under fault conditions, cable maintenance is time consuming and expensive due to digging, repairing, and refilling the site while on the other hand inconvenience to the general public is an added burden. Therefore, accuracy of the location of the fault site is imperative. While performing TDR based location diagnostics, accurate information of the propagation velocity is important so that time and velocity based calculations can provide accurate distance and location.

The velocity of wave propagation for a transmission line having air as insulation between its conductors can be calculated as:

$$v_a = \frac{1}{\sqrt{\varepsilon_o \mu_o}} = 3 \times 10^8 \frac{\text{m}}{\text{s}} \approx c \tag{6}$$

which is approximately the velocity of light in vacuum. However, when the insulation is not air or another low-pressure gaseous medium, the velocity is reduced by the velocity factor (VF) which is determined as:

$$VF = \frac{1}{\sqrt{\varepsilon_r \mu_r}} \approx \frac{1}{\sqrt{\varepsilon_r}} \tag{7}$$

The relative permeability $\mu_r \approx 1$ for dielectric materials due to their non-ferrous properties, so the VF primarily depends on the relative permittivity of the dielectric ε_r. VF is defined as the ratio of the propagation speed of light or electromagnetic waves in a medium to the speed in vacuum. Therefore, the calculated wave propagation speed of a cable $v_{c,c}$ can be expressed as:

$$v_{c,c} = c \times VF \tag{8}$$

The diameter of the cable used in the study is 26 mm, cross-linked polyethylene (XLPE) is the main insulation while a semiconducting compound material is used in conductor and insulation screens. The data sheet does not provide any information on the wave propagation speed for this cable. Considering the $\varepsilon_r = 2.2\ldots2.4$ for XLPE, the $v_{c,c}$ is in the range of $2.02\times10^8\ldots1.93\times10^8$ m/s. However, in order to verify the propagation speed, it is necessary to determine the pulse velocity experimentally as well.

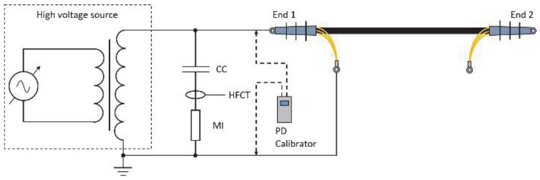

FIGURE 8. **Laboratory test setup for online measurement of PDs in the MV cable (electrical layout); CC- coupling capacitor; MI- measuring impedance of commercial system.**

The propagation velocity can be measured using a PD calibration device, which is connected in parallel to the tested cable, as illustrated in Fig. 8. The PD calibrator is connected to End 1 and the HFCT used to detect PD signals is installed in series with the coupling capacitor (CC) and the measuring impedance of the commercial PD measurement system. The original (the PD pulse injected into End 1) and the reflected signal (from End 2) are captured by the HFCT (see Fig. 9), the time difference of arrival (TDoA) is determined, and considering the distance the pulse travels is twice the length of the cable, the experimental propagation velocity $v_{c,m}$ is determined as:

$$v_{c,m} = \frac{2l_c}{t_d} = \frac{2 \times 199.3}{2.285 \times 10^{-6}} = 1.745\times10^8 \frac{\mathrm{m}}{\mathrm{s}} \tag{9}$$

The difference between the calculated and measured speed is 9%. The difference can be mainly attributed to the presence of semiconducting screens on the conductor and insulation. The aging of XLPE insulation has also been shown to have an effect on the wave propagation speed, although the cable used in this investigation is manufactured in 2016 and has not experienced aging in field service. The effect of the semiconducting screens and aging has been investigated in [19], [20]. In further analysis, the experimentally acquired value will be used, as it takes into account all the possible effects influencing propagation speed and provides the most accurate information of pulse velocity.

B. EXPERIMENTAL SETUP FOR PD INVESTIGATIONS ON MV CABLES

The test setup used for measuring PDs is depicted in Fig. 10 (physical layout) while the principle electric schematic is shown in Fig. 8. For measurement of wave propagation velocity, the PD calibrator was used as shown with dotted line connection. For PD measurements, the PD calibrator was replaced by the high voltage source as shown in Fig. 8. The source has a variable power supply and at the voltage level 13.5 kV the PD started to emerge. In order to have a better signal-to-noise ratio, the applied voltage was raised to 20 kV. The cable terminations are designated as End 1 and End 2 of the cables. A coupling capacitor (1 nF) was connected at End 1 of the cable while the cable is open ended at End 2.

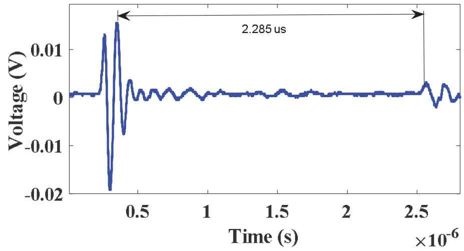

FIGURE 9. **Original and reflected pulses injected with PD calibrator in the tested cable.**

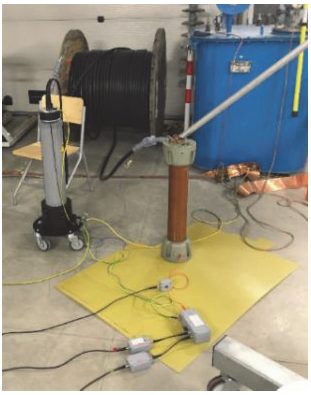

FIGURE 10. **Laboratory test setup for online measurement of PDs in the MV cable (physical layout).**

The HFCT has a 15-mm round primary window, the HFCT parameters are:

- Transfer ratio 1:10;
- Bandwidth 0.5 to 80 MHz (-3 dB).

The HFCT output was connected to a digital storage oscilloscope (DSO) with sampling frequency 2 GS/s.

In addition to the equipment used for recording the waveforms of PD pulses, a commercial PD measuring system was used for simultaneously monitoring other parameters, such as PD apparent charge magnitude, repetition rate etc. The commercial system included a coupling capacitor (CC) which was connected in series with the measuring impedance (MI). The impedance and CC in combination work effectively as a voltage divider and the signal acquired from the measuring impedance was used to record the applied voltage waveform using above mentioned high frequency DSO.

In this work, single end measurements are used and the captured data is shown in Fig. 11. The data is recorded

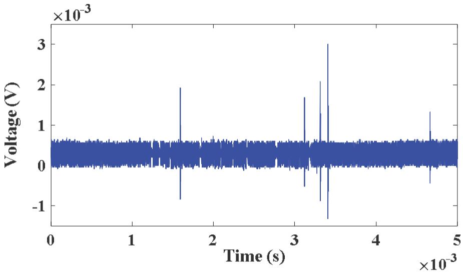

FIGURE 11. PD data of the MV cable measured with HFCT at 20 kV over one voltage quarter-cycle.

with a sampling period of 5×10^{-9} s and is stored in comma-separated values (CSV) format that can easily be imported to Matlab for further analysis on a personal computer.

V. DETECTION AND LOCATION OF THE PD SOURCES

Several measurements have been taken in order to analyze the PD activity. The measurements are recorded subject to the limitation of the number of points (1,000,000 samples) that the DSO can store for a single measurement and a suitable sampling frequency (0.2 GHz) is used to capture the PD signals reliably.

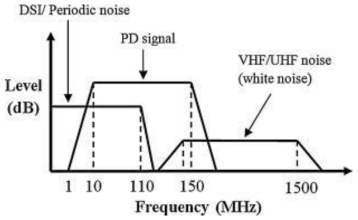

FIGURE 12. Spectra of noise and PD signal [21].

Presence of noise is a critical issue during field measurements and extracting useful signals having lower amplitude is a major challenge. The common sources of noise are: discrete spectral interference (DSI), periodical pulses, random pulses, white noise, and reflections. Figure 12 describes the presence of the noise and PD signals based on their frequency ranges and dB levels [21]. A variety of methods have been reported based on digital signal processing (DSP) techniques denoising such as finite impulse response (FIR) filters, infinite impulse response (IIR) filters, fast Fourier transform (FFT) [21]–[23]. In this work, discrete wavelet transform (DWT) technique presented in [21] has been used. The denoised signal, which presented a better signal-to-noise ratio, is shown in Fig. 13.

For analyzing the individual PD pulses in the time domain, two PD signals have been chosen as shown circled in Fig. 13. These PD signals have been identified based on the post-first pulse behavior that mainly includes reflections and the distances at which they occur. Figure 14 presents PD type 1 having two reflections at certain intervals following the first (original) PD pulse while in case of the PD type 2 shown in Fig. 15, three pulses are observed following the original PD pulse. Considering the apparent behavior, further investigation is made based on TDR principles. The analysis can be proceeded further with two basic findings. Firstly, PD activity is present on the cable line, which means there is at least one insulation defect. Secondly, two types of reflection behaviors indicate the presence of two PD sources at different locations. However, further investigation will explore the PD happening along the line in more detail.

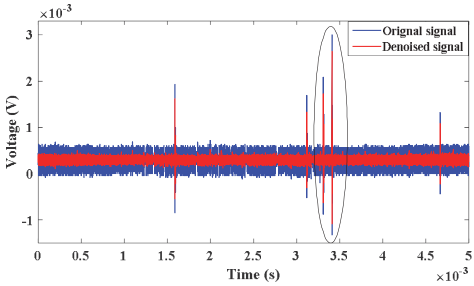

FIGURE 13. Denoising of the measured PD data.

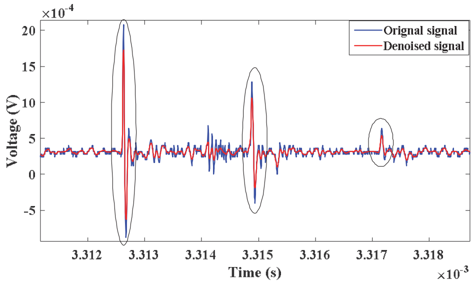

FIGURE 14. PD type 1, PD data identified as potential PDs from a PD source.

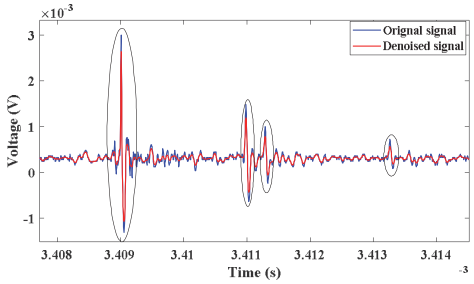

FIGURE 15. PD type 2, PD data identified as potential PDs from a PD source.

A. PD TYPE 1

Figure 16 is re-plotted starting with time zero for better understanding of the TDR analysis. It is observed that Pulse 1 or the

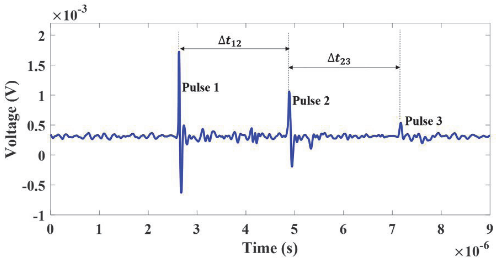

FIGURE 16. TDR based analysis of PD type 1.

original pulse appears at $t = 2.63$ μs, Pulse 2 appears at $t = 4.88$ μs while Pulse 3 appears at $t = 7.17$ μs. Considering the length of the cable (two way length) is 398.6 m and the propagation velocity is 1.745×10^8 m/s, it can be assumed that any pulse appearing within the time frame 2.284 μs, which is the time it takes for the pulse to travel twice the length of the cable, after Pulse 1 will be the 1st reflection of Pulse 1. The time difference between Pulse 1 and Pulse 2 is $\Delta t_{12} = 2.25$ μs. Recalling equation (5), the fault location can be determined as:

$$x_1 = l - \frac{\Delta t_{12} v_p}{2} = 2.56 \text{ m} \tag{10}$$

where x_1 is the distance of the PD fault from the cable End 1, at which the HFCT is connected for PD measurements. It can be seen that Pulse 3 appears at a time difference $\Delta t_{23} = 2.285$ μs after the second pulse. The lattice diagram presented in Fig. 17 for the located PD defect can be used to further explore the observed propagation behavior.

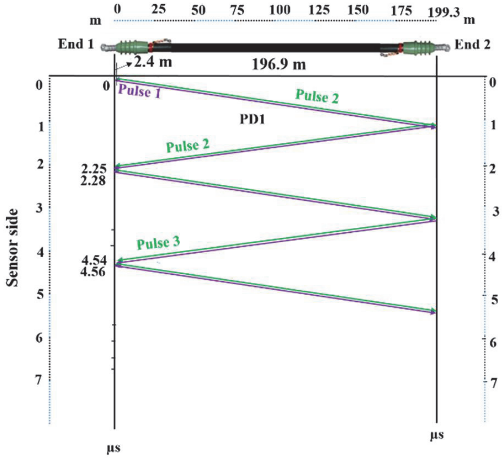

FIGURE 17. Lattice diagram to study the propagation behavior of PD type 1 along the cable.

Considering the PD defect is located at a distance of 2.56 m from End 1, the PD pulse is incepted at the defect site and starts to propagate towards both ends of the cable. Assigning a reference time, the pulse covering the distance of 2.56 m reaches the HFCT at $t_1 = 0$ s as Pulse 1 while towards the other end of the cable, the pulse is reflected from End 2, continues its propagation towards End 1, is measured by the HFCT as Pulse 2 at a time of $t_2 = 2.255$ μs. The time 2.255 μs corresponds to a distance of 2.255 μs $\times$ 1.745×10^8 m/s $= =$ 393.5 m. After having been recorded and the reflection from End 1, it travels towards End 2 and reaches End 1 (as Pulse 3) again.

On the other hand, when Pulse 1 is measured by HFCT at instant $t_1 = 0$ s, it also reflects from End 1 and travels towards End 2. Having reflected from End 2, it also travels towards End 1. This is a time when both the pulses are moving towards End 1 with Pulse 1 following the Pulse 2 at a distance of 5.12 m and reaches End 1 at a time of 2.28 μs. The difference of the ToA is 0.029 μs between Pulse 2 and Pulse 1, which is so small that the two pulses cannot be distinguished during the whole measurement time frame. In addition, comparing the amplitude of the PD pulses after each reflection, significant attenuation can be observed and after Pulse 3, the PD pulse amplitude is so small that it is merged into the noise and cannot be observed any further.

This propagation continues under the effect of two critical characteristic factors of the cable: attenuation and dispersion. These two factors affect the PD pulses in two ways respectively: the decrease in amplitude of the pulse and the increase of the pulse width [24], [25]. After a certain amount of distance travelled along the cable, the pulses 'disappear' due to decreased amplitude. The number of reflections after which the pulses disappear also depends on the length of the cable. In other words, the attenuation and dispersion depend on the distance that the pulses travel along the cable.

B. PD TYPE 2

The second type of PD signals are shown in Fig. 18. Considering the zero reference point in the plot, the first (original) PD signal Pulse 1 is measured at 2.61 μs and its first reflection Pulse 2 is captured at 4.585 μs. Similarly, the further reflections Pulse 3 and Pulse 4 are measured at times 4.895 μs and 6.87 μs, respectively. As analyzed above for PD type 1, the first pulse and its first reflection are used to determine the location of the PD fault, while the rest of the reflections are

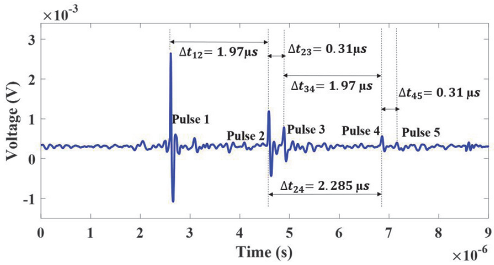

FIGURE 18. TDR based analysis of PD type 2.

important to confirm the determined location and to further study the propagation behavior of these PD pulses between the cable ends. The TDoA between Pulse 1 and Pulse 2 is $\Delta t_{12} = 1.97\ \mu$s. Due to differences in ToA as compared to PD type 1, the location of the corresponding PD fault from End 1 (measuring point) x_2 is calculated using (5) as:

$$x_2 = l - \frac{\Delta t_{12} v_p}{2} = 27.42 \text{ m}$$

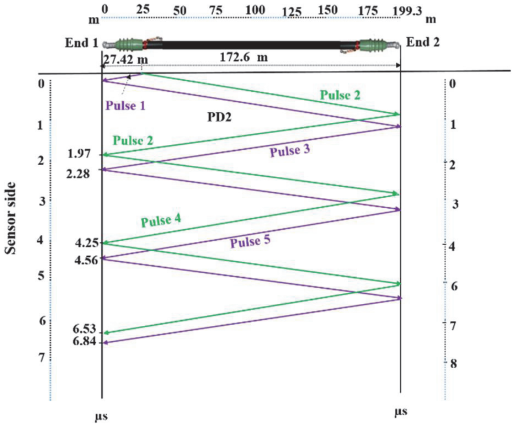

FIGURE 19. **Lattice diagram to study the propagation behavior of PD type 2 along the cable.**

The lattice diagram for PD type 2 is shown in Fig. 19 and because of the relatively greater distance from the measuring end as compared to PD type 1, the reflected pulses can be distinguished visually. Incepted at the defect site (27.42 m from End 1), Pulse 1 reaches the measuring point at $t = 0$ and at the same time Pulse 2 was travelling towards End 2. In the meanwhile, Pulse 1 is reflected from End 1 and starts to propagate towards End 2 following the Pulse 2 at a distance of 54.84 (2×27.42 m). After being reflected, Pulse 2 and Pulse 3 reach End 1 and are captured at times 1.97 μs and 2.28 μs, respectively. Similarly, continuing after their reflections from End 1 and returning after reflections from End 2, the pulses are captured as Pulse 4 and Pulse 5 at times 6.53 μs and 6.84 μs. The lattice diagram explains the propagation behavior of PD type 2 and confirms the location of the PD fault at 27.42 m from cable End 1.

In summary, PD emission is a continuous activity that emits numerous PD pulses during each voltage cycle. This is obvious and it has been analyzed that the time delay between all the pulses and their respective reflected pulses is the same for the same PD source. In case there are two or more PD sources located at different locations, there should be two or more sets of PD pulses and the time differences of the respective PD pulses should be the same. A study encompassing more reflections provides further insight about the PD sources. In this paper, the experimental investigation is presented that encompasses a cable having two PD sources at different locations. Analysis is made to differentiate the PD signals coming from different PD sources and a location diagnostic is performed.

VI. FAULT LOCATION ACCURACY AND DISCUSSION

The location of both PD defects has been determined and they appear to be at a distance of 24.86 m from each other (x_2 - x_1), based on investigation of their individual pulses. Comparing both signals of PD type 1 and PD type 2 in a time reference where the original (first) pulses are simultaneous, it can be seen that the time difference of the reflected pulses ($\Delta\ t = 0.286\ \mu$s) confirms the distance between both faults on the cable as shown in Fig. 20. Having dual confirmation of the location of the PD defects, the experimental findings have to be compared with the real location of the defects which caused the PD.

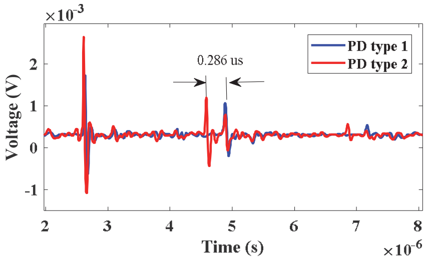

FIGURE 20. **Comparison of PD type 1 and PD type 2 signals for location validation.**

The MV cable used in this experimental investigation has two defects. The locations of both defects have been manually measured at $x_{1m} = 2.4$ m and $x_{2m} = 27.8$ m while the experimentally inferred distances are $x_1 = 2.56$ m and $x_2 = 27.42$ m. The comparison of the manually measured and located using TDR distances shows an error of $\Delta x_1 = 0.16$ m and $\Delta x_2 = 0.38$ m. This still indicates a good match of the real and determined location of the PD faults.

The slight mismatch in defect locations can be due to effective length of the cable, taking into account the termination part and the end of the cable shielding; the finite signal sampling rate as well. Although the distance of the defect points from the cable end was measured diligently, it is still subjected to various measurement errors. The manually measured distances were determined using the sequential numeric meter markings inscribed on the cable sheath during manufacturing and a tape measure to determine the distance of the cable lugs and the defective spots from the nearest meter marker. The cable ends were unrolled from a drum, therefore some residual bending is also a possible source of measurement errors. To account for these factors, the manually measured distances are presented with a conservative accuracy of 0.1 m.

Apart from the aforementioned sources of error, the sampling period can also cause minor errors in a systemic manner. In this work, the measurements have been recorded with a sampling period of 5×10^{-9} s. This means the measurements are recorded with a spatial resolution of 0.872 m. Therefore, there is always a possibility of an error of 0.872 m in terms of distance inherent to the measured waveforms. The issue of the sampling period can also affect the location diagnostics in another way. Assuming that two or more PD sources are at a very small distance from each other on the cable, for example at a distance of less than a meter. Because of the limitation of the sampling period, most likely they will be identified as the same PD source. Considering the particle aspects, such PD sources should be considered as the 'parts' of the same defect site while digging or repair is being made and visual analyses will be important for further confirmation.

The individual PD pulse analysis presented in this work describes the basic idea and methodology of the proposed technique of PD source detection and their location. The analyses are made for several data frames of half power cycles spanning 10 ms. Regarding continuous PD monitoring, one might raise concerns about the feasibility of the proposed technique regarding processing of such a huge amount of data having a high number of PD pulses. When it comes to continuous online condition monitoring of the cables, a comprehensive approach can be developed based on the measurement/data acquisition system and algorithm based processing for automated detection of the PD signals, identification of the number of PD sources, and their location.

While using DSO, a trigger can be adjusted at a certain threshold level to capture the data when a PD pulse appears. The length of the data (of PD signals) to be captured can be selected considering the length of the cable and the sampling period. The length of the data segment should be long enough to accommodate the reflections of the pulses, considering attenuation in the cable. The algorithm can be developed to mark the time of peaks appearing for incident and reflected pulses. The TDoA of the first two pulses (original and the reflected) determines the location of the defects. The data frames, presenting the same TDoA, will belong to the same PD source. Similarly, analysis encompassing all of the incoming data frames will continuously determine if there is a single PD fault or more and where they are located.

In this work, single cable/phase is used to implement the proposed location technique. In case of three phase cable installations which is the usual case in the real networks, the presented technique can be extended accordingly. At the joints and terminations, the shielding of each of the cable/phase is separated and three HFCT sensors should be installed i.e., one sensor for each shielding. During faulty conditions, the emerged PD signals from defective cable/phase will be measured by the corresponding sensor and the fault location can be determined by using TDR techniques as presented above. It should be noted that in this case, the corresponding sensor (installed around the shielding of defective cable) will measure the strongest amplitude of the PD signal, while the other two sensors may measure a weak PD signal induced due to capacitive /inductive coupling between the three phases.

VII. CONCLUSIONS

Due to aging and operational stresses insulation defects develop in cable insulation which cause PD. PD location in underground cable networks is of critical importance. Accuracy of fault location can improve the efficiency of the maintenance system for underground cable assets significantly, especially considering the factors such as repair time, cost, and discomfort to the general public due to power interruptions and on-site repairs. A cable section or branch can be long up to 500-1000 m and can have multiple defects, which can cause PDs simultaneously. When the PD measurements are made, it contain all the information of the ongoing PD activity along the affected cable. If multiple PD sources are active, analysis of the PD signals is quite complex. Reflections of the PD signals plays important role for separation of the PD sources while performing TDR based analysis.

In this work, experimental investigation was made on a 200 m long MV power cable that has two PD sources at different locations. It is proposed that the wave propagation velocity of the cable should be determined experimentally which will enable to locate the PD faults with increase accuracy. TDR based measurement methodology has been adopted by using single end measurements using HFCT sensor installed at one end of the cable. The presented study describes the methodology for two PD sources. However, in case several PD sources are present at several locations, a brief discussion is presented for implementation of an 'automated' monitoring system based on principles of the proposed technique.

Although XLPE has emerged as a robust dielectric insulation that makes the insulation of a cable sections quite reliable. However, joints and terminations are always needed and are the most vulnerable components of an MV cable. When the PD measurements are performed at a certain part of the cable feeder having number of joints/terminations, there is a possibility that more than one locations are suffering with the PD defects simultaneously. In this case, the presented methodology will be useful to identify and locate the PD sources efficiently. This scenario is more likely in the paper insulated cable that are installed decades ago and have increased number of joints due to number of repairs during operation.

As the networks are reaching to their capacity limits, high temperature superconducting (HTS) cables are introduced as a potential solution for carrying significantly higher voltage and currents along with much lower losses as compared to conventional power cables. The presence of liquid nitrogen based cooling in the HTS cable is an added capability that reduces the thermal stresses significantly to avoid the defects in dielectric insulation layers. Similarly, the dielectric insulation is mechanically more protected because of inner and outer cryostat. Such features can improve the issues of dielectric deterioration in these cables to a great extent. However, the cable joints and terminations are still the threat of the PD inception. Being new installations, it is proposed to 'embed' the PD sensors at the suitable locations along the cable feeder during HTS cable installation that will improve the reliability of the network by early detection and location of the possible PD defects using proposed location technique.

ACKNOWLEDGEMENT

The authors would like to thank Prof. Guillermo Robles from University Carlos III de Madrid, Spain for valuable discussions while working on the similar topics there.

REFERENCES

[1] *Utilization of Underground and Overhead Power Lines in the City of New York*, Office Long-Term Planning Sustainability, New York, NY, USA, Dec. 2013.

[2] S. Swingler, J. Daly, and R. Woschitz, ''Statistics of AC underground cables in power networks,'' CIGRE Brochure, vol. 338, 2007.

[3] *Finland's Seventh National Communication under the United Nations Framework Convention on Climate Change*, Ministry Environ., Helsinki, Finland, 2017.

[4] R. Sarathi, K. H. Oza, C. L. G. P. Kumar, and T. Tanaka, ''Electrical treeing in XLPE cable insulation under harmonic AC voltages,'' *IEEE Trans. Dielectr. Electr. Insul.*, vol. 22, no. 6, pp. 3177–3185, Dec. 2015.

[5] P. L. Lewin, J. Steele-Davies, S. M. Rowland, V. Catterson, C. Johnstone, and C. Walton, ''The state of the art of condition monitoring: Where do we go from here?'' in *Proc. INSUCON*, May 2013, pp. 58–66.

[6] E. F. Steennis, P. Wagenaars, P. van der Wielen, P. Wouters, Y. Li, T. Broersma, and P. Bleeker, ''Guarding MV cables on-line: With travelling wave based temperature monitoring, fault location, PD location and PD related remaining life aspects,'' *IEEE Trans. Dielectr. Electr. Insul.*, vol. 23, no. 3, pp. 1562–1569, Jun. 2016.

[7] W. J. K. Raymond, H. A. Illias, A. H. A. Bakar, and H. Mokhlis, ''Partial discharge classifications: Review of recent progress,'' *Measurement*, vol. 68, pp. 164–181, May 2015.

[8] H. Illias, G. Altamimi, N. Mokhtar, and H. Arof, ''Classification of multiple partial discharge sources in dielectric insulation material using Cepstrum analysis–artificial neural network,'' *IEEJ Trans. Elect. Electron. Eng.*, vol. 12, no. 3, pp. 357–364, 2017.

[9] C. Boya, M. Ruiz-Llata, J. Posada, and J. A. Garcia-Souto, ''Identification of multiple partial discharge sources using acoustic emission technique and blind source separation,'' *IEEE Trans. Dielectr. Electr. Insul.*, vol. 22, no. 3, pp. 1663–1673, Jun. 2015.

[10] L. Hao, A. Contin, J. Hunter, P. L. Lewin, D. J. Swaffield, C. Walton, and M. Michel, ''A new method for automatic multiple partial discharge classification,'' in *Proc. 17th Int. Symp. High Voltage Eng.*, Hanover, Germany, 2011, pp. 1–6.

[11] M. M. Yaacob, M. A. Alsaedi, J. R. Rashed, A. M. Dakhil, and S. F. Atyah, ''Review on partial discharge detection techniques related to high voltage power equipment using different sensors,'' *Photonic Sensors*, vol. 4, no. 4, pp. 325–337, 2014.

[12] A. R. Mor, P. H. F. Morshuis, P. Llovera, V. Fuster, and A. Quijano, ''Localization techniques of partial discharges at cable ends in off-line single-sided partial discharge cable measurements,'' *IEEE Trans. Dielectr. Electr. Insul.*, vol. 23, no. 1, pp. 428–434, Feb. 2016.

[13] G.-Y. Kwon, C.-K. Lee, Y. H. Lee, S. J. Chang, C.-K. Jung, and Y. J. Shin, ''Offline fault localization technique on HVDC submarine cable via time–frequency domain reflectometry,'' *IEEE Trans. Power Del.*, vol. 32, no. 3, pp. 1626–1635, Jun. 2017.

[14] M. Shafiq, K. Kauhaniemi, G. Robles, M. Isa, and L. Kumpulainen, ''Online condition monitoring of MV cable feeders using Rogowski coil sensors for PD measurements,'' *Electr. Power Syst. Res.*, vol. 167, pp. 150–162, Feb. 2019.

[15] M. Bawart, M. Marzinotto, and G. Mazzanti, ''Diagnosis and location of faults in submarine power cables,'' *IEEE Elect. Insul. Mag.*, vol. 32, no. 4, pp. 24–37, Jul./Aug. 2016.

[16] G. Robles, M. Shafiq, and J. M. Martínez-Tarifa, ''Multiple partial discharge source localization in power cables through power spectral separation and time-domain reflectometry,'' *IEEE Trans. Instrum. Meas.*, to be published.

[17] H. N. Johnson, ''Propagation of high frequency partial discharge signal in power cables,'' Ph.D. dissertation, Univ. New South Wales, Sydney, NSW, Australia, 2009.

[18] M. Shafiq, M. Lethonen, L. Kutt, G. A. Hussain, and M. Hashmi, ''Effect of terminating resistance on high frequency behaviour of Rogowski coil for transient measurements,'' *Elektronika Elektrotechnika*, vol. 19, no. 7, pp. 22–28, 2013.

[19] M. Gavita, ''Influence of the semi-conducting screens on the wave propagation characteristics of medium voltage extruded cables,'' Ph.D. dissertation, Royal Inst. Technol., Stockholm, Sweden, 2003.

[20] Y. Li, P. A. A. F. Wouters, P. Wagenaars, P. C. J. M. van der Wielen, and E. F. Steennis, ''Temperature dependent signal propagation velocity: Possible indicator for MV cable dynamic rating,'' *IEEE Trans. Dielectr. Electr. Insul.*, vol. 22, no. 2, pp. 665–672, Apr. 2015.

[21] G. A. Hussain, M. Shafiq, L. Kumpulainen, F. Mahmood, and M. Lehtonen, ''Performance evaluation of noise reduction method during on-line monitoring of MV switchgear for PD measurements by non-intrusive sensors,'' *Int. J. Elect. Power Energy Syst.*, vol. 64, pp. 596–607, Jan. 2015.

[22] C. F. F. C. Cunha, A. T. Carvalho, M. R. Petraglia, and A. C. Lima, ''A new wavelet selection method for partial discharge denoising,'' *Electr. Power Syst. Res.*, vol. 125, pp. 184–195, Aug. 2015.

[23] N. A. Yusoff, M. Isa, H. Hamid, M. R. Adzman, M. N. K. H. Rohani, C. C. Yii, and N. N. Ayop, ''Denoising technique for partial discharge signal: A comparison performance between artificial neural network, fast Fourier transform and discrete wavelet transform,'' in *Proc. IEEE Int. Conf. Power Energy (PECon)*, Nov. 2016, pp. 311–316.

[24] D. Clark, R. Mackinlay, R. Giussani, L. Renforth, and R. Shuttleworth, ''Partial discharge pulse propagation, localisation and measurements in medium voltage power cables,'' in *Proc. 48th Int. Univ. Power Eng. Conf. (UPEC)*, Sep. 2013, pp. 1–6.

[25] M. Tozzi, ''Partial discharge in power distribution electrical systems: Pulse propagation models and detection optimization,'' Ph.D. dissertation, Dept. Elect. Eng., Univ. Bologna, Bologna, Italy, 2010.

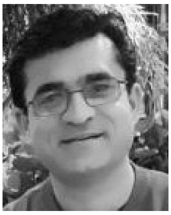

MUHAMMAD SHAFIQ received the M.Sc. degree from UET, Lahore, Pakistan, in 2007, and the Ph.D. degree from Aalto University, Finland, in 2014. From 2001 to 2009, he was a Lecturer and an Assistant Professor with IUB, Pakistan, and from 2015 to 2017, he was a Researcher within industrial organizations in Finland. He is currently an Assistant Professor with the Department of Electrical Engineering and Energy Technology, University of Vaasa, Finland. His research interests include power systems and high voltage engineering while the topics of his research interest include, partial discharge diagnostics, condition monitoring of power system components, and design of sensors for high frequency measurements.

IVAR KIITAM was born in Tallinn, Estonia, in 1992. He received the B.Sc. and M.Sc. degrees in electrical power engineering from the Tallinn University of Technology (TalTech), in 2014 and 2017, respectively, where he is currently pursuing the Ph.D. degree with the Department of Electrical Power Engineering and Mechatronics. His main research interests include medium voltage power cable and covered conductor insulation diagnostics.

PAUL TAKLAJA received the M.Sc. and Ph.D. degrees in electrical power engineering from the Tallinn University of Technology, Tallinn, Estonia, in 2007 and 2012, respectively, where he is currently a Senior Lecturer Teaching Assistant with the Department of Electrical Power Engineering. His research interest includes essentially high-voltage engineering issues.

LAURI KÜTT received the B.Sc. degree in computer and automation technology and the M.Sc. degree in electrical power engineering from the Tallinn University of Technology, Estonia, in 2002 and 2004, respectively, where he is currently a Professor with the Department of Electrical Power Engineering. His current research topics include partial discharge measurements and power quality in distribution networks.

KIMMO KAUHANIEMI was born in Kankaanpää, Finland, in 1963. He received the M.Sc. and Dr.Tech. degrees in electrical engineering from the Tampere University of Technology, Finland, in 1987 and1993, respectively. He was with the VTT Technical Research Centre of Finland. He is currently a Professor and the Head of the Smart Electric Systems (SES) Research Group in electrical engineering with the University of Vaasa, Finland. He has long-term experience on transient simulation of various power systems. His research interests include electricity distribution systems, relay protection, smart grids, and microgrids.

IVO PALU was born in Rakvere, Estonia, in1979. He graduated from the Tallinn University of Technology (TalTech). He received the Ph.D. degree in electrical power engineering, in 2009. He has taught various courses, including wind energy and electrical materials. He is currently a Professor and the Director of the Department of Electrical Power Engineering and Mechatronics, TalTech. His main research interests include wind turbine co-operation with thermal power plants and grid integration of new energy sources. He is a member of the Board of Estonian Society for Electrical Power Engineering and the supervisory Board of Estonian Power Company Eesti Energia AS.

• • •

Appendix 4

Publication IV

Kiitam, I.; Shafiq, M.; Taklaja, P.; Parker, M.; Palu, I.; Kütt, L. (2021); Characteristic Pulse Pattern Features of Different Types of Partial Discharge Sources in Power Cables. IEEE PES/IAS PowerAfrica Conference. IEEE, 1–5.

2021 IEEE PES/IAS PowerAfrica

Characteristic Pulse Pattern Features of Different Types of Partial Discharge Sources in Power Cables

Ivar Kiitam
Student Member, IEEE
Tallinn University of Technology
Tallinn, Estonia
ivar.kiitam@taltech.ee

Muhammad Shafiq
Member, IEEE
Tallinn University of Technology
Tallinn, Estonia
muhammad.shafiq@taltech.ee

Paul Taklaja
Tallinn University of Technology
Tallinn, Estonia
paul.taklaja@taltech.ee

Martin Parker
Tallinn University of Technology
Tallinn, Estonia
martin.parker@taltech.ee

Ivo Palu
Member, IEEE
Tallinn University of Technology
Tallinn, Estonia
ivo.palu@taltech.ee

Lauri Kütt
Member, IEEE
Tallinn University of Technology
Tallinn, Estonia
lauri.kutt@taltech.ee

Abstract— **The measurement of partial discharges (PD) is an important approach used in identifying the presence of defects in high voltage insulation. This paper investigates various parameters characteristic to different types of PD, which can be used for the purposes of achieving more effective PD source discrimination. Measurements were performed on three distinct PD sources using a high-frequency current transformer to detect pulses. Parameters to characterize the PD activity were calculated, including statistical, pulse width, pulse interval and sequential pulse voltage differences. The degree of positive and negative half-cycle asymmetry was also determined. The results obtained indicate that the most significant differences in the parameter values, which can be used to distinguish between different source types, are associated with pulse count, pulse peak values, PD occurrence phase, pulse widths, sequential pulse intervals, voltage differences and correlation between pulse waveforms.**

Keywords— corona, internal discharge, partial discharge, pattern recognition, surface discharge

I. INTRODUCTION

The measurement of partial discharges (PD) is an important technique used in electrical insulation diagnostics. It provides information regarding the presence of processes which cause degradation of dielectric materials and can provide an indication regarding the need to renew insulation systems. There has been increasing interest in equipment monitoring and condition-based maintenance over the last years. PD monitoring in high-voltage equipment has the potential to provide information regarding the state of insulation and early notice of impending potential faults, particularly for equipment which does not produce PD during normal operation.

There are different types of PD, which do not possess an equally detrimental effect on insulation. PD is generally regarded to be either corona discharge, internal (or void) discharge or surface discharge. Corona discharge is usually not a critical issue, as it does not directly degrade the solid or liquid insulation. Surface discharge and internal discharge are more problematic, as the energetic particles involved in the discharge process interact with the insulation and eventually, significant attrition of the insulating materials will occur, which may result in breakdown and subsequent component failure and loss of electrical supply. Modern XLPE (cross-linked polyethylene) insulated power cables and insulation composed of organic materials is particularly susceptible to the detrimental effects of PD.

Measurement results of PD must be analyzed and interpreted to make inferences regarding the number, type and locations of PD sources. This can sometimes be very complicated and usually requires assessment by an experienced specialist. There is potential in the prospect of automating this analysis process. Computer-aided pattern recognition would enable to make an initial assessment of PD activity and ascertain whether it indicates an acute problem. This would obviate, to an extent, the requirement for specialist interpretation and enable differentiation between harmful PD (e.g., internal discharge in a cable joint) and benign PD (e.g., corona discharge at a cable termination). It is known that different types of PD will present with distinctly different phase-resolved partial discharge (PRPD) patterns [1] as well as different PD-producing defects which produce the same type of PD but with a different geometry [2].

Several methods have previously been explored to accomplish PD pattern recognition and various approaches to characterize PD are utilized. Common parameters used to quantify PD activity include average discharge current, average discharge power, pulse repetition rate, peak discharge value and quadratic rate [3]. Statistical analysis of PD datasets, e.g. pulse count vs phase, is utilized to extract parameters such as mean value, variance, skewness, kurtosis or phase asymmetry [4]. Because these datasets can be very large, methods to reduce its dimensionality and computation time as well as to extract important features have also been used [5]. Mapping techniques such as principal component analysis, discriminant analysis and t-distributed stochastic neighbor embedding have also been explored [6], [7]. The density-based spatial clustering algorithm for applications with noise has also been successfully used in PD source discrimination [8].

The development of artificial intelligence has also affected PD analysis. Methods based on neural networks and machine learning have been applied to PD analysis, as well as support vector machines, fuzzy logic-based classifiers, hidden Markov models, self-organizing maps, inductive inference algorithms, rough set theory-based classifiers and sparse representation classifiers [5], [9], [10]. Applying texture analysis algorithms and extracting fractal features of PD patterns have also been proposed [6].

This research work is supported by the project PSG632 funded by the Estonian Research Council.

978-1-6654-0311-5/21/$31.00 ©2021 IEEE

Another approach to PD analysis is to study the features of individual pulses and the sequence of pulses, i.e., the time interval and voltage difference between pulses [11]. If the number of PD sources is low, this approach, i.e., pulse sequential analysis, can provide useful insight into the nature of the PD source. Individual pulse parameters include e.g., peak value, width, area-under-the-curve or rise times and fall times [6]. Studying how PD parameters change with small variations in energizing voltage can also be used to distinguish PD sources [12].

In this paper, aspects of the aforementioned methods have been combined into a singular approach to identify a large variety of distinguishing features of different types of PD. 25 different numeric parameters are calculated for the detected PD activity and the parameters which can be qualitatively used to distinguish the sources from each other and identify unique characteristics are determined. The appropriate use of these parameters can be the basis of further advanced classification algorithms to be employed in PD pattern recognition.

II. TEST SETUP FOR PARTIAL DISCHARGE MEASUREMENT

Three PD sources were studied in a laboratory environment, each of which represents a distinct PD type, as shown in Fig. 1. The sources were energized, one at a time, with 50 Hz AC voltage and the PD pulses were measured, at a voltage slightly above the partial discharge inception voltage (PDIV), using a high-frequency current transformer. The PD was recorded using a digital storage oscilloscope (DSO) with a sampling rate of 250 MS/s. The sources of PD and the related voltage levels are:

- corona discharge – a pin-plane electrode configuration, high voltage is applied to pin (PDIV 11 kV; PDs measured at 12 kV)
- internal discharge – a cut made into the outer sheath of a medium voltage power cable, which penetrates into the insulation (PDIV 6.5 kV; PDs measured at 8 kV)
- surface discharge – a damaged cable termination (PDIV 8 kV; PDs measured at 10 kV)

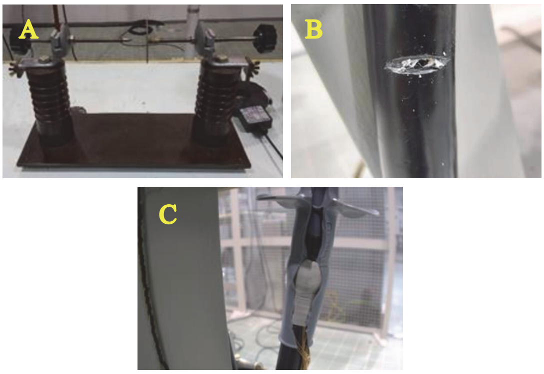

Fig. 1. PD sources used in the tests: A – corona, B – internal discharge, C – surface discharge

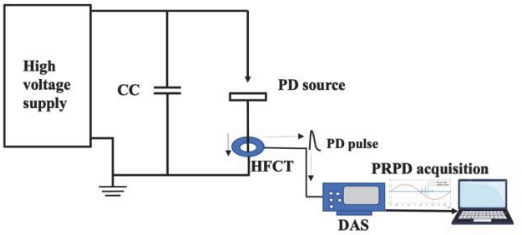

Fig. 2. General schematic of test setup. CC – coupling capacitor, HFCT – high frequency current transformer, DAS – digital storage oscilloscope

III. DATA PROCESSING AND PD-RELATED PARAMETERS

The measured data were processed in MATLAB to yield a series of characteristic quantities to represent each type of PD source. Software-based data manipulation included the following stages:

- PD data denoising
- pulse identification and quantification
- accumulating pulse parameters extracted from full-cycle PD data into arrays to describe PD activity during the positive and negative half-cycles
- calculating characteristic parameters for half-cycles of both polarity
- plotting the necessary graphs

From the measured data, the PD-related parameters were calculated. Based on these, the sources are compared and their utility for differentiating different types of PD sources is evaluated:

- pulse count N
- maximum peak pulse value p_{max}
- minimum peak pulse value p_{min}
- mean peak pulse value p_{mean}
- normalized standard deviation of pulse peak value σ_{pr} ($\sigma_{pn} = \sigma_p / p_{mean}$)
- first pulse time t_f (the smallest discharge epoch observed during any half-cycle of either positive or negative polarity)
- last pulse time t_l (the largest discharge epoch observed during any half-cycle of either positive or negative polarity)
- phase span of PD T_{PD} ($T_{PD} = t_l - t_f$)
- maximum pulse width w_{max}
- minimum pulse width w_{min}
- mean pulse width w_{mean}
- pulse width standard deviation σ_w
- pulse width span w_{span} ($w_{span} = w_{max} - w_{min}$)
- maximum pulse interval (intervals are considered for cycles during which at least two pulses occurred during the same half-cycle) τ_{max}
- minimum pulse interval τ_{min}
- mean pulse interval τ_{mean}
- pulse interval standard deviation σ_τ

- pulse interval normalized standard deviation $\sigma_{\tau r}$ ($\sigma_{\tau n} = \sigma_{\tau} / \tau_{mean}$)
- maximum voltage difference between pulses ΔU_{max} (the difference of the instantaneous value of the energizing voltage during subsequent PD pulses; voltage differences are considered for cycles during which at least two pulses occurred during the same half-cycle. The absolute values of voltage differences are considered, due to the possibility of both positive and negative values depending on whether the pulses occur before or after the peak of the half-cycle)
- minimum voltage difference between pulses ΔU_{min}
- mean voltage difference between pulses ΔU_{mean}
- normalized standard deviation of voltage difference between pulses $\sigma_{\Delta Un}$ ($\sigma_{\Delta Un} = \sigma_{\Delta U} / \Delta U_{mean}$; here also the absolute values of voltage differences are used to calculate the standard deviation)
- correlation coefficient of pulses r (the Pearson correlation coefficient is calculated for the pulses with the smallest and largest width and for both polarities of pulses. The samples captured from 200 ns before the pulse peak to 800 ns after the peak are considered. Pulses originating from the same source are, in general, expected to present with a similar shape, which is the reason this parameter is used.)
- pulse interval – peak value normalized standard deviation (this parameter is associated with the effect of space charges on PD activity. For every two consecutive pulses occurring during the rising portion of every half-cycle at times t_{i-1} and t_i, the first with a peak value of p_{i-1}, the parameter $I_i = (t_i - t_{i-1}) / p_{i-1}$ is calculated. The mean value I_{mean} and standard deviation σ_I are calculated and $\sigma_{In} = \sigma_I / I_{mean}$
- voltage difference – peak value normalized standard deviation (This parameter is also associated with the effect of space charges on PD activity. For every two consecutive pulses occurring during the rising portion of every half-cycle at instantaneous voltage values of U_{i-1} and U_i, the first of which has a peak value of p_{i-1}, the parameter $V_i = (U_i - U_{i-1}) / p_{i-1}$ is calculated. The mean value V_{mean} and standard deviation σ_V are calculated and $\sigma_{Vn} = \sigma_V / V_{mean}$.

The pulse width refers to the width of the pulse at half of the peak value. The values of all of the aforementioned parameters were determined for PD activity for both the positive and negative half-cycle of the applied voltage using each source. In addition, the relative value was calculated for each parameter, i.e., the parameter value of the positive half-cycle was divided by the value of the negative half-cycle to determine the asymmetry of PD behavior between the positive and negative half-cycles with regard to the parameter being considered.

IV. RESULTS AND DISCUSSION

The PRPD patterns of each of the PD sources are presented in Fig. 3. Additionally, the negative polarity pulses with the maximum and minimum width at half value for every PD source are also provided in Fig.-s 4–6. Table I contains the calculated parameters describing the PD activity from each source. The results are based on the PD activity recorded over 7 full AC voltage cycles.

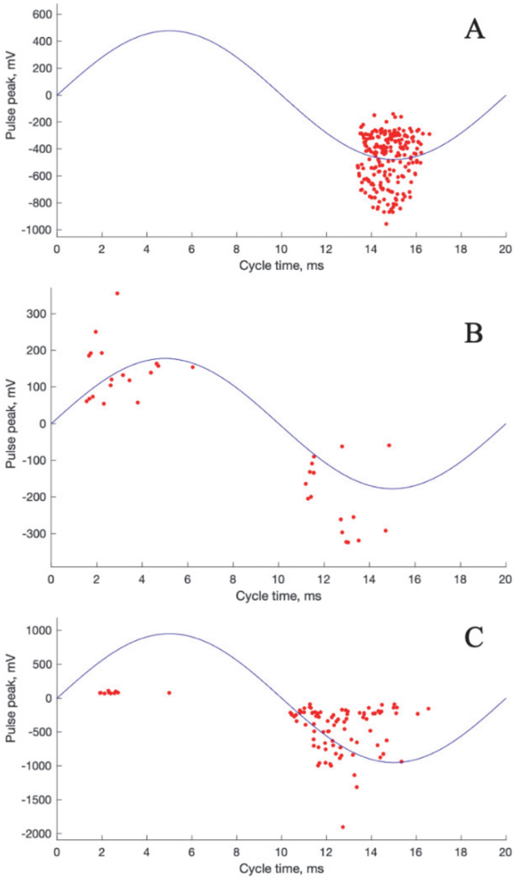

Fig. 3. Phase-resolved partial discharge patterns for each of the PD sources: A – corona, B – internal discharge, C – surface discharge

The results of the tests indicate that there are numerous parameters which may be used to distinguish different types of PD sources. While the behavior of PD is somewhat different in any real-world case, the features of PD activity are inherently linked to the mechanism which produces it. The behavior of PD sources is also influenced by the degree to which the energizing voltage exceeds the inception voltage, e.g. higher voltages would also invoke corona discharge during the positive half-cycle. The presented measurements were collected at voltages which best represent the difference in behavior of PD sources. The parameters which provided the strongest indication of difference between the sources are (also marked in bold in Table I):

A. *Pulse count*

Corona and surface discharge have strong asymmetry between pulse counts over the positive and negative half-cycles. If the voltage is low enough, there might even be a complete absence of pulses during the positive half-cycle, as is the case with corona discharge in this test. In case of internal discharge, the pulse counts are quite similar during both half-cycles.

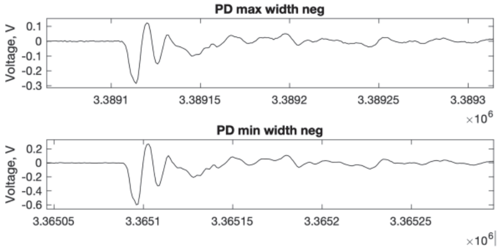

Fig. 4. Negative pulses with maximum and minimum width recorded with the corona source

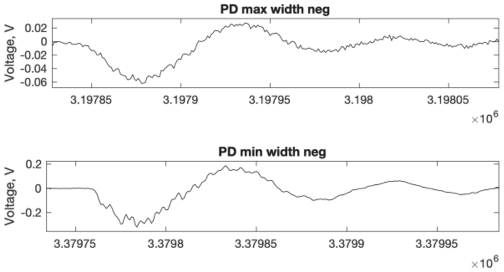

Fig. 5. Negative pulses with maximum and minimum width recorded with the internal PD source

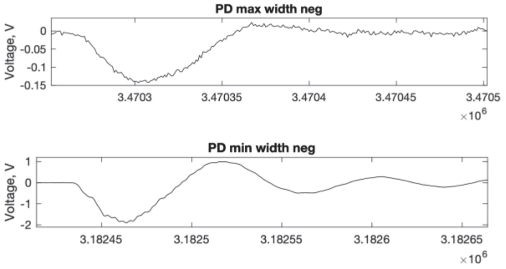

Fig. 6. Negative pulses with maximum and minimum width recorded on the surface PD source

B. *Maximum peak value of the pulse*

In case of internal discharge, the peak value is approximately equal during both the positive and negative half-cycles. In case of surface discharge, the maximum value is significantly smaller during the positive half-cycle compared to the negative half-cycle.

C. *Mean peak value of the pulse*

Similarly to the maximum peak pulse value, the asymmetry of mean peak value is substantially larger in case of surface discharge compared to internal discharge. In case corona discharges occur during both the positive and negative half-cycles, it is expected to see much larger peaks during the positive half-cycle [12].

D. *Phase span*

The phase span of internal discharges is similar for both half-cycles. In case of both corona and surface discharges, the phase span is notably smaller or nonexistent for the positive half-cycle. This can be explained with the increased supply of electrons during the negative half-cycle.

TABLE I
PARAMETERS CHARACTERIZING PARTIAL DISCHARGE IN THE THREE TYPES OF SOURCES, FOR POSITIVE AND NEGATIVE HALF-CYCLES AND RELATIVE TO EACH OTHER

	Corona	**Internal**			**Surface**		
Parameters	**neg**	**pos**	**neg**	**pos/ neg**	**pos**	**neg**	**pos/ neg**
pulse count	209	18	16	1.13	10	92	0.11
max peak (mV)	956	355	324	1.10	111	1902	0.06
min peak (mV)	139	54	59	0.91	68	90	0.76
mean peak (mV)	472	143	201	0.71	82	432	0.19
norm. std. dev. peak	0.39	0.53	0.48	1.12	0.16	0.76	0.21
first pulse time (ms)	3.39	1.56	1.19	1.31	1.91	0.39	4.88
last pulse time (ms)	6.59	6.22	4.86	1.28	5.00	6.54	0.76
phase span (ms)	3.20	4.67	3.67	1.27	3.08	6.15	0.50
pulse width max (ns)	36	164	164	1.00	148	236	0.63
pulse width min (ns)	32	104	116	0.90	132	144	0.92
pulse width mean (ns)	32	142	139	1.02	140	160	0.88
pulse width std. dev. (ns)	1.0	13.6	12.1	1.12	5.1	12.1	0.42
pulse width span (ns)	4	60	48	1.25	16	92	0.17
max interval (ms)	0.37	3.57	1.97	1.82	2.61	1.52	1.72
min interval (ms)	0.04	0.34	1.37	0.25	0.60	0.01	73.5
mean interval (ms)	0.09	1.56	1.67	0.93	1.27	0.40	3.22
std. dev. interval (ms)	0.05	0.88	0.20	4.37	1.15	0.27	4.29
norm. std. dev. interval	0.49	0.57	0.12	4.67	0.91	0.68	1.33
max voltage diff. (kV)	0.36	5.44	6.01	0.91	4.50	2.53	1.78
min voltage diff. (kV)	~0	1.08	2.54	0.42	1.93	0.03	57.8
mean voltage diff. (kV)	0.09	3.48	4.85	0.72	2.83	0.94	3.00
norm. std. dev. voltage diff.	0.97	0.41	0.24	1.69	0.51	0.61	0.84
correlation of pulse waveforms	0.98	0.96	0.97	0.99	0.99	0.64	1.54
norm. std. dev. interval-peak	0.56	0.40	0.60	0.66	0.93	0.86	1.08
norm. std. dev. voltage diff. -peak	0.99	0.45	0.46	0.99	0.54	0.87	0.62

E. *Pulse width parameters*

The width of PD pulses is closely related to the discharge mechanism. Provided that detection equipment with a suitably high bandwidth is used, as is the case in this study, it is possible to distinguish PD pulses from different sources based on pulse width. The detector properties and transmission line characteristics will also have an impact on the pulse shape and consequently, the measured pulse shape is always somewhat distorted. Regardless, the measured pulses exhibit distinctly different width characteristics, which can be exploited to identify different PD sources.

The width of corona pulses was significantly smaller than that of the pulses from other sources, providing a reliable criterion to identify the existence of this type of discharge. Also, there was small variability in the width of pulses. The width of internal and surface discharge pulses was similar, although in case of internal discharges, the maximum pulse width was equal for both polarities. The maximum and mean pulse widths of surface discharge are notably larger during the negative half-cycle.

F. *Pulse interval parameters*

The time gap between pulses can also provide information regarding the PD sources, as this is greatly affected by the space charges deposited at the source from previous PD activity, or, particularly in case of corona discharge, lack thereof. As expected, the mean interval is smallest for corona and largest for internal PD. In case of surface PD, the mean interval is significantly smaller for the negative half-cycle. Also, the mean interval of internal PD is approximately equal for both polarities.

G. *Voltage difference parameters*

As expected, the smallest variability in the applied voltage differences between subsequent pulses is observed with internal discharge, also the maximum voltage difference between pulses during the same half-cycle is approximately equal for both polarities. This is also reflected when taking into account the magnitude of the preceding pulse (last row of Table I), as the value was lower than in case of corona and surface discharge.

H. *Correlation of pulse shape at max and min pulse widths*

The Pearson correlation coefficient was in most cases relatively high (> 0.95), as is to be expected in case there is only one active PD source. The only exception to this was the negative half-cycle of the surface discharge with a correlation of 0.64. This reflects the large difference in the maximum and minimum pulse widths, which can also be observed in Fig. 6.

I. *Applicability of the parameters in distinguishing PD sources*

From these data, it can be inferred that there are numerous possibilities to distinguish different types of PD sources. In simple cases, with only one source, it is often not particularly difficult to make an accurate assessment of the type and nature of the PD source. With multiple simultaneous active sources however, the diagnosis can be challenging. Exploiting as many of the previously discussed parameters in the analysis of PD activity, in an appropriate manner, can aid in the diagnosis of PD activity. Some parameters, e.g. pulse width, can provide a strong indication regarding the presence of corona. Others, e.g. pulse interval parameters, can provide suggestive indications, but not always a conclusive diagnosis. The nature of the equipment being tested, e.g. cable, transformer or GIS, and their typical defects should also be considered.

V. CONCLUSION

Several PD-related parameters were calculated based on measurements performed on three different PD sources, each of which represented a distinct type of PD: corona discharge, internal discharge and surface discharge. The values of these parameters were calculated for both the positive and negative half-cycle and the asymmetry of the parameters was also considered by determining the positive half-cycle value relative to the negative half-cycle value. The parameters which provided the most significant degree of difference between the sources and can be used in distinguishing multiple simultaneous PD sources, are:

- pulse count
- peak values (maximum, mean and standard deviation)
- phase of PD pulses (first pulse, last pulse, phase span)
- pulse width (minimum, maximum, mean standard deviation, span)
- sequential pulse intervals
- sequential pulse voltage differences
- correlation between pulse waveforms

Using these parameters to analyze PD activity can provide numerous approaches to identify simultaneous active PD sources and component defects. The parameters could also be used for computer-aided PD recognition algorithms. Further work can involve developing these methods and testing their feasibility for on-site implementation.

REFERENCES

[1] H. Illias, Teo Soon Yuan, A. H. A. Bakar, H. Mokhlis, G. Chen and P. L. Lewin, "Partial discharge patterns in high voltage insulation," *2012 IEEE International Conference on Power and Energy (PECon)*, 2012, pp. 750-755.

[2] D. A. Fynes-Clinton, D. R. Cornish and C. Nyamupangedengu, "Partial Discharge Patterns of Typical Installation Defects in MV Power Cable Terminations," *19th International Symposium on High Voltage Engineering*, Pilsen, Czech Republic, 2015.

[3] IEC 60270 *High-voltage test techniques – Partial discharge measurements.*

[4] N. C. Sahoo, M. M. A. Salama and R. Bartnikas, "Trends in partial discharge pattern classification: a survey," in *IEEE Transactions on Dielectrics and Electrical Insulation*, vol. 12, no. 2, pp. 248-264, April 2005.

[5] W. J. K. Raymond, H. A. Illias, A. H. A. Bakar and H. Mokhlis, "Partial Discharge Classifications: Review of Recent Progress," *Measurement*, vol. 68, pp. 164-181, 2015.

[6] A. Krivda, "Automated recognition of partial discharges," in *IEEE Transactions on Dielectrics and Electrical Insulation*, vol. 2, no. 5, pp. 796-821, Oct. 1995.

[7] M. Wu, H. Cao, J. Cao, H. Nguyen, J. B. Gomes and S. P. Krishnaswamy, "An overview of state-of-the-art partial discharge analysis techniques for condition monitoring," in *IEEE Electrical Insulation Magazine*, vol. 31, no. 6, pp. 22-35, November-December 2015.

[8] L. Hao, P. Lewin, D. Swaffield and C. Walton, "A New Method for Automatic Multiple Partial Discharge Classification," in XVII International Symposium on High Voltage Engineering, Hannover, Germany, 2011.

[9] T. K. Abdel-Galil, R. M. Sharkawy, M. M. A. Salama and R. Bartnikas, "Partial Discharge Pulse Pattern Recognition Using an Inductive Inference Algorithm," *IEEE Transactions on Dielectrics and Electrical Insulation*, vol. 12, no. 2, pp. 320-327, 2005.

[10] S. Biswas, D. Dey, B. Chatterjee and S. Chakravorti, "An Approach Based on Rough Set Theory for Identification of Single and Multiple Partial Discharge Source," *Electrical Power and Energy Systems*, vol. 46, pp. 163-174, 2013.

[11] D. Benzerouk, "Pulse Sequence Analysis and Pulse Shape Analysis: Methods to Analyze Partial Discharge Processes", Dr.-Ing. dissertation, University of Siegen, 2008.

[12] M. Shafiq, I. Kiitam, P. Taklaja, A. Hussain, L. Kütt and K. Kauhaniemi, "Characterization of Corona and Internal Partial Discharge under Increasing Electrical Stress using Time Domain Analysis," *2020 IEEE Electrical Insulation Conference (EIC)*, 2020, pp. 217-220.

Curriculum vitae

Personal data

Name:	Ivar Kiitam
Date of birth:	16.01.1992
Place of birth:	Tallinn
Citizenship:	Estonia

Contact data

E-mail:	ivar.kiitam@gmail.com

Education

2017–2021	Tallinn University of Technology – PhD
2015–2017	Tallinn University of Technology – MSc
2011–2014	Tallinn University of Technology – BSc
2008–2011	Tallinn Secondary Science School

Language competence

Estonian	fluent, first language
English	fluent
Russian	intermediate
German	basic

Professional employment

2017–2021	Tallinn University of Technology – Early stage researcher
2015–2017	Tallinn University of Technology – Engineer
2013–2014	Tallinn University of Technology – Laboratory assistant
2013	Elering AS – internship
2012	E-Service AS – internship

Elulookirjeldus

Isikuandmed

Nimi:	Ivar Kiitam
Sünniaeg:	16.01.1992
Sünnikoht:	Tallinn
Kodakondsus:	Eesti

Kontaktandmed

E-post:	ivar.kiitam@gmail.com

Hariduskäik

2017–2021	Tallinna Tehnikaülikool – PhD
2015–2017	Tallinna Tehnikaülikool – MSc
2011–2014	Tallinna Tehnikaülikool – BSc
2008–2011	Tallinna Reaalkool

Keelteoskus

Eesti keel	kõrgtase, emakeel
Inglise keel	kõrgtase
Vene keel	kesktase
Saksa keel	algtase

Teenistuskäik

2017–2021	Tallinna Tehnikaülikool – doktorant-nooremteadur
2015–2017	Tallinna Tehnikaülikool – insener
2013–2014	Tallinna Tehnikaülikool – laborant
2013	Elering AS – praktikant
2012	E-Service AS – praktikant

ISSN 2585-6901 (PDF)
ISBN 978-9949-83-770-0 (PDF)